SONOCRYSTALLIZATION AND SONOFRAGMENTATION

BY

HYO NA KIM

DISSERTATION

Submitted in partial fulfillment of the requirements
for the degree of Doctor of Philosophy in Chemistry
in the Graduate College of the
University of Illinois at Urbana-Champaign, 2017

Urbana, Illinois

Doctoral Committee:

Professor Kenneth S. Suslick, Chair
Professor Catherine J. Murphy
Professor Hong Yang
Assistant Professor Prashant K. Jain

Abstract

Acoustic cavitation occurs when ultrasound is applied to a liquid. Bubbles are generated, oscillate, expand and, when specific criteria are met, implosively collapse. These collapses generate hot spots and shockwaves. Hot spots have intense local temperatures (~5,000 K) and pressures (~1,000 atm), and a rapid heating and cooling rate (> 10^{10} K s^{-1}). Shockwaves can induce crystallization, *i.e.*, sonocrystallization, or break existing crystals, *i.e.*, sonofragmentation in solid-liquid mixtures.

The sonofragmentation of ionic and molecular crystals is discussed in **Chapters 2** and **3**. When ultrasound was applied to slurries of ionic or molecular crystals, crystal breakage occurred not by interparticle collision but by direct interactions between crystals and shockwaves. Sonofragmentation rates depended strongly on the strength of the crystal material, as described by its Vickers hardness or Young's modulus. This is a mechanochemical extension of the Bell–Evans–Polanyi Principle or Hammond's Postulate: *i.e.*, activation energies for solid fracture correlate with the binding energies of solids. In addition, from comparisons of sonofragmentation patterns between ionic and molecular crystals, it was confirmed that the sonofragmentation of ionic crystals was more sensitive to changes in material hardness than that of molecular crystals. Finally, two possible mechanisms of particle breakage via sonofragmentation were suggested: particle breakage from defects formed by shock-induced compression-expansion of the initial crystal and particle breakage from defects created during shock-induced bending or torsion of the initial crystal.

In **Chapters 4** and **5**, the sonocrystallization of pharmaceutical agents having inherently low water solubility is discussed. **Chapter 4** describes the development of a spray

sonocrystallization system. Spray sonocrystallization produced nano-scale carboxyphenyl salicylate crystals (c.a. 100 nm) with a narrow size distribution. The crystal size was controllable by changing the initial solute concentration. In **Chapter 5**, carbamazepine crystals were produced via various crystallization methods, including spray sonocrystallization. Crystal sizes, solubility and dissolution rates were compared among carbamazepine crystals generated by five different crystallization methods. Spray sonocrystallization produced the smallest crystals and resulted in the most rapid observed dissolution rate in water.

Table of Contents

Chapter 1

Introduction

1.1 Acoustic cavitation

Ultrasound is an oscillating sound pressure wave over a frequency range of 15 kHz to 10 MHz.[1] When ultrasonic waves pass through a liquid with sufficient amplitude, the negative pressure exceeds the local tensile strength of the liquid and bubbles are created.[2-4] Bubbles are typically generated near pre-existing impurities (e.g., gas-filled crevices in dust motes), which oscillate and grow during cycles of compression and expansion. When the growing bubbles reach a specific size they efficiently absorb energy from ultrasound waves during a single compression–expansion cycle.[1, 5-6] This is called the resonant size. The resonant size depends on the frequency of the irradiated ultrasound, which is approximately 170 μm for a 20 kHz ultrasound.[1] At the resonant size, bubbles grow rapidly during a single cycle of ultrasound waves due to efficient energy absorption. Since bubbles cannot be sustained without absorption of energy, they implosively collapse after reaching the resonant size. This process is referred to as acoustic cavitation (Figure 1.1).

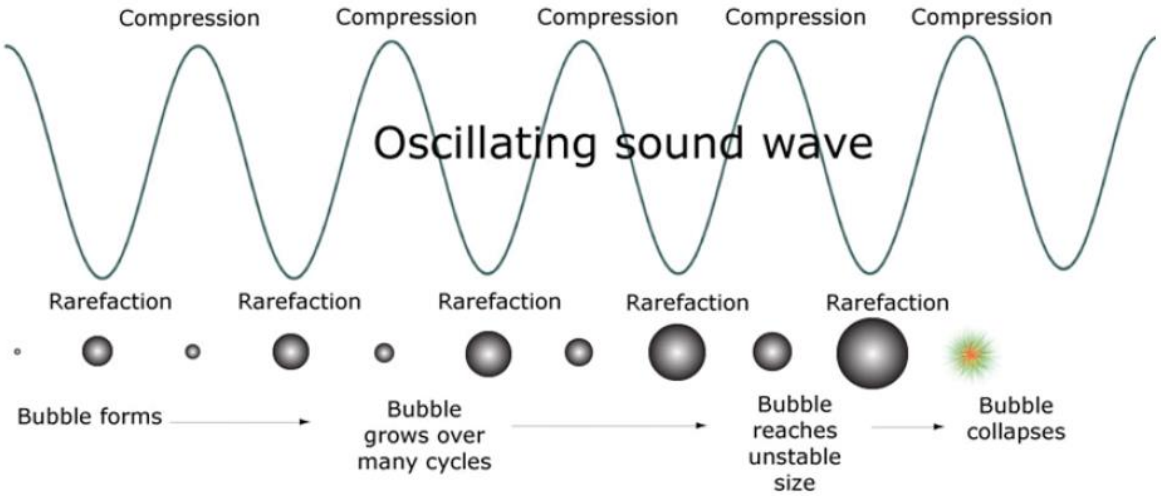

Figure 1.1 Graphical summary of acoustic cavitation. When ultrasound is applied to a liquid, acoustic cavitation occurs: bubbles are formed in the liquid, oscillate and expand, and, finally, implosively collapse.[6]

There are both chemical and physical effects of acoustic cavitation. Ultrasonic wavelengths in liquid vary from approximately 1 mm to 10 cm, which is much larger than the molecular size scale. Thus, the chemical and physical effects of ultrasound do not occur by direct interactions between ultrasound and chemical species, but by the process of acoustic cavitation.[2, 4, 7] The collapse of bubbles produces hot spots, which have intense local temperatures (~5,000 K) and pressures (~1,000 atm), and a rapid heating and cooling rate (> 10^{10} K s^{-1}),[8-11] and shockwaves. Shockwaves have velocities as high as ~ 4,000 m/s and high-pressure amplitudes of 106 kPa.[12]

The physical effects of ultrasound are more diverse in heterogeneous systems (solid–liquid systems), than in homogeneous systems. When a bubble collapses near a significantly larger surface or particle, the bubble no longer collapses spherically and a high-speed liquid stream with a velocity > 100 m/s is generated (i.e., microjet).[13-14] The liquid moves toward the surface of the solid material, which deforms it or changes its chemical composition.[1, 15] Additionally,

shockwaves generated from acoustic cavitation cause high velocity collisions between micron-sized solid particles (i.e., interparticle collisions).[16-17] Also, shockwaves can directly interact with particles and induce breakage (i.e., sonofragmentation).[18]

Sonocrystallization is crystallization induced by ultrasound, and was first report by Alfred Loomis in 1927.[19] In that report, the author investigated the ultrasonic effects of crystallization, among other diverse physical and chemical influences. From the 1950s to the 1970s, sonocrystallization was actively studied in the former Soviet Union.[20-23] Since that time, sonocrystallization of various materials and the modification of diverse experimental parameters have been reported.[24-26] Since the 1980s, the industrial use of sonocrystallization has increased due to advances in equipment, and currently, sonocrystallization is common for generating crystals in pharmaceutical and fine chemicals sectors.[27-29] Despite considerable research, a fundamental understanding of sonocrystallization, especially the mechanism of action, remains incomplete.

1.2 Nucleation

There are two steps in crystallization: nucleation and crystal growth. Molecules in a solution coagulate to form nuclei, and grow into visible crystals.[30] Nucleation is classified by the addition of seed crystals and spontaneity (Figure 1.2).[31] Primary nucleation refers to nucleation in systems that do not already contain crystals. Primary nucleation can be either homogeneous or heterogeneous. Homogeneous nucleation occurs spontaneously, while heterogeneous nucleation is induced by foreign surfaces or particles. Secondary nucleation refers to nucleation from crystals found in a supersaturated system during crystallization.

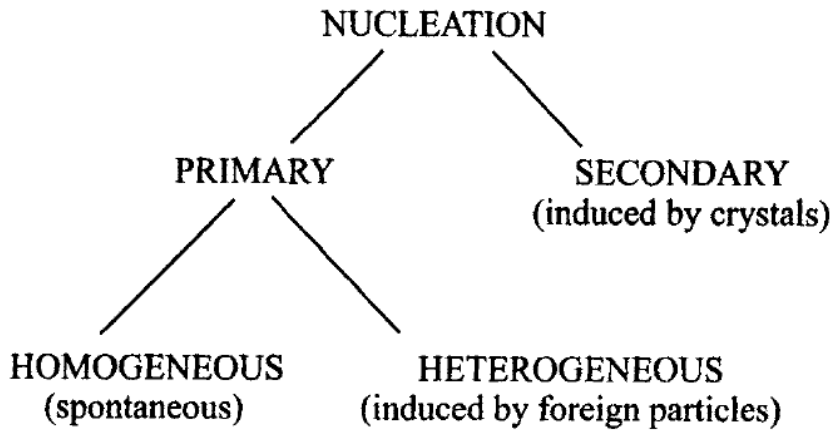

Figure 1.2 Classification of nucleation.[31]

Coagulation and redissolution of molecules or clusters occurs continuously in a supersaturated solution with surface excess free energy (ΔG_s) and volume excess free energy (ΔG_v) (Figure 1.3). Surface excess free energy is the excess free energy coupled between the surface of a small solid cluster and the bulk of the solid; it is the barrier to formation of the surface of a nucleus. Volume excess free energy is the excess free energy between a large particle and the solute, and is required for the transition from solute to a nucleus. The overall free energy (ΔG) is the sum of the free energies, as described by the following:

$$\Delta G = \Delta G_s + \Delta G_v$$

$$= 4\pi r^2\gamma + \frac{4}{3}\pi r^3 \Delta G_v$$

where r = the radius of a cluster assumed as a sphere; G_v = the free energy change of the transformation per unit volume; and γ = interfacial tension between the developing crystalline surface and the supersaturated solution in which it is located.

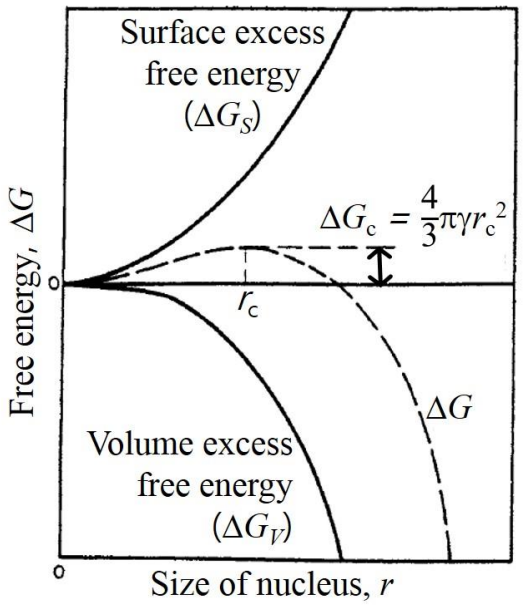

Figure 1.3 Crystallization kinetics. Volume excess free energy (ΔG_v) favors aggregation whereas surface excess free energy (ΔG_s) allows dissolution. Thus, formation of nuclei is a compromise between volume and surface term.[31]

A nucleus forms when a cluster has a higher overall excess free energy than the so-called critical free energy (ΔG_{crit}).

$$\Delta G_{crit} = \frac{4}{3}\pi\gamma r_c^2$$

A cluster reaches the critical free energy when the radius of the cluster reaches a critical size (r_c). If the size of a cluster is equal to or greater than the critical size, nucleation occurs, while if the size of the cluster is smaller than the critical size, it re-dissolves into the solution.

1.3 Effects of ultrasound on nucleation

1.3.1 Induction time

Induction time (t_{ind}) is the elapsed time between supersaturation and the appearance of crystals (Figure 1.4).[31] It is composed of three parts, including the relaxation time (t_r), stable nucleus time (t_n) and nucleus growing time (t_g). The relaxation time is the time required for the crystallized solution to achieve a quasi-steady-state distribution of molecular clusters, while the stable nucleus time and nucleus growing time are the times required for the formation of a stable nucleus and its growth to a detectable size, respectively. In some systems, especially those with a low degree of supersaturation, massive nucleation occurs following a latent period (t_{lp}). The concentration of the crystallized solution remains relatively constant during the induction time and latent period. Following the latent period, widespread crystal growth occurs and the concentration of the solution changes rapidly and significantly.

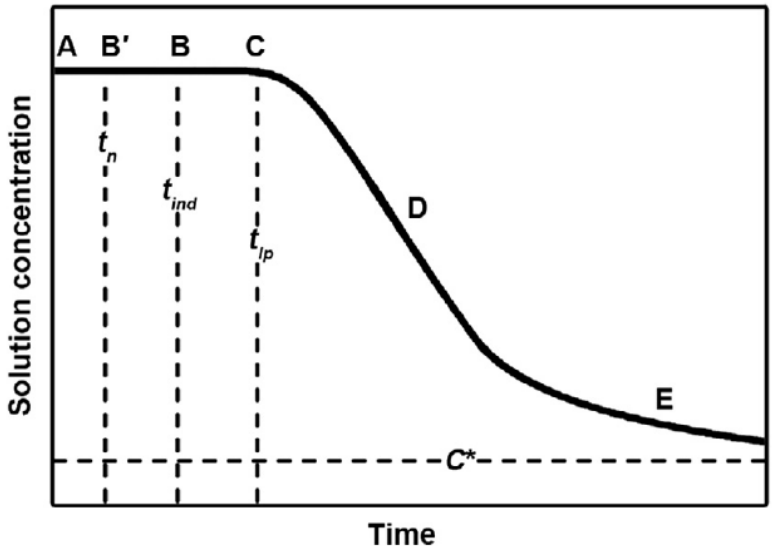

Figure 1.4 A desupersaturation curve. There is lag time between the point of supersaturation (A) and nucleation (B'). Initial nuclei grow until they are a detectable size (B). The concentration of the solution remains relatively constant for some time (C) and then it changes

Figure 1.4 (cont.) dramatically (D) due to rapid crystal growth. Finally, it reaches the equilibrium concentration (E). C* = equilibrium saturation, t_n = nucleation time, t_{ind} = induction time, and t_{lp} = latent period.[31]

Ultrasonic irradiation reduces induction time due to the improved micro-scale mixing and turbulence caused by acoustic cavitation. When the induction time decreases, the rate of appearance of crystals accelerates. Thus, the number of produced crystals increases, while their sizes decrease.

Z. Guo *et al.* studied the effects of ultrasound on induction time using saturated roxithromycin solutions.[32] In this study, saturated roxithromycin solutions were mixed with water (antisolvent) under ultrasonic irradiation and the induction time was assessed using a He–Ne laser recorder. Notably, induction time was reduced when sonocrystallization was performed (Figure 1.5). Additionally, the difference in induction time between sonocrystallization and stirring crystallization increased as the supersaturated ratio of the solution decreased.

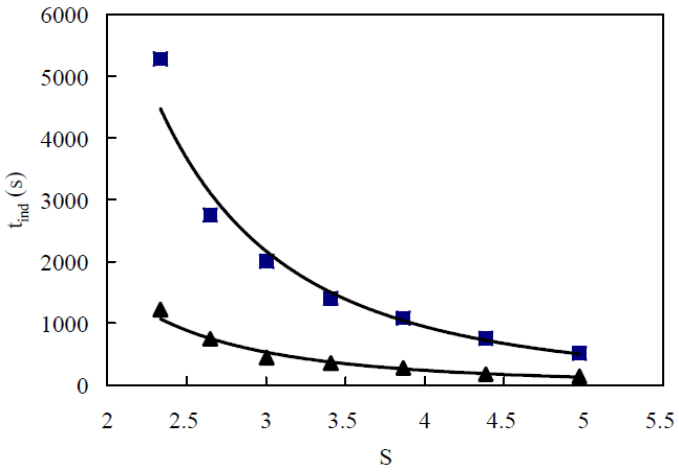

Figure 1.5 Influence of ultrasound on the induction time (t_{ind}) of roxithromycin solution having different supersaturated ratios (S) in presence (▲) and absence (■) of ultrasound.[32]

Those authors also assessed the induction time of $BaSO_4$ under ultrasonic irradiation and found that the induction time of sonocrystallization was shorter than that for stirring crystallization.[33] Furthermore, it was confirmed that sonication with high amplitude ultrasound waves decreased induction time more than sonication with low amplitude waves (Figure 1.6).

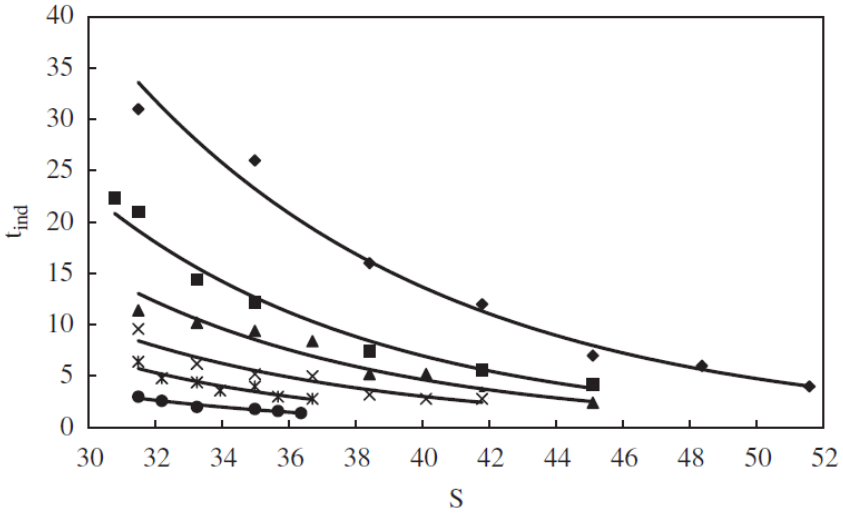

Figure 1.6 Influence of ultrasound on the induction time (t_{ind}) of $BaSO_4$ solution having different supersaturated ratio (S). The amplitude of 750W ultrasonic processor modified as 0% (♦, no ultrasound), 21% (■), 31% (▲), 41% (x), 51% (*), and 61% (●).[33]

1.3.2 Metastable zone width

The metastable zone width (MZW) is the area between an equilibrium saturation curve and the experimentally observed supersaturation point at which nucleation occurs spontaneously (Figure 1.7).[31] For the generation of crystals, the status of a solution changes from stable to metastable to labile (unstable). There are several ways to generate crystals, including cooling (ABCD line), evaporation or addition of an antisolvent (AB'C' line), a combination of cooling and evaporation, or cooling and the addition of an antisolvent (AB''C''

line).

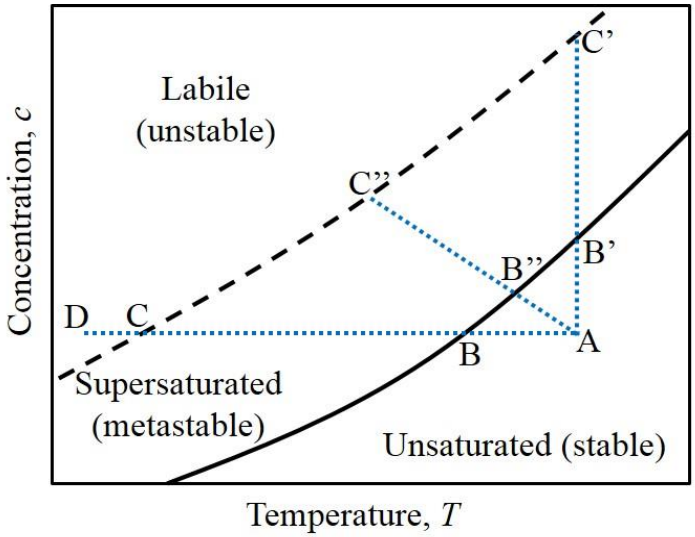

Figure 1.7 Solubility-supersaturation diagram. Solid line is a solubility curve of a solution. Dashed line is a supersaturation curve which represents temperatures and concentrations at which uncontrolled spontaneous crystallization occurs.[31]

When a solution is ultrasonically irradiated, the MZW decreases. During sonocrystallization, gas-filled crevices surrounding dust motes behave as new nucleation sites causing an increase in the rate of nucleation.[30, 34] Additionally, microscale mixing and turbulence improves from the collapse of bubbles during sonocrystallization.[35-38] They accelerate diffusion of solutes and increases the nucleation rate. Due to such increased nucleation sites and improved mixing efficiency, sonocrystallization reduces the MZW.

The effects of ultrasound on the MZW were confirmed during the crystallization of p-aminobenzoic acid (PABA).[39] Cooling crystallization of PABA was performed at a constant cooling rate of 1 °C/min during sonication or with stirring. The nucleation temperature was determined by detecting the appearance of the first crystals becoming visible to the naked eye.

As shown in Figure 1.8, nucleation occurred at lower levels of saturation during sonication compared to stirring.

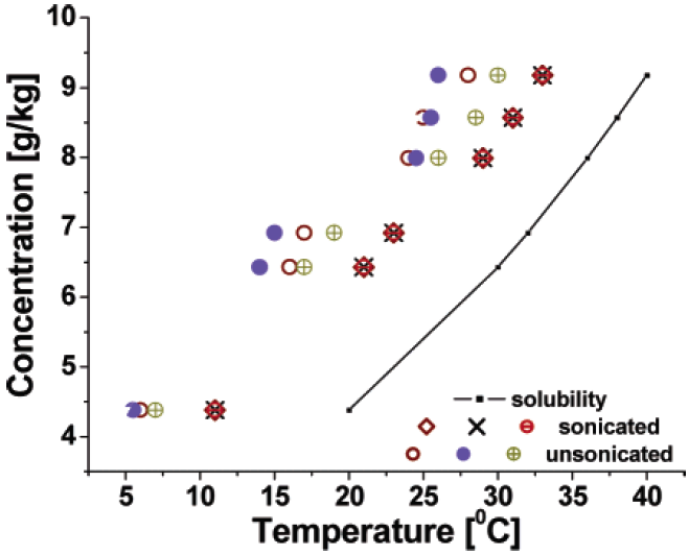

Figure 1.8 Effect of ultrasound on metastable zone width of p-aminobenzoic acid crystallization. For sonocrystallization, 20 kHz and 2.1 W/cm^2 of ultrasound was used. For the unsonicated cases, a magnetic stirring bar was used to stir the solution at 300 rpm.[39]

Another example of a reduction in MZW under sonication is the antisolvent crystallization of benzoic acid.[40] A saturated benzoic acid solution was prepared using absolute ethanol, and mixed with water (antisolvent) by either conventional magnetic stirring or ultrasonic irradiation at room temperature. As shown in Figure 1.9, MZW decreases significantly on ultrasonic irradiation of the benzoic acid solution.

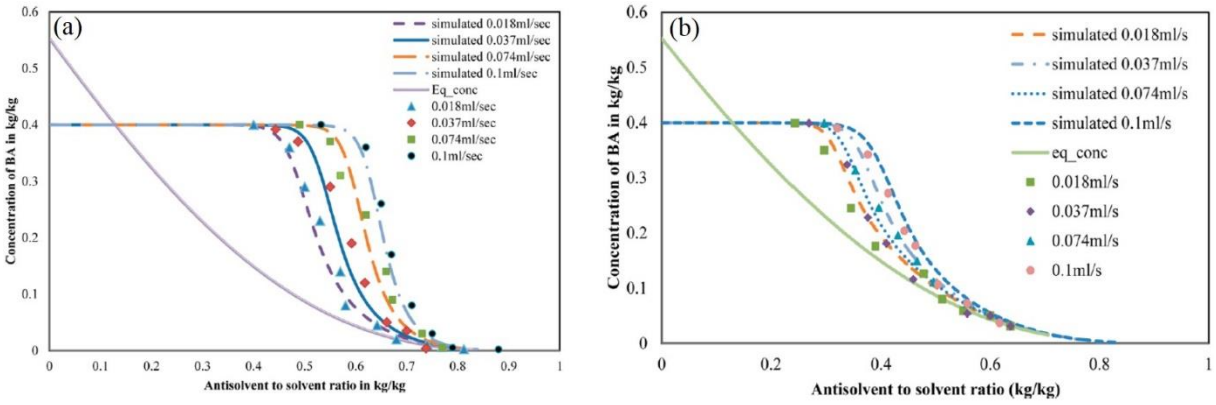

Figure 1.9 Simulated and experimental results of MZW change of benzoic acid with various addition rates of antisolvent (a) with stirring (a magnetic bar, 400 rpm) and (b) under sonication (20 kHz, 8 W/cm^2). For each graph, the Eq_conc line is solubility curve of benzoic acid.[40]

1.3.3 Critical excess free energy

Ultrasound promotes nucleation by reducing the critical excess free energy (ΔG_{crit}). When ultrasound is irradiated to a solution, bubbles are generated.[2-4] At the bubble-solution interface, half a solute molecule is solvated by the solvent, while the other half is not due to contact with the bubble. Such contacts decrease the solvation rate. Re-dissolution of the solute molecule is then prevented, increasing the coagulation of molecules in the solution.[41] Thus, the critical excess free energy (ΔG_{crit}) for nucleation is reduced (Figure 1.3), while the nucleation rate increases.[30-31]

1.3.4 Interparticle collisions and sonofragmentation

Ultrasound increases the rate of secondary nucleation by affecting the number of secondary nucleation sites. Under ultrasonic irradiation, the crystals generated from primary

nucleation collide or interact with shockwaves.[42-44] Due to these occurrences, pre-existing crystals are fragmented and become sites of secondary nucleation.[34, 45]

Chow *et al.* investigated sonocrystallization of ice crystals in sucrose solution, which formed ice dendrites (Figure 1.10).[46-48] Primary nucleation produced the ice dendrites, which subsequently fragmented due to continuous sonication. During prolonged sonication, secondary nucleation occurred around the fragmented crystals and cavitation spots. From corresponding images of these events, it was confirmed that ultrasound affected primary and secondary nucleation events.

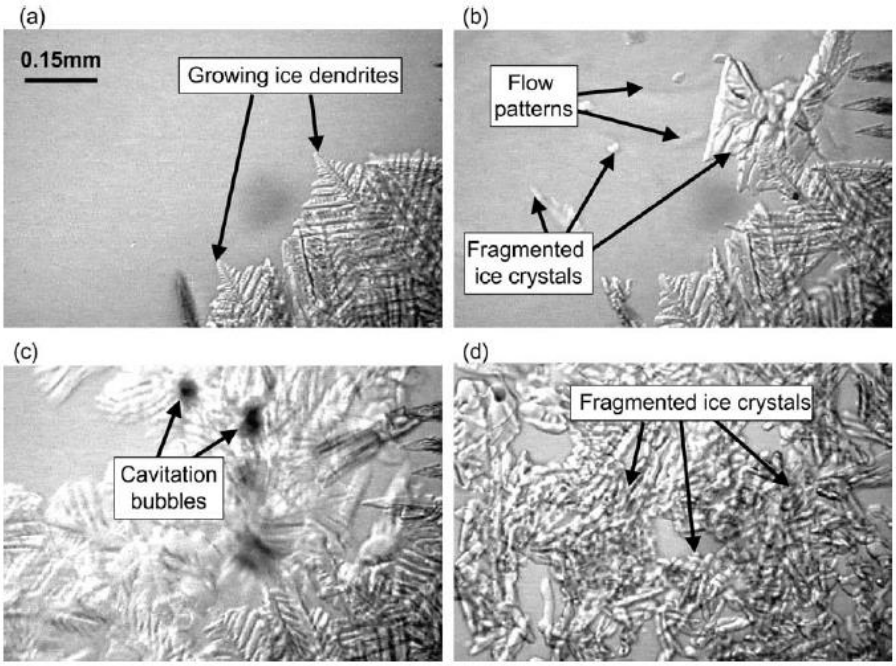

Figure 1.10 Optical micrographs of sonocrystallization and sonofragmentation of ice dendrites in a 15 wt% sucrose solution. (a) primary nucleation and crystal growth (no ultrasound), (b) flow patterns and breakage of ice dendrites after 1.36 seconds of sonication, (c) sonofragmentation of ice crystals after 2.38 seconds of sonication, and (d) secondary nucleation and crystal growth after 17.38 seconds of sonication.[46]

1.4 Advantages of sonocrystallization

1.4.1 Reduction of crystal size

Sonocrystallization is an effective method to generate small crystals. Induction time, MZW and excess free energy are reduced under sonication. Additionally, interparticle collisions and sonofragmentation can occur during sonication. Owing to these effects, rates of primary and secondary nucleation increase and sonocrystallization produces large numbers of small crystals.

Sonocrystallization can produce smaller crystals than other methods, and recently, Gogate *et al*. investigated the effects of ultrasound on crystal size using mefenamic acid.[49] Saturated mefenamic acid solutions were prepared at 60 °C and cooled to room temperature. During the cooling process, either 20 kHz and 30 W/cm^2 of ultrasound was applied for 30 minutes, or stirring was performed at 200 rpm using a magnetic bar. Figure 1.11 shows the significant reduction in crystal size that was observed when the solution was sonicated.

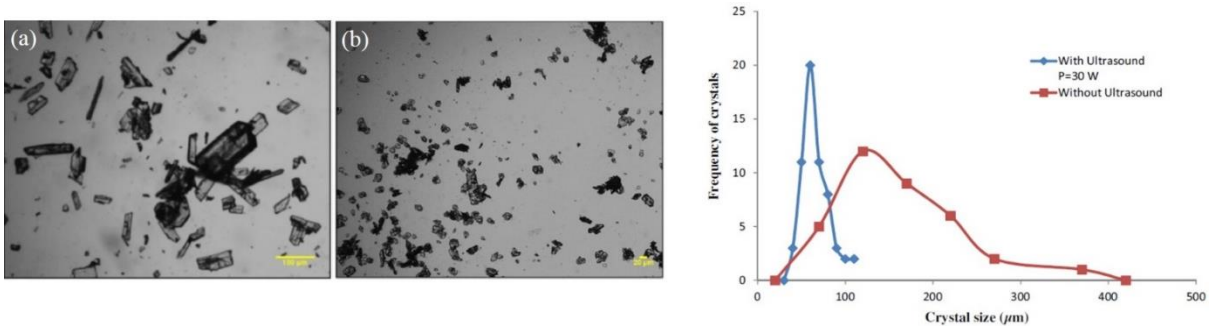

Figure 1.11 Effect of ultrasound on crystal size of mefenamic acid. (Left) optical microscopic images of mefenamic acid crystals generated by cooling crystallization (a) without sonication (stirring) and (b) with sonication. Scale bars are 100 and 20 μm, respectively. (Right) Crystal size distribution of mefenamic acid.[49]

1.4.2 Reduction of crystal size distribution

Sonocrystallization produces crystals with a narrow size distributions. Acoustic cavitation causes vigorous mixing and turbulence in a solution, which prevents crystals from agglomerating. Also, crystals generated via sonocrystallization are unaffected by the size of the seed crystals. During seed crystallization, the size range of the seed crystals greatly impacts the size distribution of the final crystals. However, since sonocrystallization does not require seed crystals, there is no effect of the size of the starting crystals.

Changing ultrasonic conditions controls the crystal size distribution. Paracetamol was used to assess the effects of ultrasonic waves on crystal size distributions.[50] Antisolvent crystallization was performed using saturated paracetamol and water under sonication, and the intensity and frequency of the ultrasound was modified. From the comparisons between Figures 1.12 and 1.13, ultrasound reduced the size distribution of paracetamol crystals. Additionally, when the intensity and frequency of the irradiated ultrasound increased, the size distribution of crystals reduced (Figure 1.13).

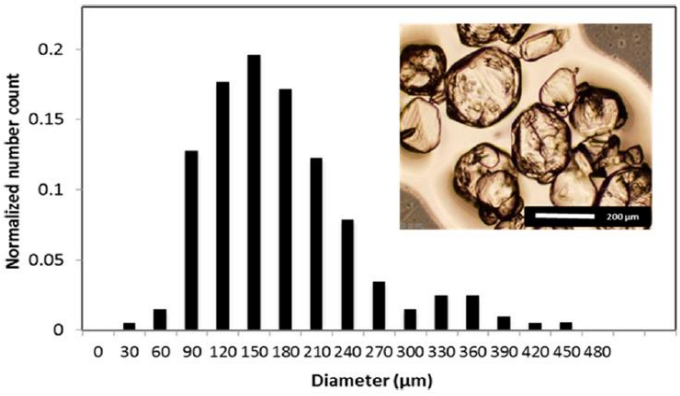

Figure 1.12 Crystal size distribution and optical microscope image of paracetamol generated via antisolvent crystallization with stirring (800 rpm).[50]

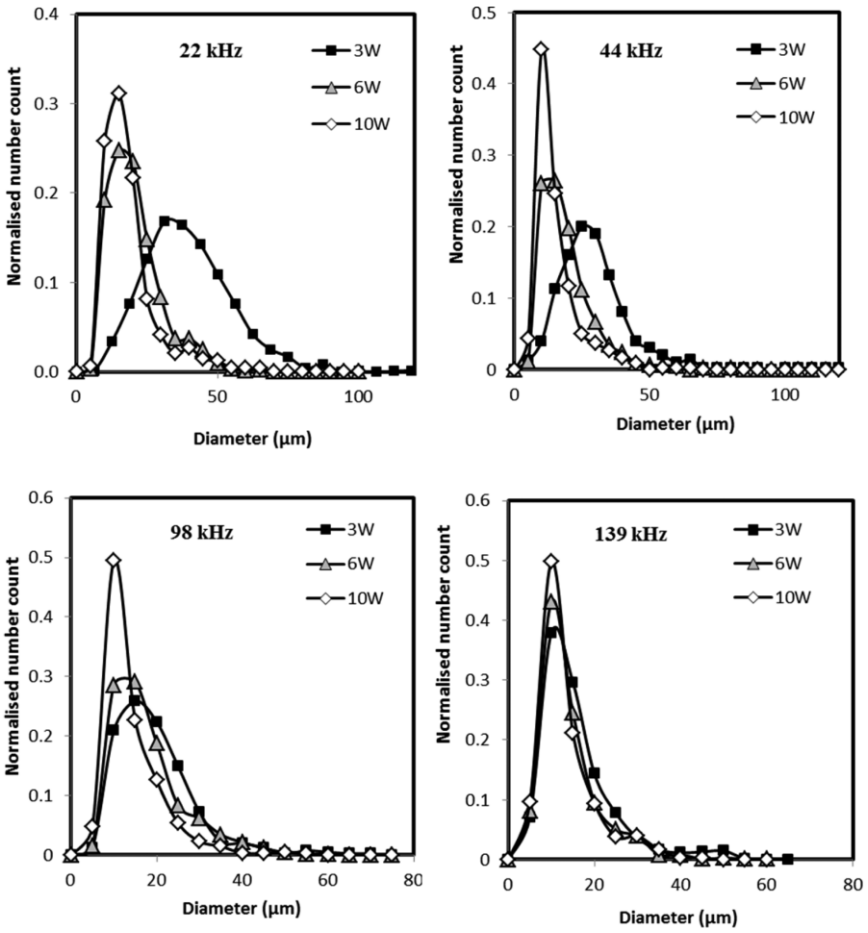

Figure 1.13 Crystal size distributions of paracetamol crystals produced via antisolvent sonocrystallization.[50]

1.4.3 Controllable polymorphism

Polymorphisms can be effected by sonocrystallization. Polymorphism is the ability of a solid material to exist in more than one form or structure.[51] Polymorphs have different stabilities under certain conditions, and the preferred form depends on the condition in which the polymorphs are formed or stored. It is unknown how ultrasound controls the polymorphism of a material.[52-54]

Sonocrystallization generally converts crystals from their kinetically favored form to one

that is thermodynamically favored. A typical example is that of calcium carbonate, which exists in three different forms, including calcite (the most stable form under ambient conditions), aragonite (metastable) and vaterite (the least stable form).[55] Without sonication, vaterite, which is the kinetically favored form, was generated. However, the percentage of calcite, which is the thermodynamically favored form, increased as sonication time or intensity increased (Figure 1.14).[55] Thus, more intense or extended periods of sonication might promote the ground state polymorph due to the improved mass transport and local heating from acoustic cavitation.

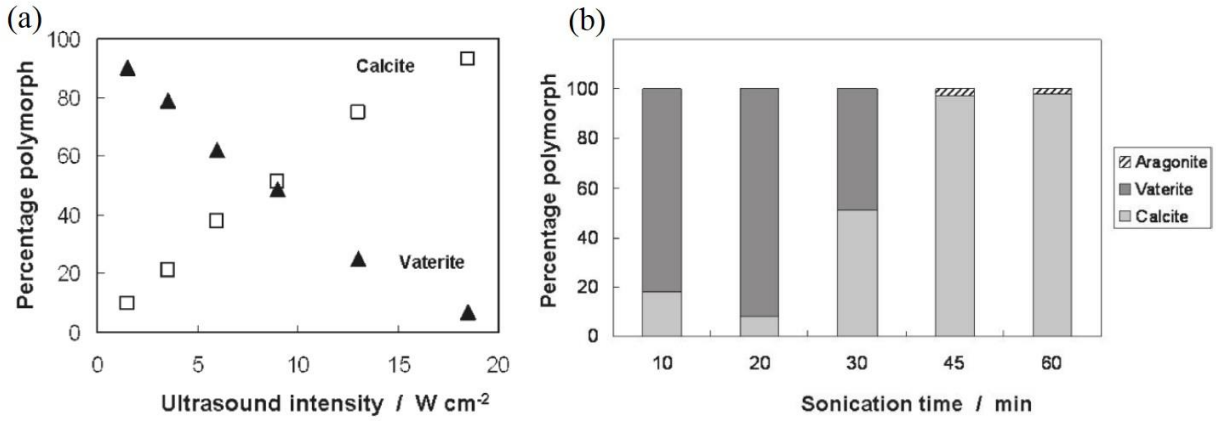

Figure 1.14 Variation of composition of $CaCO_3$ polymorphs under sonication (20 kHz): (a) the effect of intensity of ultrasound with 30 minutes of sonication, and (b) the effect of sonication time with 13 W/cm^2 of sonication.[55]

Conversely, sonocrystallization can sometimes produce a less thermodynamically stable polymorph. Paracetamol exists as either form I (stable) or form II (metastable), and given the difference in stability between the forms, form II has higher solubility.[56] When a supersaturated paracetamol solution was cooled without sonication, plate-like crystals (form I) were generated. However, with sonication, needle-like crystals (form II) were formed

(Figure 1.15). The generation of less stable forms from sonocrystallization has been reported; however, until now, no clear explanations were provided.[50, 56-60]

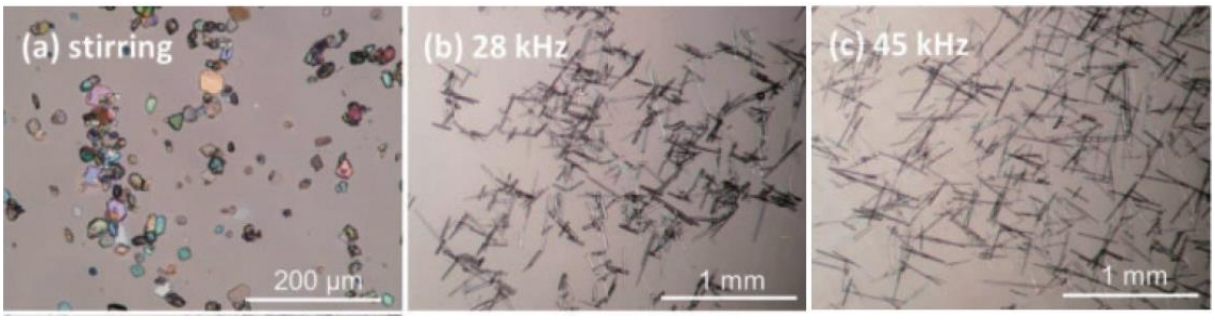

Figure 1.15 Optical microscopic images of paracetamol polymorphs: (a) form I produced by stirring (150 rpm), (b) form II generated via ultrasonic irradiation with 28 kHz, and (c) form II crystallized via ultrasonic irradiation with 45 kHz.[56]

1.5 Various parameters of sonocrystallization

1.5.1 Frequency of ultrasound

Changes in ultrasound frequencies affect the bubble dynamics.[61] At low ultrasonic frequencies, cavitation bubbles experience positive and negative pressure ultrasound waves for extended periods of time because wavelengths increase as frequencies decrease. Thus, the bubble oscillation amplitude is large since the size of the bubble differs substantially during compression and expansion periods.[62-63] Conversely, high ultrasonic frequencies shorten the wavelength of the ultrasound and the lifetime of the cavity is reduced. There are many cavitation bubbles and the power of collapse from each bubble is weak.[64-65] It is very difficult, however, to compare different frequencies due to changes in the number of cavitating bubbles, which is highly dependent on the specific apparatus used.

Koda *et al.* produced liposomes under ultrasonic irradiation and assessed the effects of

irradiation frequency on their size. Three different frequencies (43, 143 and 480 kHz) were applied at a fixed intensity (8 W/cm^2). It was observed that the size of the liposomes decreased as the sonic frequency decreased, due to changes in bubble dynamics (Figure 1.16).[66]

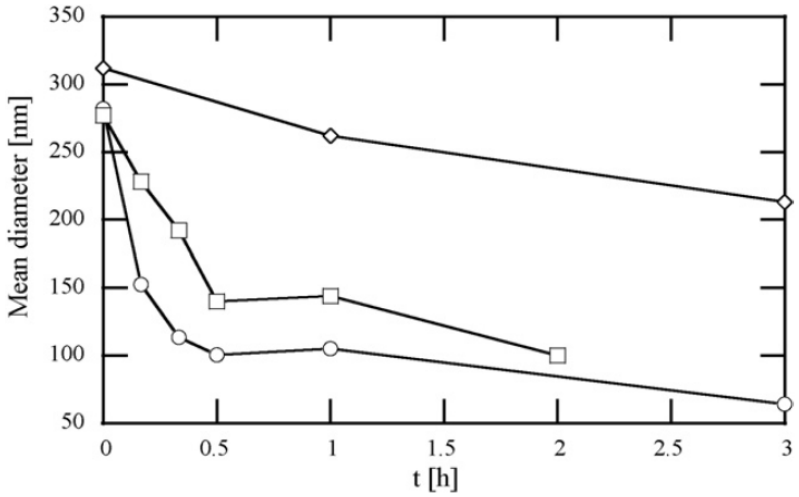

Figure 1.16 The effect of frequency of ultrasound on crystal size of liposome. The ultrasonic power was 8 W/cm^2, and the frequencies were 43 kHz (○), 133 kHz (□), and 480 kHz (◊), respectively.[66]

Another study investigated the effects of the frequency of ultrasound waves on MZW.[67] Cooling crystallization of paracetamol was tested without or with ultrasonic irradiation at multiple frequencies (from 41 to 1,140 kHz), and the MZW was calculated as the difference between the nucleation temperature and the saturation temperature. When the frequency of the ultrasound increased, the MZW decreased (Figure 1.17).

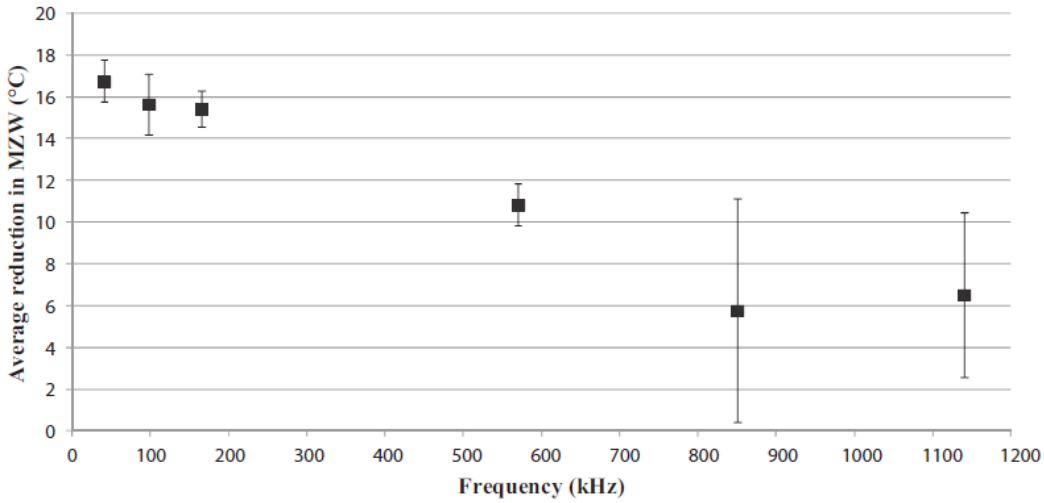

Figure 1.17 The effect of ultrasound frequency on reduction of MZW of paracetamol. The amount of reduced MZW is the difference of MZW of cooling crystallization of paracetamol without and with sonication (8 W/cm^2). The cooling crystallization and cooling sonocrystallization experiments were performed at least three times for each frequency. The dots are the average reduction of MZW and the error bars are the standard deviations.[67]

1.5.2 Intensity of ultrasound

When ultrasound intensities increase, the size of generated crystals decreases. Increased sonication intensities cause more vigorous microscale mixing and turbulence, which causes solutes to diffuse more rapidly.[68] Due to the accelerated diffusion of solute, induction time and MZW are reduced and the nucleation rate increases. Also, the vigorous microscale mixing and turbulence helps to prevent crystals from agglomerating.[69] The effect of ultrasound intensity was investigated during sonocrystallization of roxithromycin.[70] The intensity was adjusted from 5 to 15 W/cm^2, which caused the average crystal size to decrease (Figure 1.18).

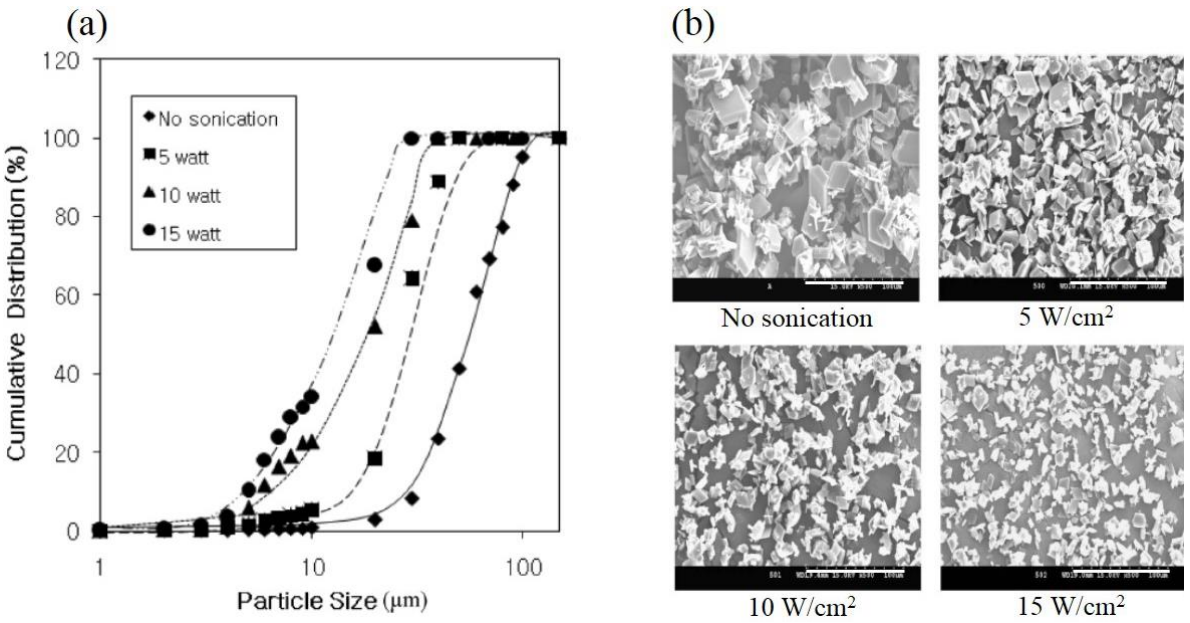

Figure 1.18 The effect of intensity of ultrasound on crystallization of roxithromycin: (a) cumulative crystal size distributions and (b) SEM images of roxithromycin with different sonication intensities. For all sonication experiments, the solution was sonicated at 22.5 kHz for 10 minutes. Scale bars are 100 μm.[70]

1.5.3 Sonication time

As sonication time increases, crystal sizes decrease and become more uniform. For short sonication time, solution and precipitants are not mixed uniformly.[62] The generated crystals from the solution are irregularly shaped and various sized. Thus, prolonged sonication time improves mixing and prevents crystals from aggregating.[71-72] Kougoulos *et al*. investigated the effects of sonication duration on crystal size using adipic acid and found a significant difference in crystal size according to whether sonication was applied or not (Figure 1.19).[73] Furthermore, crystal size was reduced as sonication duration increased. As we will see, this is often due to sonofragmentation of the crystals formed.

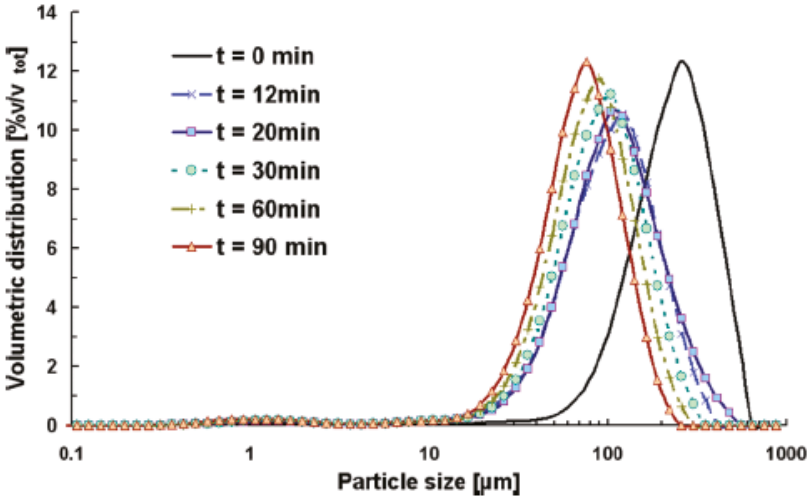

Figure 1.19 Effect of sonication time on partice size and size distribution of adipic acid. For sonication experiments, the adipic acid solution was sonicated at 20 kHz and 8.5 W/cm^2. For the control experiment, stirring was performed with a magnetic stirring bar (200 rpm).[73]

1.5.4 Types of ultrasound generator and configurations for sonocrystallization

Multiple types of ultrasonic generators exist and provide many different experimental configurations for sonocrystallization. Ultrasound generators are typically ultrasonic baths, horns and plate transducers (Figure 1.20).

Figure 1.20 Different types of ultrasound generators: (a) ultrasonic bath,[74] (b) ultrasonic horn,[75] and (c) ultrasonic plate transducer.[76]

Sonicating baths are standard laboratory equipment and are typically used to disperse particles

in liquid. Such sonicators are easily accessed, but are only available in batch configurations.[77-78] Ultrasonic horns are also used to perform sonocrystallization and offer batch or flowing configurations (Figure 1.21).[40, 68, 79-83]

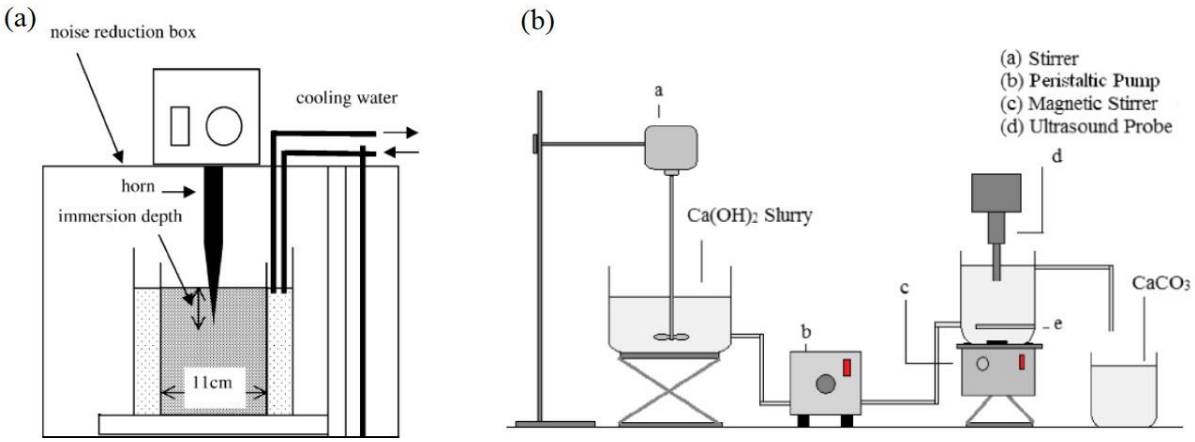

Figure 1.21 Configurations of sonocrystallization with an ultrasonic horn: (a) batch crystallization[68] and (b) flow crystallization of calcium carbonate.[82]

For flowing configurations, it is necessary to use specialized crystallization cells and additional equipment, such as a peristaltic pump for circulation. However, flowing configurations produce crystals continuously if the solution is injected continuously. Another type of ultrasound generator is the plate transducer, which generates a wide range of ultrasound frequencies. It is essential for sonocrystallization when high frequencies (> 100 kHz) are required.[84] With the ultrasonic plate transducer, a batch configuration is used for crystallization.

1.6 Applications

1.6.1 Pharmaceutical agents

Sonocrystallization is used widely to produce pharmaceutical agents (PAs), since it can

control crystal sizes, distributions, and polymorphisms.[24, 27-29] Reductions in PA size increase the dissolution rate and solubility, especially for nanocrystals.[85-88] Also, control of polymorphisms decreases the probability of side effects.[89-90] For PAs, control of such properties (i.e., size and polymorphism) is important because they directly affect delivery to target organs and work to treat a disease. In fact, multiple PAs, including acetylsalicylic acid, paracetamol, phenacetin, carbamazepine, etc., have been generated via sonocrystallization to decrease size and size distributions, and/or to control polymorphism (Figure 1.22).[50, 56, 67, 69, 91-94]

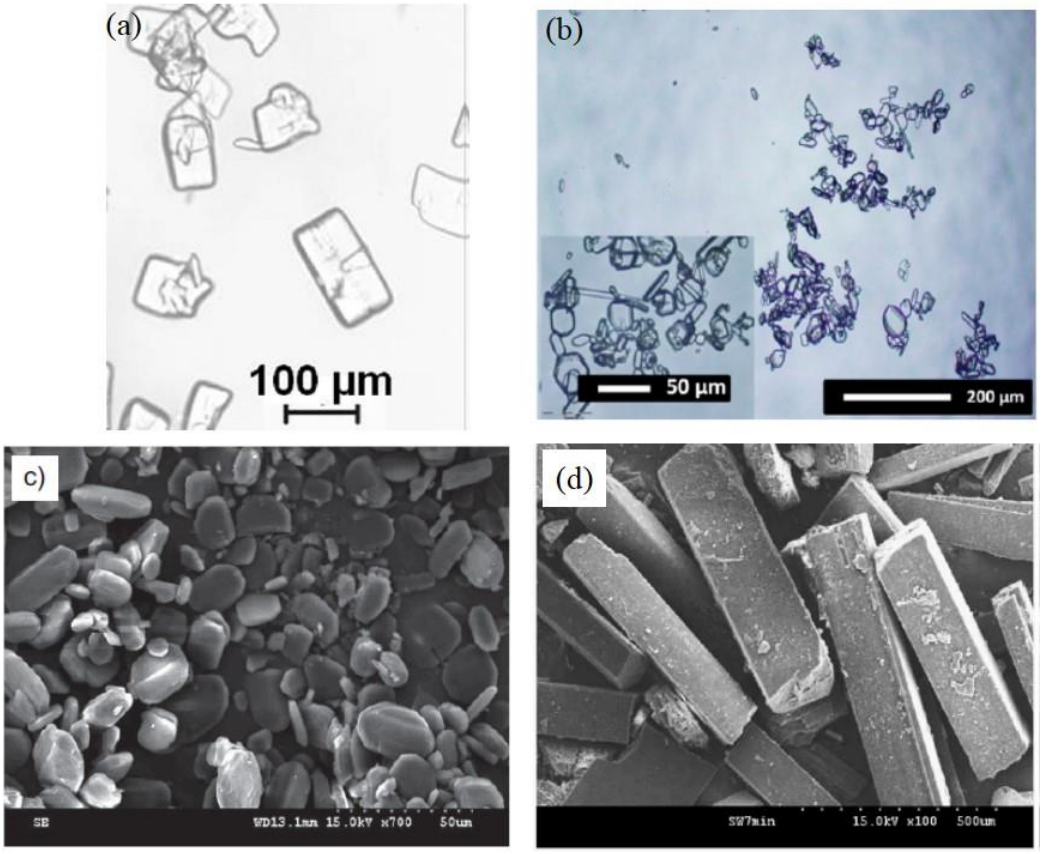

Figure 1.22 Microscopic images of APs generated by sonocrystallization. Optical microscopic images of (a) acetylsalicylic acid[91] and (b) paracetamol.[50] SEM images of (c) phenacetin[69] and (d) carbamazepine.[92]

1.6.2 Nanoparticles and nanostructures

Sonocrystallization is used to generate nanocrystals, since it is an effective method for producing small particles.[95-97] Qian *et al*. reported ultrasonic irradiation as a new method for generating zinc oxide nanocrystals.[98] The conventional method was time consuming, taking 2 days; however, sonication (20 kHz), generated nanocrystals in 3 minutes. Moreover, nanocrystals were formed, using ultrasonic irradiation without the addition of heptane, in 25 minutes (Figure 1.23).

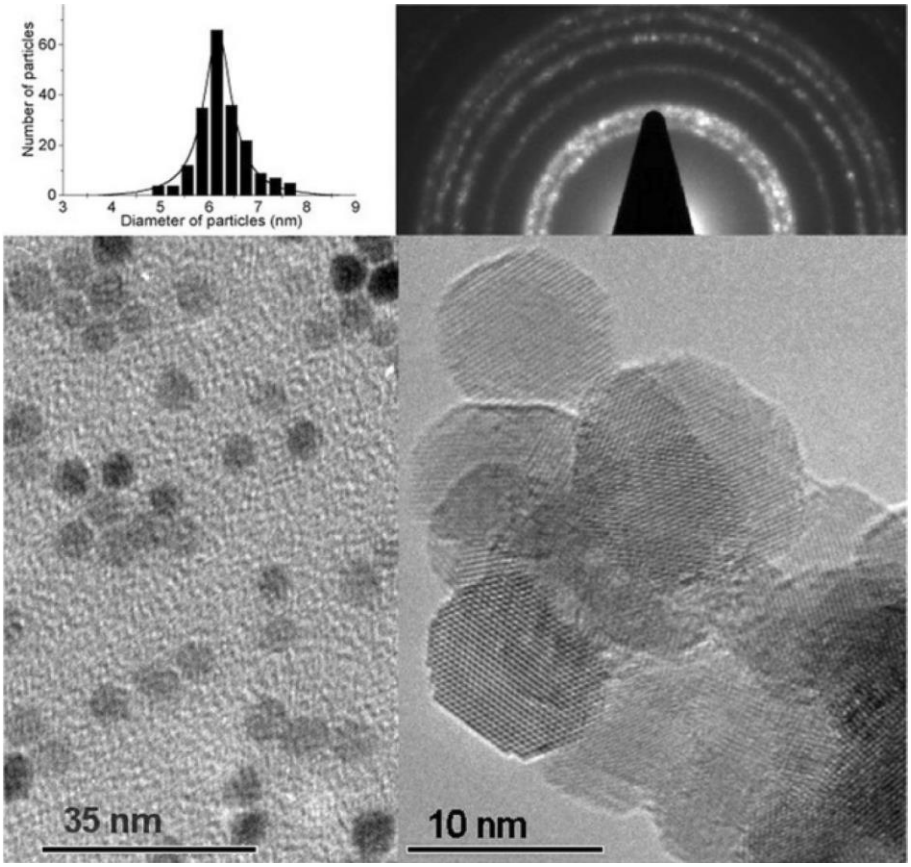

Figure 1.23 Characterizations of zinc oxide nanocrystals produced by sonocrystallization: particle size distribution, electron diffraction pattern and TEM images.[98]

It is possible to produce a variety of nanostructures via sonocrystallization. Li *et al.* produced nanofibers and fibrillar networks using ultrasonic irradiation.[99] *N*-lauroyl-L-glutamic acid di-*n*-butylamide (GP-1) were dissolved in octanol or propylene glycol at 120 ˚C and quenched to room temperature in an ultrasonic water bath (35 kHz, 1–4 W/cm^2) for 0–2 min. Using sonication, the product was a nanofiber network structure and without sonication, spherulitic particles were formed (Figure 1.24). The network structure exhibited an enhanced storage modulus and gelation capability compared to the spherulitic particles.

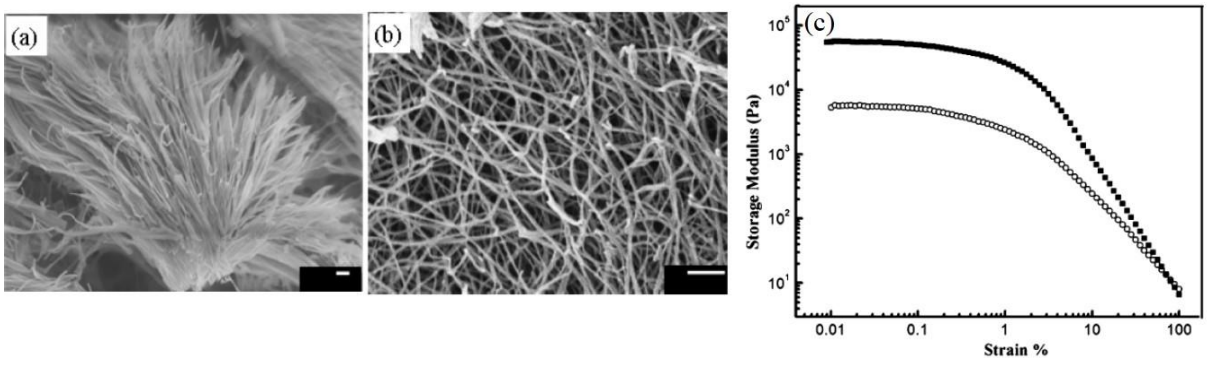

Figure 1.24 GP-1 nanostructures generated without sonication or with sonication: SEM imagers of GP-1 (a) spherulitic structures produce without sonication and (b) 3D interconnected fiber network structures with 1 minutes of sonication, and (c) storage modulus of the 2 wt % GP-1/PG gels formed without ultrasound (□) and with ultrasound (■), respectively. Scale bars are 500 nm.[99]

Hayward *et al.* reported on the generation of perylene diimide (PDI) nanowires using sonocrystallization. PDI and poly(3-hexylthiophene) were dissolved in 1,2-dicholorobenzene at 120 ˚C and cooled to 20 ˚C with or without sonication.[100] Notably, sonocrystallization produced narrower, straighter and less agglomerated PDI nanowires than the cooling crystallization without sonication (Figure 1.25 Left). The relatively good control of

sonocrystallized nanowire sizes allowed for the preparation of smooth films (Figure 1.25 Right).

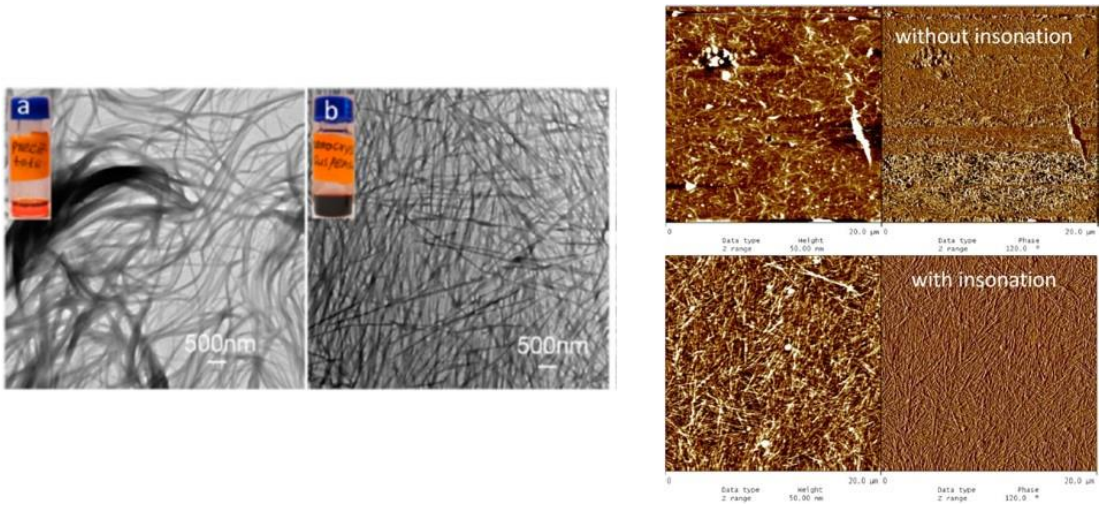

Figure 1.25 (Left) SEM images of PDI nanowire produce by (a) cooling crystallization without sonication and (b) sonocrystallization. For the sonocrystallization, the PDI solution was irradiated with 35 kHz of ultrasound for 2 hours. (Right) AFM images of PDI nanowire films.[100]

1.7 Sonofragmentation

In a liquid-solid mixture, acoustic cavitation causes various physical phenomena. If a bubble grows near a solid particle larger than the resonant size of the bubble, the bubble is deformed due to the asymmetric environment.[1, 6] This asymmetry causes the bubble to collapse asymmetrically, and a fast-moving stream of liquid (i.e., microjet) is formed.[13-14] The microjet moves toward the solid particles and causes surface deformation or changes in the chemical composition of the surface.[1, 15]

When solid particles in the mixture are smaller than the resonant size of the bubble, the

shockwave that is generated by acoustic cavitation causes interparticle collisions.[16-17, 101] Also, shockwaves interact directly with solid particles, causing sonofragmentation.[18, 102-103] Interparticle collisions and sonofragmentation affect the average particle size and size distribution, both by reducing the size of existing crystals and creating secondary nucleation sites.[104]

The effect of the shockwaves generated by acoustic cavitation in liquid-solid systems depends on the type of solid in the system. When slurries of metal powders were irradiated using ultrasound, interparticle collisions occurred.[16-17] The velocity of the colliding particles was sufficient to cause intense localized heating, plastic deformation, spot-welding and melting (Figure 1.26) of various low-melting point metals (e.g., Zn, Ni, Co, Mo). However, high-melting point metals (e.g., W) were not affected to the same extent.

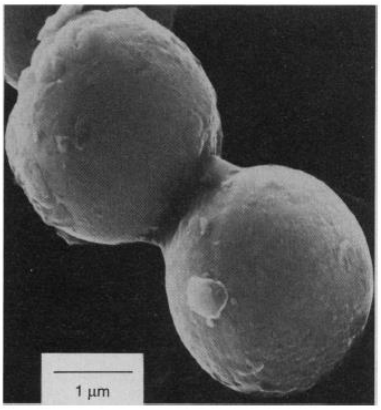

Figure 1.26 SEM image of zinc particles after sonication. 20 wt% of zinc slurry was sonicated by an ultrasonic horn (20 kHz and 50 W/cm^2) for 30 minutes. Localized melting was caused by high-velocity interparticle collisions and particles were agglomerated.[16]

Sonication of molecular crystals causes sonofragmentation by means of direct interactions between particles and shockwaves. Suslick *et al*. explored the sonication of an aspirin slurry

under multiple experimental conditions.[18] They suggested four possible mechanisms of particle breakage under sonication, including interparticle collision, particle–horn collision, particle–wall collision and direct interaction between particles and shockwaves (i.e. sonofragmentation). As shown in Figure 1.27, interparticle collisions rarely affect particle breakage. Additionally, particle–horn and particle–wall collisions were negligible contributors to fragmentation. Thus, the authors concluded that direct interactions between particles and shockwaves were the main causes of fragmentation.

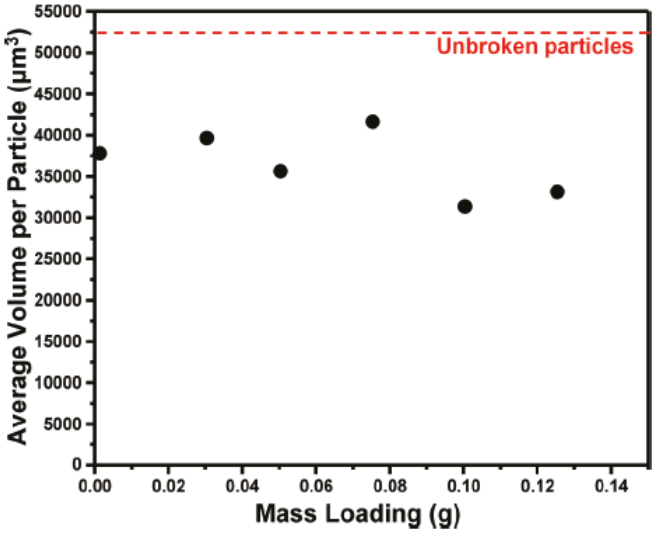

Figure 1.27 Effect of quantity of particle loading on final particle size after sonication for 10 seconds. Ultrasound was 20 kHz and 5.5 W/cm^2. All masses were dispersed in 5 ml of dodecane.[18]

1.8 Conclusion

Since the 1920s, when sonocrystallization was first discovered, there have been numerous studies on sonocrystallization investigating modification of control variables and test materials. Sonocrystallization has been developed for use in diverse industrial fields, including

pharmaceuticals. However, there are still open questions, such as a basic understanding of the mechanism of sonocrystallization and sonofragmentation.

1.9 References

1. Suslick, K. S., Sonochemistry. *Science* **1990,** *247* (4949), 1439-1445.

2. Leighton, T. G., *The acoustic bubble*. Academic Press: Cambridge, 1994.

3. Jones, S. F.; Evans, G. M.; Galvin, K. P., Bubble nucleation from gas cavities - a review. *Advances in Colloid and Interface Science* **1999,** *80* (1), 27-50.

4. Brennen, C. E., *Cavitation and bubble dynamics*. Cambridge University Press: Cambridge, 2014.

5. Suslick, K. S., Ultrasound - Its chemical, physical and biological effects. *Interdisciplinary Science Reviews* **1990,** *15* (2), 190-191.

6. Leong, T.; Ashokkumar, M.; Kentish, S., The fundamentals of power ultrasound - a review. *Acoustics Australia* **2011,** *39* (2), 54-63.

7. Suslick, K. S., The chemical effects of ultrasound. *Scientific American* **1989,** *260* (2), 80-86.

8. McNamara, W. B.; Didenko, Y. T.; Suslick, K. S., Sonoluminescence temperatures during multi-bubble cavitation. *Nature* **1999,** *401* (6755), 772-775.

9. McNamara, W. B.; Didenko, Y. T.; Suslick, K. S., Pressure during sonoluminescence. *Journal of Physical Chemistry B* **2003,** *107* (30), 7303-7306.

10. Flannigan, D. J.; Suslick, K. S., Plasma formation and temperature measurement during single-bubble cavitation. *Nature* **2005,** *434* (7029), 52-55.

11. Suslick, K. S.; Flannigan, D. J., Inside a collapsing bubble: sonoluminescence and the conditions during cavitation. *Annual Review of Physical Chemistry* **2008,** *59*, 659-683.

12. Pecha, R.; Gompf, B., Microimplosions: cavitation collapse and shock wave emission on a nanosecond time scale. *Physical Review Letters* **2000,** *84* (6), 1328-1330.

13. Lauterborn, W.; Vogel, A., Morden optical techniques in fluid mechanics. *Annual Review of Fluid Mechanics* **1984,** *16*, 223-244.

14. Blake, J. R.; Keen, G. S.; Tong, R. P.; Wilson, M., Acoustic cavitation: the fluid dynamics of non-spherical bubbles. *Philosophical Transactions of the Royal Society a-Mathematical Physical and Engineering Sciences* **1999,** *357* (1751), 251-267.

15. Suslick, K. S., Application of ultrasound to materials chemistry. *MRS Bulletin* **1995,** *20* (4), 29-34.

16. Doktycz, S. J.; Suslick, K. S., Interparticle collisions driven by ultrasound. *Science* **1990,** *247* (4946), 1067-1069.

17. Prozorov, T.; Prozorov, R.; Suslick, K. S., High velocity interparticle collisions driven by ultrasound. *Journal of the American Chemical Society* **2004,** *126* (43), 13890-13891.

18. Zeiger, B. W.; Suslick, K. S., Sonofragmentation of molecular crystals. *Journal of the American Chemical Society* **2011,** *133* (37), 14530-14533.

19. Richards, W. T.; Loomis, A. L., The chemical effects of high frequency sound waves I. A preliminary survey. *Journal of the American Chemical Society* **1927,** *49*, 3086-3100.

20. Kapustin, A., *The effects of ultrasound on the kinetics of crystallization*. Springer Science & Business Media: Berlin, 2012.

21. Polotski.Ig; Ovsiyenk.Dy; Khodov, Z. L.; Sosnina, Y. G.; Baselyuk, G. Y.; Kushnir, V. K., Effect of an ultrasound on perfection of melt-grown aluminium single crystals. *Physics of Metals and Metallography* **1966,** *21* (5), 81.

22. Belyaev, V. K.; Reshetny, II, Effect of ultrasound on growth and dissolution of single crystals in a drop of solution. *Soviet Physics Acoustics-Ussr* **1967,** *12* (3), 312.

23. Vasilev, B. P.; Vinograd.Kn, Amplification of high-intensity ultrasound in cadmium sulfide single crystals. *Soviet Physics Solid State,Ussr* **1967,** *9* (5), 1052.

24. de Castro, M. D. L.; Priego-Capote, F., Ultrasound-assisted crystallization (sonocrystallization). *Ultrasonics Sonochemistry* **2007,** *14* (6), 717-724.

25. Sander, J. R. G.; Zeiger, B. W.; Suslick, K. S., Sonocrystallization and sonofragmentation. *Ultrasonics Sonochemistry* **2014,** *21* (6), 1908-1915.

26. Gajendragadkar, C. N.; Gogate, P. R., Intensified recovery of valuable products from whey by use of ultrasound in processing steps - A review. *Ultrasonics Sonochemistry* **2016,** *32*, 102-118.

27. Cains, P. W.; Martin, P. D.; Price, C. J., The use of ultrasound in industrial chemical synthesis and crystallization. 1. Applications to synthetic chemistry. *Organic Process Research & Development* **1998,** *2* (1), 34-48.

28. Ruecroft, G.; Hipkiss, D.; Ly, T.; Maxted, N.; Cains, P. W., Sonocrystallization: the use of ultrasound for improved industrial crystallization. *Organic Process Research & Development* **2005,** *9* (6), 923-932.

29. Castillo-Peinado, L. D.; de Castro, M. D. L., The role of ultrasound in pharmaceutical production: sonocrystallization. *Journal of Pharmacy and Pharmacology* **2016,** *68* (10), 1249-1267.

30. Beckmann, W., *Crystallization: basic concepts and industrial applications*. John Wiley & Sons: New York, 2013.

31. Mullin, J. W., *Crystallization*. Butterworth-Heinemann: Oxford, 2001.

32. Guo, Z.; Zhang, M.; Li, H.; Wang, J.; Kougoulos, E., Effect of ultrasound on anti-solvent crystallization process. *Journal of Crystal Growth* **2005,** *273* (3-4), 555-563.

33. Guo, Z.; Jones, A. G.; Li, N., The effect of ultrasound on the homogeneous nucleation

of BaSO4 during reactive crystallization. *Chemical Engineering Science* **2006,** *61* (5), 1617-1626.

34. Zhang, Z.; Sun, D. W.; Zhu, Z. W.; Cheng, L. N., Enhancement of crystallization processes by power ultrasound: current state-of-the-art and research advances. *Comprehensive Reviews in Food Science and Food Safety* **2015,** *14* (4), 303-316.

35. Parvizian, F.; Rahimi, M.; Faryadi, M., Macro- and micromixing in a novel sonochemical reactor using high frequency ultrasound. *Chemical Engineering and Processing* **2011,** *50* (8), 732-740.

36. Jordens, J.; Bamps, B.; Gielen, B.; Braeken, L.; Van Gerven, T., The effects of ultrasound on micromixing. *Ultrasonics Sonochemistry* **2016,** *32*, 68-78.

37. Monnier, H.; Wilhelm, A. M.; Delmas, H., The influence of ultrasound on micromixing in a semi-batch reactor. *Chemical Engineering Science* **1999,** *54* (13-14), 2953-2961.

38. Monnier, H.; Wilhelm, A. M.; Delmas, H., Effects of ultrasound on micromixing in flow cell. *Chemical Engineering Science* **2000,** *55* (19), 4009-4020.

39. Gracin, S.; Uusi-Penttila, M.; Rasmuson, A. C., Influence of ultrasound on the nucleation of polymorphs of p-aminobenzoic acid. *Crystal Growth & Design* **2005,** *5* (5), 1787-1794.

40. Ramisetty, K. A.; Pandit, A. B.; Gogate, P. R., Ultrasound-assisted antisolvent crystallization of benzoic acid: effect of process variables supported by theoretical simulations. *Industrial & Engineering Chemistry Research* **2013,** *52* (49), 17573-17582.

41. Vekilov, P. G., Nucleation. *Crystal Growth & Design* **2010,** *10* (12), 5007-5019.

42. Guo, Z.; Jones, A. G.; Li, N.; Germana, S., High-speed observation of the effects of ultrasound on liquid mixing and agglomerated crystal breakage processes. *Powder Technology*

2007, *171* (3), 146-153.

43. Raman, V.; Abbas, A., Experimental investigations on ultrasound mediated particle breakage. *Ultrasonics Sonochemistry* **2008,** *15* (1), 55-64.

44. Wagterveld, R. M.; Boels, L.; Mayer, M. J.; Witkamp, G. J., Visualization of acoustic cavitation effects on suspended calcite crystals. *Ultrasonics Sonochemistry* **2011,** *18* (1), 216-225.

45. Agrawal, S. G.; Paterson, A. H. J., Secondary nucleation: mechanisms and models. *Chemical Engineering Communications* **2015,** *202* (5), 698-706.

46. Chow, R.; Blindt, R.; Chivers, R.; Povey, M., The sonocrystallisation of ice in sucrose solutions: primary and secondary nucleation. *Ultrasonics* **2003,** *41* (8), 595-604.

47. Chow, R.; Blindt, R.; Kamp, A.; Grocutt, P.; Chivers, R., The microscopic visualisation of the sonocrystallisation of ice using a novel ultrasonic cold stage. *Ultrasonics Sonochemistry* **2004,** *11* (3-4), 245-250.

48. Chow, R.; Blindt, R.; Chivers, R.; Povey, M., A study on the primary and secondary nucleation of ice by power ultrasound. *Ultrasonics* **2005,** *43* (4), 227-230.

49. Iyer, S. R.; Gogate, P. R., Ultrasound assisted crystallization of mefenamic acid: Effect of operating parameters and comparison with conventional approach. *Ultrasonics Sonochemistry* **2017,** *34*, 896-903.

50. Bhangu, S. K.; Ashokkumar, M.; Lee, J., Ultrasound assisted crystallization of paracetamol: crystal size distribution and polymorph control. *Crystal Growth & Design* **2016,** *16* (4), 1934-1941.

51. Nangia, A., Conformational polymorphism in organic crystals. *Accounts of Chemical Research* **2008,** *41* (5), 595-604.

52. Louhi-Kultanen, M.; Karjalainen, M.; Rantanen, J.; Huhtanen, M.; Kallas, J.,

Crystallization of glycine with ultrasound. *International Journal of Pharmaceutics* **2006,** *320* (1-2), 23-29.

53. Kurotani, M.; Hirasawa, I., Polymorph control of sulfamerazine by ultrasonic irradiation. *Journal of Crystal Growth* **2008,** *310* (21), 4576-4580.

54. Hatakka, H.; Alatalo, H.; Louhi-Kultanen, M.; Lassila, I.; Haeggstrom, E., Closed-loop control of reactive crystallization part II: polymorphism control of L-glutamic acid by sonocrystallization and seeding. *Chemical Engineering & Technology* **2010,** *33* (5), 751-756.

55. Price, G. J.; Mahon, M. F.; Shannon, J.; Cooper, C., Composition of calcium carbonate polymorphs precipitated using ultrasound. *Crystal Growth & Design* **2011,** *11* (1), 39-44.

56. Mori, Y.; Maruyama, M.; Takahashi, Y.; Ikeda, K.; Fukukita, S.; Yoshikawa, H. Y.; Okada, S.; Adachi, H.; Sugiyama, S.; Takano, K.; Murakami, S.; Matsumura, H.; Inoue, T.; Yoshimura, M.; Mori, Y., Selective crystallization of metastable phase of acetaminophen by ultrasonic irradiation. *Applied Physics Express* **2015,** *8* (6).

57. Lee, Y. L.; Ristic, R. I.; DeMatos, L. L.; Martin, C. M., Crystallisation pathways of polymorphic triacylglycerols induced by mechanical energy. In *Xiv International Conference on Small-Angle Scattering*, Ungar, G., Ed. 2010; Vol. 247.

58. Tripathi, R.; Biradar, S. V.; Mishra, B.; Paradkar, A. R., Study of polymorphs of progesterone by novel melt sonocrystallization technique: a technical note. *Aaps Pharmscitech* **2010,** *11* (3), 1493-1498.

59. Sarkar, A.; Ragab, D.; Rohani, S., Polymorphism of progesterone: a new approach for the formation of form II and the relative stabilities of form I and form II. *Crystal Growth & Design* **2014,** *14* (9), 4574-4582.

60. Hermanto, M. W.; Yeoh, A.; Soh, B.; Chow, P. S.; Tan, R. B. H., Robust crystallization process development for the metastable delta-form of pyrazinamide. *Organic Process*

Research & Development **2015,** *19* (12), 1987-1996.

61. Nalajala, V. S.; Moholkar, V. S., Investigations in the physical mechanism of sonocrystallization. *Ultrasonics Sonochemistry* **2011,** *18* (1), 345-355.

62. Li, H.; Wang, J. K.; Bao, Y.; Guo, Z. C.; Zhang, M. Y., Rapid sonocrystallization in the salting-out process. *Journal of Crystal Growth* **2003,** *247* (1-2), 192-198.

63. Lee, J.; Ashokkumar, M.; Kentish, S. E., Influence of mixing and ultrasound frequency on antisolvent crystallisation of sodium chloride. *Ultrasonics Sonochemistry* **2014,** *21* (1), 60-68.

64. Ichitsubo, T.; Matsubara, E.; Kai, S.; Hirao, M., Ultrasound-induced crystallization around the glass transition temperature for Pd40Ni40P20 metallic glass. *Acta Materialia* **2004,** *52* (2), 423-429.

65. Nii, S.; Takayanagi, S., Growth and size control in anti-solvent crystallization of glycine with high frequency ultrasound. *Ultrasonics Sonochemistry* **2014,** *21* (3), 1182-1186.

66. Yamaguchi, T.; Nomura, M.; Matsuoka, T.; Koda, S., Effects of frequency and power of ultrasound on the size reduction of liposome. *Chemistry and Physics of Lipids* **2009,** *160* (1), 58-62.

67. Jordens, J.; Gielen, B.; Braeken, L.; Van Gerven, T., Determination of the effect of the ultrasonic frequency on the cooling crystallization of paracetamol. *Chemical Engineering and Processing* **2014,** *84*, 38-44.

68. Nishida, I., Precipitation of calcium carbonate by ultrasonic irradiation. *Ultrasonics Sonochemistry* **2004,** *11* (6), 423-428.

69. Su, C. S.; Liao, C. Y.; Jheng, W. D., Particle size control and crystal habit modification of phenacetin using ultrasonic crystallization. *Chemical Engineering & Technology* **2015,** *38* (1), 181-186.

70. Park, M. W.; Yeo, S. D., Antisolvent crystallization of roxithromycin and the effect of ultrasound. *Separation Science and Technology* **2010,** *45* (10), 1402-1410.

71. Li, J. Q.; Bao, Y.; Wang, J. K., Effects of sonocrystallization on the crystal size distribution of cloxacillin benzathine crystals. *Chemical Engineering & Technology* **2013,** *36* (8), 1341-1346.

72. Belkacem, N.; Salem, M. A. S.; AlKhatib, H. S., Effect of ultrasound on the physico-chemical properties of poorly soluble drugs: Antisolvent sonocrystallization of ketoprofen. *Powder Technology* **2015,** *285*, 16-24.

73. Narducci, O.; Jones, A. G.; Kougoulos, E., An assessment of the use of ultrasound in the particle engineering of micrometer-scale adipic acid crystals. *Crystal Growth & Design* **2011,** *11* (5), 1742-1749.

74. http://bandelin.com.

75. http://www.sonics.com.

76. http://www.weber-ultrasonics-america.com.

77. Crespo, R.; Martins, P. M.; Gales, L.; Rocha, F.; Damas, A. M., Potential use of ultrasound to promote protein crystallization. *Journal of Applied Crystallography* **2010,** *43*, 1419-1425.

78. Kiani, H.; Zhang, Z. H.; Delgado, A.; Sun, D. W., Ultrasound assisted nucleation of some liquid and solid model foods during freezing. *Food Research International* **2011,** *44* (9), 2915-2921.

79. Hatkar, U. N.; Gogate, P. R., Process intensification of anti-solvent crystallization of salicylic acid using ultrasonic irradiations. *Chemical Engineering and Processing* **2012,** *57-58*, 16-24.

80. Bhoi, S.; Sarkar, D., Modelling and experimental validation of ultrasound assisted

unseeded batch cooling crystallization of L-asparagine monohydrate. *Crystengcomm* **2016,** *18* (25), 4863-4874.

81. Jiang, M.; Papageorgiou, C. D.; Waetzig, J.; Hardy, A.; Langston, M.; Braatz, R. D., Indirect ultrasonication in continuous slug-flow crystallization. *Crystal Growth & Design* **2015,** *15* (5), 2486-2492.

82. Shirsath, S. R.; Sonawane, S. H.; Saini, D. R.; Pandit, A. B., Continuous precipitation of calcium carbonate using sonochemical reactor. *Ultrasonics Sonochemistry* **2015,** *24*, 132-139.

83. Jamshidi, R.; Rossi, D.; Saffari, N.; Gavriilidis, A.; Mazzei, L., Investigation of the effect of ultrasound parameters on continuous sonocrystallization in a millifluidic device. *Crystal Growth & Design* **2016,** *16* (8), 4607-4619.

84. Wohlgemuth, K.; Ruether, F.; Schembecker, G., Sonocrystallization and crystallization with gassing of adipic acid. *Chemical Engineering Science* **2010,** *65* (2), 1016-1027.

85. Buckton, G.; Beezer, A. E., The relationship between particle size and solubility. *International Journal of Pharmaceutics* **1992,** *82* (3), R7-R10.

86. Wu, W. J.; Nancollas, G. H., A new understanding of the relationship between solubility and particle size. *Journal of Solution Chemistry* **1998,** *27* (6), 521-531.

87. Kesisoglou, F.; Panmai, S.; Wu, Y. H., Nanosizing - oral formulation development and biopharmaceutical evaluation. *Advanced Drug Delivery Reviews* **2007,** *59* (7), 631-644.

88. O'Mahony, M.; Leung, A. K.; Ferguson, S.; Trout, B. L.; Myerson, A. S., A process for the formation of nanocrystals of active pharmaceutical ingredients with poor aqueous solubility in a nanoporous substrate. *Organic Process Research & Development* **2015,** *19* (9), 1109-1118.

89. Lu, J.; Rohani, S., Polymorphism and crystallization of active pharmaceutical ingredients (APIs). *Current Medicinal Chemistry* **2009,** *16* (7), 884-905.

90. Beckmann, W., Crystallization of pharmaceutical compounds polymorphs, pseudo-polymorphs and particle formation. *Engineering in Life Sciences* **2003,** *3* (3), 113-120.

91. Eder, R. J. P.; Schrank, S.; Besenhard, M. O.; Roblegg, E.; Gruber-Woelfler, H.; Khinast, J. G., Continuous sonocrystallization of acetylsalicylic acid (ASA): control of crystal size. *Crystal Growth & Design* **2012,** *12* (10), 4733-4738.

92. Park, M. W.; Yeo, S. D., Antisolvent crystallization of carbamazepine from organic solutions. *Chemical Engineering Research & Design* **2012,** *90* (12), 2202-2208.

93. Bucar, D. K.; Elliott, J. A.; Eddleston, M. D.; Cockcroft, J. K.; Jones, W., Sonocrystallization yields monoclinic paracetamol with significantly improved compaction behavior. *Angewandte Chemie-International Edition* **2015,** *54* (1), 249-253.

94. Thorat, A. A.; Dalvi, S. V., Solid-state phase transformations and storage stability of curcumin polymorphs. *Crystal Growth & Design* **2015,** *15* (4), 1757-1770.

95. Xu, M.; Lu, Y. N.; Liu, Y. F.; Shi, S. Z.; Qian, T. S.; Lu, D. Y., Sonochemical synthesis of monosized spherical BaTiO3 particles. *Powder Technology* **2006,** *161* (3), 185-189.

96. Dang, F.; Kato, K.; Imai, H.; Wada, S.; Haneda, H.; Kuwabara, M., Growth of BaTiO3 nanoparticles in ethanol-water mixture solvent under an ultrasound-assisted synthesis. *Chemical Engineering Journal* **2011,** *170* (1), 333-337.

97. Schoenitz, M.; Joseph, S.; Bunjes, H.; Scholl, S., Application of ultrasound in a micro heat exchanger for crystallization of solid lipid nanoparticles. *Chemical Engineering & Technology* **2013,** *36* (6), 1075-1079.

98. Qian, D.; Jiang, J. Z.; Hansen, P. L., Preparation of ZnO nanocrystals via ultrasonic irradiation. *Chemical Communications* **2003,** (9), 1078-1079.

99. Wang, R. Y.; Liu, X. Y.; Li, J. L., Engineering molecular self-assembled fibrillar networks by ultrasound. *Crystal Growth & Design* **2009,** *9* (7), 3286-3291.

100. Bu, L. J.; Dawson, T. J.; Hayward, R. C., Tailoring ultrasound-induced growth of perylene diimide nanowire crystals from solution by modification with poly(3-hexyl thiophene). *Acs Nano* **2015,** *9* (2), 1878-1885.

101. Suslick, K. S.; Casadonte, D. J.; Doktycz, S. J., The effects of ultrasound on nickel and copper powders. *Solid State Ionics* **1989,** *32-3*, 444-452.

102. Gopi, K. R.; Nagarajan, R., Advances in nanoalumina ceramic particle fabrication using sonofragmentation. *Ieee Transactions on Nanotechnology* **2008,** *7* (5), 532-537.

103. Jordens, J.; Appermont, T.; Gielen, B.; Van Gerven, T.; Braeken, L., Sonofragmentation: effect of ultrasound frequency and power on particle breakage. *Crystal Growth & Design* **2016,** *16* (11), 6167-6177.

104. Myerson, A. S., *Handbook of industrial crystallization*. Butterworth-Heinemann: Oxford, 2002.

Chapter 2

Sonofragmentation of ionic crystals

2.1 Introduction

Mechanochemical effects change solid particles physically and chemically under mechanical action.[1-4] This includes both chemical effects when surfaces of materials are rubbed or when solids are broken.[5-7] There are many ways of inducing mechanochemistry in materials, including trituration, grinding, milling and ultrasound.[8-10] When mechanical actions are applied to solids, fracture can occur, but our fundamental understanding of the nature of the breakage of solids as a function of their chemical and mechanical properties remains limited. The fragmentation of powders in liquid slurries, especially, has received relatively little attention.[11-12] In this chapter, it was examined fundamental experiments on the fragmentation of ionic crystals during sonication of slurries and gained new insights on the mechanism of such sonofragmentation.

When a liquid is irradiated with high intensity ultrasound, acoustic cavitation occurs: i.e., bubbles form, oscillate, grow, and, under certain conditions, implosively collapse; this collapse can generate intense local heating, with hot spots created transiently with temperatures of <5000 K, pressures of Kbar, and shockwaves launched into the liquid.[13-16] If a bubble collapses near an extended solid surface (i.e., several times the size of the bubble), the collapse becomes asymmetric and a fast-moving stream of liquid (i.e., microjet) impinges on the solid surface.[17-19] In contrast, microjets do not form in slurries with fine powders (e.g., particles less than the bubble diameter), but cavitation still occurs, and shockwaves are formed.

The effect of ultrasound on liquid–solid systems depends on the type of materials sonicated. For example, when slurries of malleable powders (e.g., softer metals) were irradiated with ultrasound, interparticle collisions caused surface deformation, agglomeration, and a change in the chemical composition of the particle surface.[20-25] In contrast, sonication of slurries of brittle materials (specifically, molecular crystals) caused fragmentation of the crystals through direct interactions between crystals and shockwaves,[26] which is a major component of sonocrystallization of active pharmaceutical ingredients (APIs).[27-29] While previous studies have examined the effects of control variables (e.g., acoustic power density, frequency, liquid, etc.) on particle fragmentation,[30-34] there is only one report that examines the influence of the material properties of solids on their fragmentation under ultrasonic irradiation, and that is limited to polymeric solids.[35]

For ionic and molecular crystals (particularly for APIs), there are a few articles that examine the relationship between the mechanical properties of the particles and their breakage under dry milling or particle impaction.[36-38] Hardness and elasticity are two of the most relevant material properties related to fragmentation. There are several ways to measure the hardness of a material, but the Vickers test is the most common.[39] The Vickers hardness (H_v) of a material is defined by the degree of deformation of the surface by a diamond indenter at a given applied force. The Vickers hardness of alkali halides has been measured systematically.[40-43] The elasticity of materials is quantified by Young's modulus (E): stress (force per unit area) vs. strain (proportional deformation). For the alkali halides, Young's modulus has also been measured.[44]

In this study, six different alkali halides, having different Vickers hardness and Young's modulus values, were used to investigate the sonofragmentation patterns of ionic crystals. Various parameters, including the crystal size and control variables, were studied to determine

their effect on the fragmentation of alkali halides particles. In addition, the mechanism of sonofragmentation of ionic crystals was examined.

2.2 Experimental

2.2.1 Materials

Lithium chloride, sodium chloride, sodium bromide, potassium chloride and potassium bromide were purchased from Fisher Scientific and used as-received, unless otherwise indicated. Sodium fluoride (Sigma-Aldrich) was recrystallized in nanopure water (i.e., water deionized to >18 MΩ·cm resistance, scrubbed for organics, and passed through a 0.45 μm filter with a Barnstead NANOpure® ultrapure water purification system). Dodecane, decane, octane, heptane, and tetradecane were purchased from Sigma-Aldrich and used as-received. Silicone oils were Dow Corning 200 fluid® 100 and 350 cSt.

2.2.2 Sonofragmentation experimental setup

10 ml of dodecane was added to 15 mg of alkali halide. The slurry was allowed to thermally equilibrate at 18 °C for 5 minutes in a temperature-controlled water bath (Isotemp 1006S). This mixture was sonicated with an exponential ultrasonic horn (Sonics and Materials VCX-750, 20 kHz, 1 cm^2 Titanium tip, 10 W/cm^2) for different times. At 20 kHz, the maximum diameter of a cavitating bubble before collapse is ~ 150 μm.[45] All sonication experiments were performed using a duty cycle of 2 sec on and 8 sec off pulse cycle to reduce temperature variation. For all cases, steady state temperatures during sonication were 25 °C. Sonication times are reported as the total time exposed to ultrasound.

2.2.3 Sample preparation of four groups of sodium bromide having different crystal size

In order to check the effect of initial crystal size, a sonic sifter (Advantech Manufacturing, Berlin, WI) was used with various sieves (mesh opening sizes 53, 106, 250 and 500 μm) to separate batches of sodium bromide based on their size. The sonic sifter was used for 5 minutes. Crystals that were not sieved by the sifter were removed from the sieve. The sieved crystals were collected and sieved again with same intensity and time. This process was done total 4 times for each group of sodium bromide.

2.2.4 Effect of vapor pressure

To study of the effect of vapor pressure, 15 mg of potassium chloride was used in 10 mL of various unreactive organic liquids. All other experimental conditions were same as fragmentation experiments of various alkali halides that are described above. Heptane, octane, decane, and tetradecane were used as the slurry liquids. Each slurry was sonicated for 140 seconds.

2.2.5 Effect of viscosity

Dodecane and Dow Corning 200 Fluid (100 cSt) were mixed and viscosities of the mixtures were measured by Cannon-Fenske routine viscometer (Cannon Instrument Company, size 100, 150, 200 and 300) at 25 °C in a temperature-controlled water bath (Isotemp 1006S). The 160 cSt liquid was made from a mixture of Dow Corning 200 Fluid (100 cSt) with Dow Corning 200 Fluid (350 cSt). 15 mg of KCl was added to each of seven mixtures with viscosities ranging from 0.1 to 160 cSt, and sonicated for 140 seconds. All other experimental conditions were same as sonofragmentation experiments of various alkali halides described above.

2.2.6 Mechanism studies: interparticle collisions, particle–wall decoupling and particle–horn decoupling

Particle loading experiments were explored with various amounts of potassium chloride (from 5 to 760 mg) added to 10 mL dodecane. Sonication time was 140 seconds and the steady state temperature during sonication was 25 °C.

Particle–wall decoupling experiments were performed with a latex membrane (Trojan™ non-lubricated condom) under ultrasonic power ranging from 5 to 40 W/cm^2. The latex membrane contained a slurry of 15 mg of potassium chloride and 10 ml of dodecane, and the reactor contained 10 ml of dodecane (Figure 2.9b); the control comparison used 30 mg potassium chloride in 20 mL of dodecane (Figure 2.9a). Sonication time was 140 seconds and the steady state temperature during sonication was 25 °C.

Particle–horn decoupling experiments were investigated in an opposite way of the crystal-wall decoupling experiments. The latex membrane contained 10 ml of dodecane, and the reactor contained 15 mg of potassium chloride and 10 ml of dodecane (Figure 2.9c); the control comparison used 30 mg potassium chloride in 20 mL of dodecane (Figure 2.9a). Potassium chloride slurries were sonicated for 140 seconds with ultrasonic power ranging from 5 to 40 W/cm^2. The steady state temperature during sonication was 25 °C.

2.2.7 Characterization

An aliquot of sonicated slurry was removed using a disposable pipette for analysis by optical microscopy (Zeiss Axioskop optical/fluorescence microscope). The micrographs were captures using a Cannon PC1015 digital camera mounted to the microscope. Crystal size analysis with optical microscopic images was performed using Image-J software (National Institutes of Health, Bethesda, MD, USA). Approximately 200 particles were measured for

each experiment. Data fitting was performed using OriginPro 8.5 software (OriginLab, Northampton, MA, USA).

2.3 Results and discussion

2.3.1 Sonofragmentation of ionic crystals

Alkali halides were fragmented under ultrasonic irradiation (Figure 2.1) and their rates of fragmentation shown in Figure 2.2. The particle size decreases exponentially with length of time of sonication.

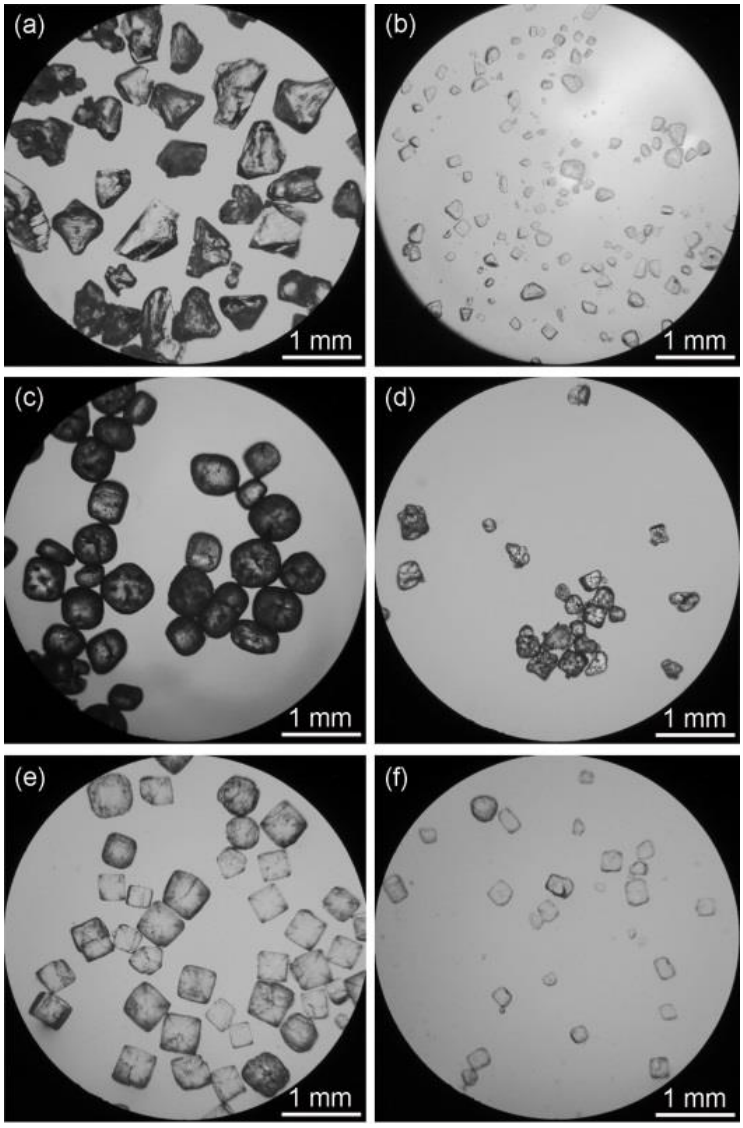

Figure 2.1 (cont.)

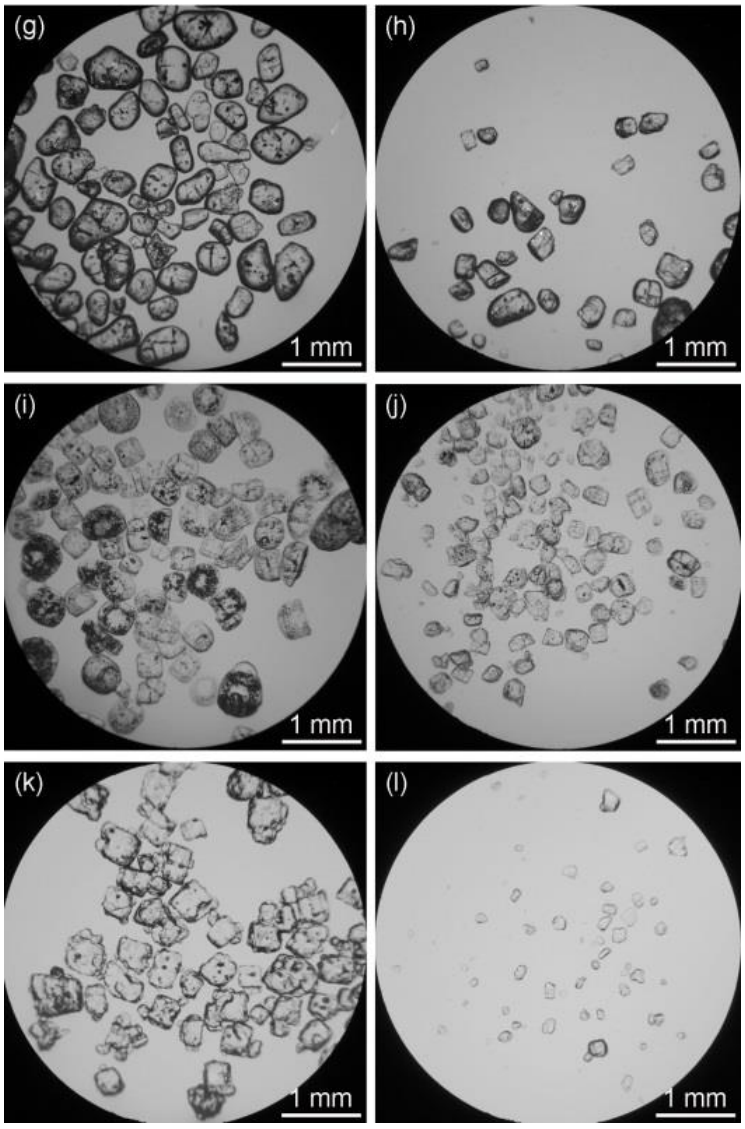

Figure 2.1 Optical micrographs of alkali halides before and after sonication. (a) Sodium fluoride before sonication and (b) after sonication 900 seconds, (c) Lithium chloride before sonication and (d) after sonication for 360 seconds, (e) Sodium chloride before sonication and (f) after sonication 310 seconds, (g) sodium bromide before sonication and (h) after sonication for 140 seconds, (i) potassium chloride before sonication and (j) after sonication for 140 seconds, (k) potassium bromide before sonication and (l) after sonication for 90 seconds. Each slurry contained 0.2 wt% of alkali halide in dodecane and was sonicated by using a titanium horn (10 W/cm^2 and 20 kHz).

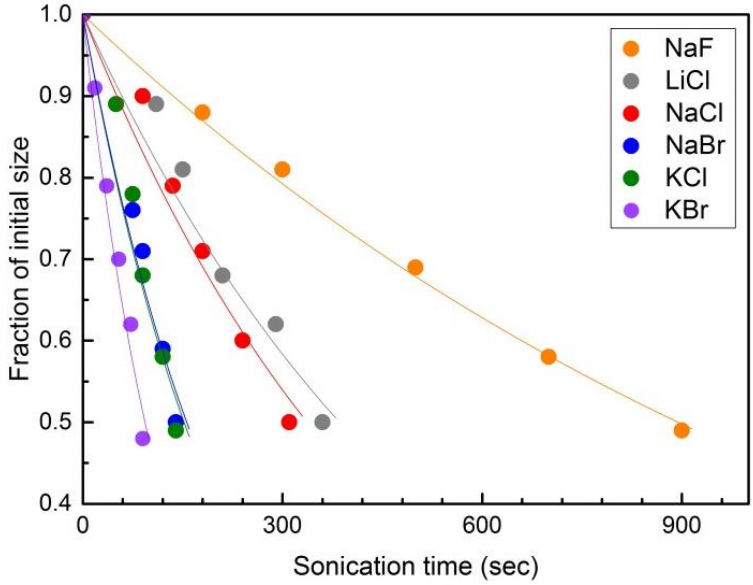

Figure 2.2 Fraction of initial crystal size versus sonication time for various alkali halides. Slurries containing 0.2 wt% of the alkali halides in dodecane were sonicated using a titanium horn (10 W/cm^2 and 20 kHz). Solid lines are exponential fits to the data. Standard deviation of each data point is less than 4 % of its average value.

The strength of ionic bonding in the alkali halide crystals increases, of course, for composed of smaller cations and anions, e.g., NaF is harder than KBr. Among the alkali halides, increased Vickers hardness and Young's modulus values requires longer sonication times to reach half the initial crystal size (Table 2.1). When the sonication time is normalized by Vickers hardness or Young's modulus, all values for fraction of initial size are distributed near a master line (Figure 2.3). That is, the rate of fragmentation monotonically decreases with increasing Vickers hardness or Young's modulus. The quantitative relationship between hardness or elasticity and rate of fragmentation is clear (Figure 2.3), but its origins are complicated especially by the critical factor of defect concentration, which will affect the mechanical strength and other properties of the materials.[46-47]

Table 2.1 Vickers hardness (H_v), Young's modulus (E), and sonication time necessary to halve the initial crystal size ($\tau_{1/2}$) of alkali halides.*

Alkali halide	H_v (GPa)	E (GPa)	$\tau_{1/2}$ (sec)	Initial crystal size (μm)
NaF	0.626	77.5	900	500
LiCl	0.243	49.8	360	580
NaCl	0.216	37.3	310	340
NaBr	0.129	29.7	140	490
KCl	0.128	26.5	140	420
KBr	0.098	22.3	90	310

*Determinations of H_v[40, 43], E[44] and $\tau_{1/2}$ were made on single crystals of the alkali halides. RSD of the initial crystal sizes were ~14%.

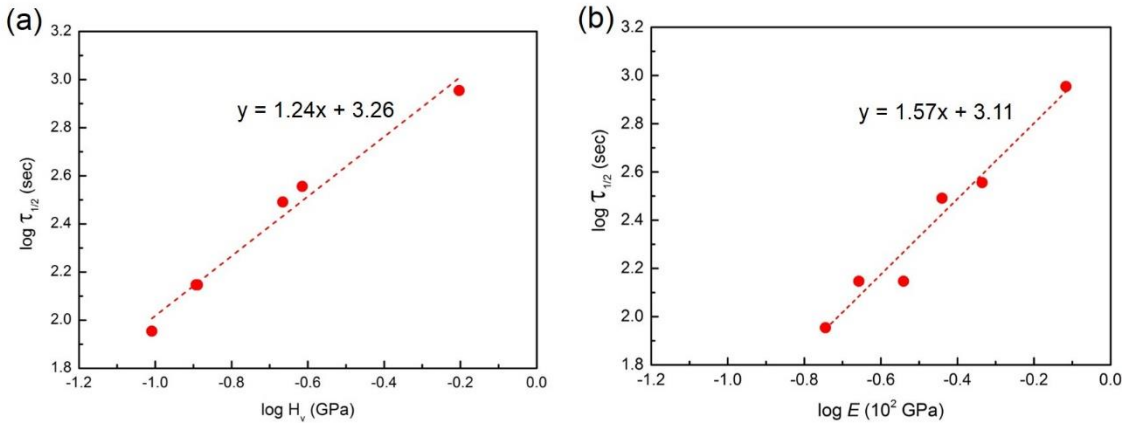

Figure 2.3 Relationship between rate of sonofragmentation and either Vickers hardness or Young's modulus. (a) log Vickers hardness (H_v) vs. log time necessary to halve the initial crystal size ($\tau_{1/2}$); and (b) log Young's modulus (E) vs. log time necessary to halve the initial crystal size ($\tau_{1/2}$). Linear fitting was applied. Standard deviation of each data point is less than 4 % of its average value.

2.3.2 Effect of initial crystal size

For these studies, it was important to establish any consequences of variation in the initial crystal size on sonofragmentation. Sodium bromide was chosen as a test sample and examined at initial crystal sizes ranging from 510 µm down to 150 µm (Figure 2.4), isolated by sieving using a sonic sifter (Advantech Manufacturing, Berlin, WI). As shown in Figure 2.5, initial crystal size had no effect on the rates of fragmentation of alkali halides over the range examined.

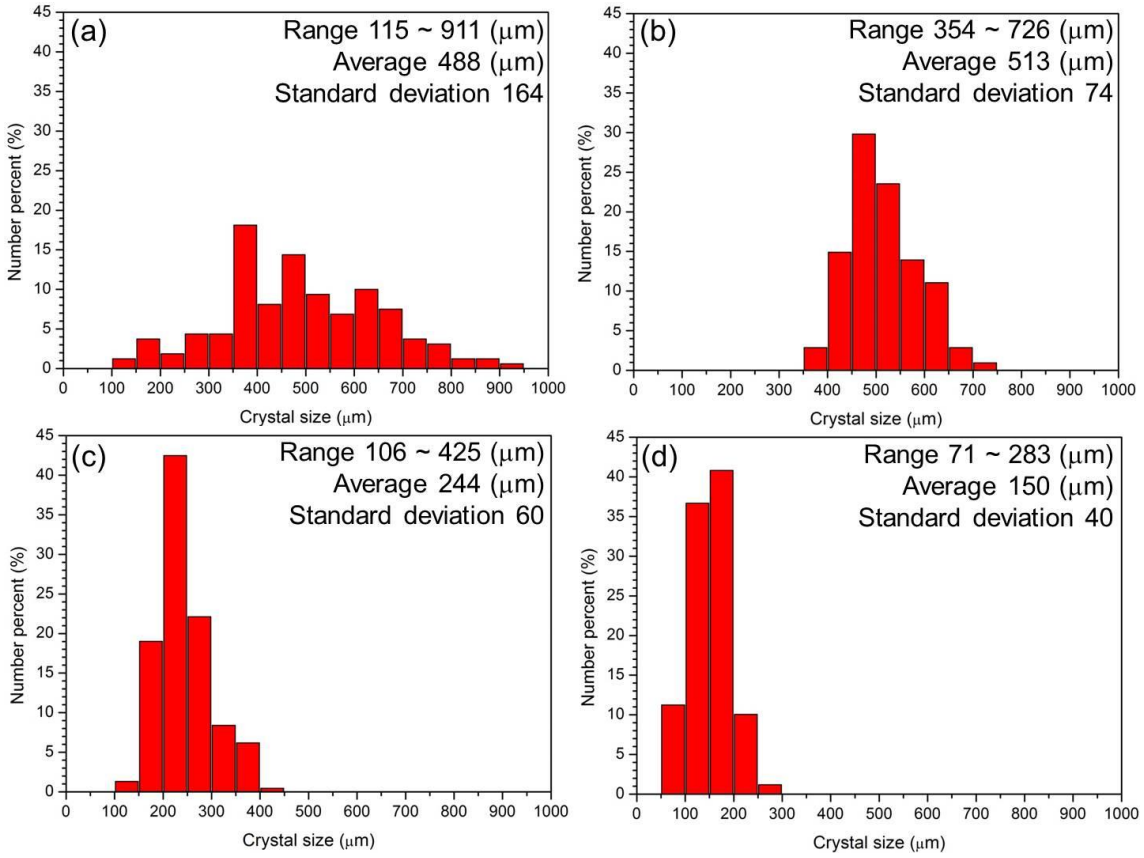

Figure 2.4 Crystal size distributions of sodium bromide (a) without sieving, (b) sieved by sonic sifter (Advantech Manufacturing, Berlin, WI), mesh openings 500 and 250 µm, (c) sieved by sonic sifter, mesh openings 250 and 106 µm, and (d) sieved by sonic sifter, mesh openings 106 and 53 µm).

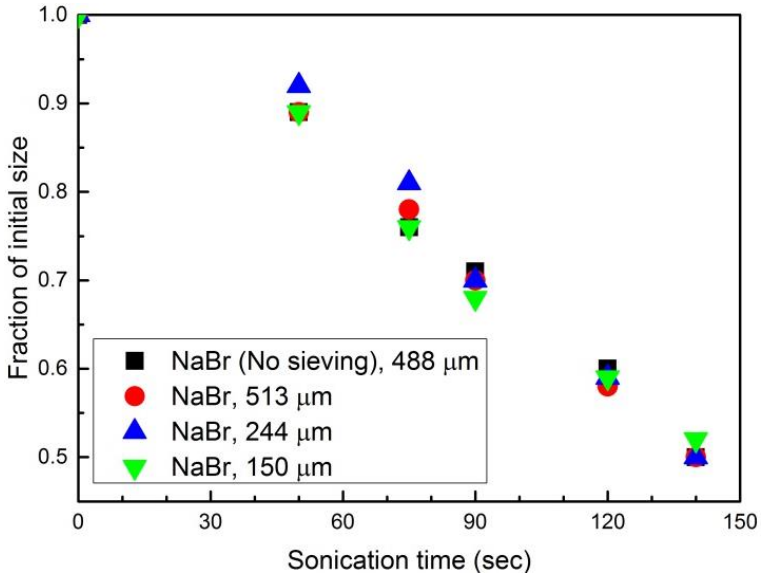

Figure 2.5 Effect of initial crystal size on fragmentation of sodium bromide. A slurry containing 0.2 wt% sodium bromide in 10 mL dodecane was sonicated using a titanium horn (10 W/cm^2 and 20 kHz). The average particle sizes for each group are given in the key. Standard deviation of each data point is less than 6 % of its average value.

2.3.3 Effect of liquid vapor pressure

We also studied various control variables to determine their effect on the rate of fragmentation, specifically liquid vapor pressure, viscosity, and slurry loading. Vapor pressure of the slurry was one of control variables examined in this study. When a bubble collapses, the mechanical energy of the expanded bubble before collapse is converted into thermal and chemical energy of the bubble contents, i.e., the sonochemical hot spot.[15, 48] High vapor pressure of polyatomic molecules inside the bubble dramatically decreases the effective temperatures formed in the hot spot both through endothermic bond dissociation of the polyatomic vapor and through the decrease in the polytropic ratio (i.e., the distribution of energy into molecular rotations, bond vibrations, and translations).[49-50] Thus, different solvent

vapor pressures might cause different rates of particle fragmentation. To test this hypothesis, several organic liquids were used to prepare various potassium chloride slurries. There was no change in the fraction of initial crystal size (Figure 2.6) as liquid vapor pressure increased from about 0.01 to 50 Torr. Thus, the vapor pressure of the slurry did not affect fragmentation of alkali halides crystals. While vapor pressure dramatically affects the temperature reached *inside* bubbles during cavitational collapse,[49-51] vapor pressure *does not* affect either the total mechanical energy of the bubble before the collapse or the bubble rebound that generates the shock wave launched into the liquid.[25, 28, 52]

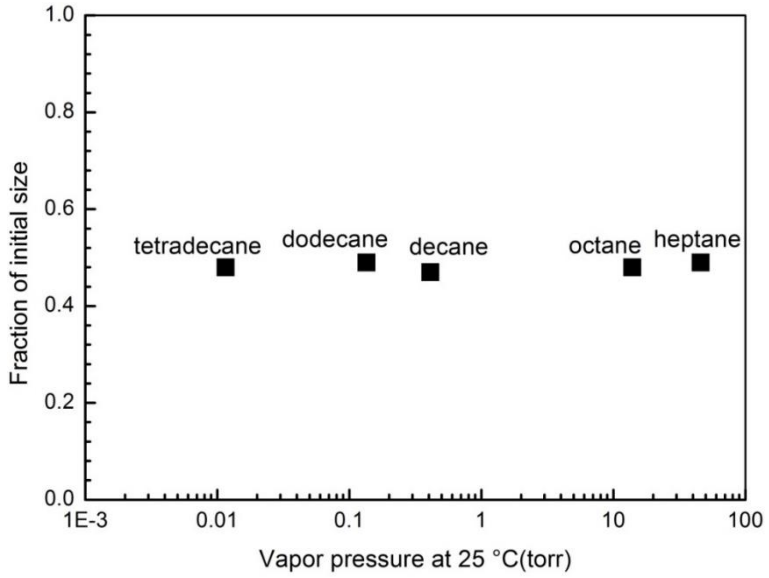

Figure 2.6 No significant effect of vapor pressure is observed on the rate of fragmentation of potassium chloride. A 0.2 wt % of potassium chloride slurry in 10 mL of an unreactive organic liquid was sonicated for 140 seconds using a titanium horn (10 W/cm^2 and 20 kHz).

2.3.4 Effect of viscosity

Viscosity may also affect the rate of fragmentation by changing relevant factors, such as the number of cavitating bubbles, bubble dynamics, drag on moving particles, and shockwave propagation.[13, 53] Dodecane and Dow Corning 200 Fluid (i.e., silicone oil) are miscible and

were combined to prepare solutions of various viscosities (Figure 2.7). Slurries of the mixed liquids and potassium chloride were sonicated, and the effect of viscosity on fragmentation was investigated. As the viscosity increased, the rate of potassium chloride fragmentation decreased, as expected (Figure 2.8). Indeed, for liquid viscosity greater than ~100 cSt, no sonofragmentation was observed.

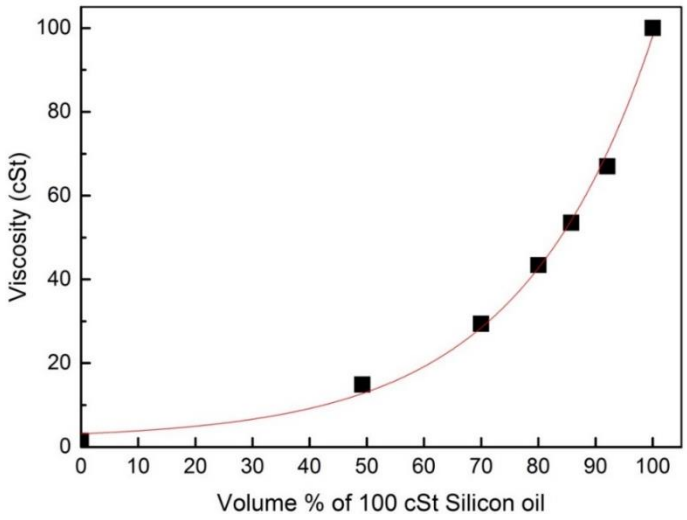

Figure 2.7 Viscosity measurements of dodecane-silicone oil mixtures. The first data point is viscosity of dodecane (0.10 cSt). The solid line is an exponential fit.

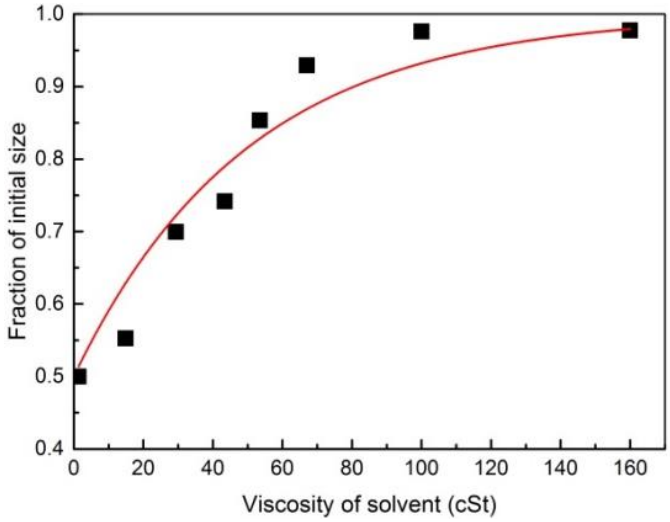

Figure 2.8 (cont.)

Figure 2.8 Effect of viscosity on fragmentation of potassium chloride. A slurry containing 0.2 wt% potassium chloride in a dodecane–silicon oil mixture was sonicated using a titanium horn (10 W/cm^2 and 20 kHz). The solid line is an exponential fit.

2.3.5 Mechanism of sonofragmentation of ionic crystals

There are four possible contributors to sonofragmentation of materials: interparticle collisions, particle–wall collisions, particle–horn collisions, and particle–shockwave/microjet interactions.[26] Previous papers on sonocrystallization have often assumed that interparticle collisions play a major role in fragmentation of growing crystals.[32, 54-56] While interparticle collisions are important for long ultrasonic irradiation of slurries of metal powders, we found recently that this is not the case for molecular solids.[26] To understand the breakage of brittle materials, we isolated each of these possible contributions to the sonofragmentation of ionic crystals and examined them separately (Figure 2.9).

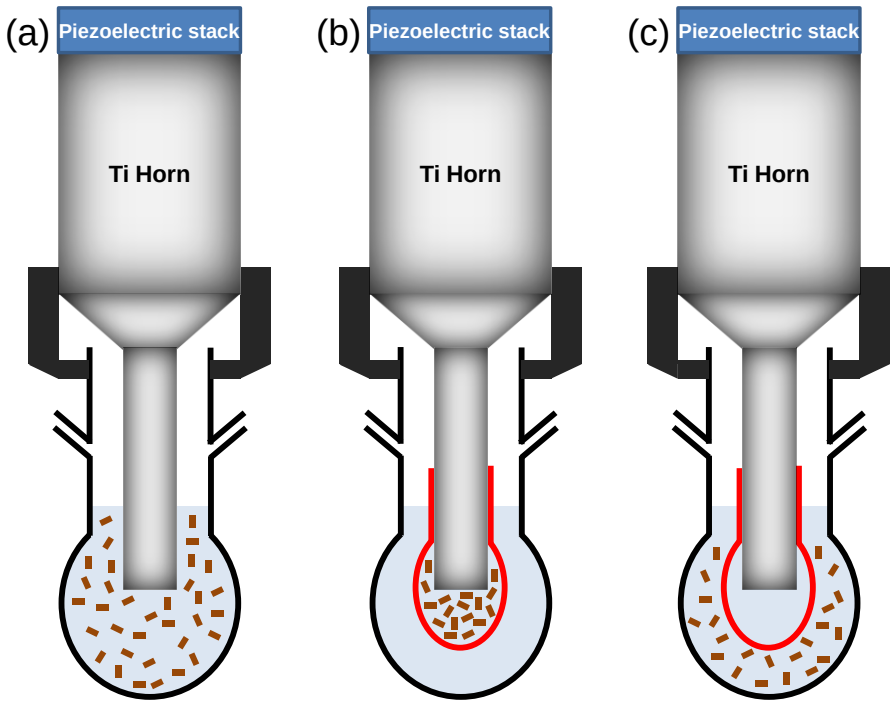

Figure 2.9 (cont.)

Figure 2.9 Experimental setups of (a) the normal apparatus showing the immersion of the titanium ultrasonic horn into the slurry, (b) decoupling experiments to eliminate particle–wall interactions, and (c) decoupling experiments to eliminate particle–horn interactions.

2.3.5.1 Interparticle collisions

First, we examined the effect of crystal loading on sonicated slurries. Various amounts of potassium chloride were loaded as a slurry into dodecane (10 mL). Regardless of the loading of the slurry, the rate of crystal fragmentation was *not significantly affected*: 140 sec of sonication (10 W/cm^2, 20 kHz) reduced the initial crystal size to 0.50(3) for slurries ranging from 0.07 to 10 wt% (Figure 2.10). Thus, *interparticle collisions do not contribute significantly to the sonofragmentation of these crystals*.

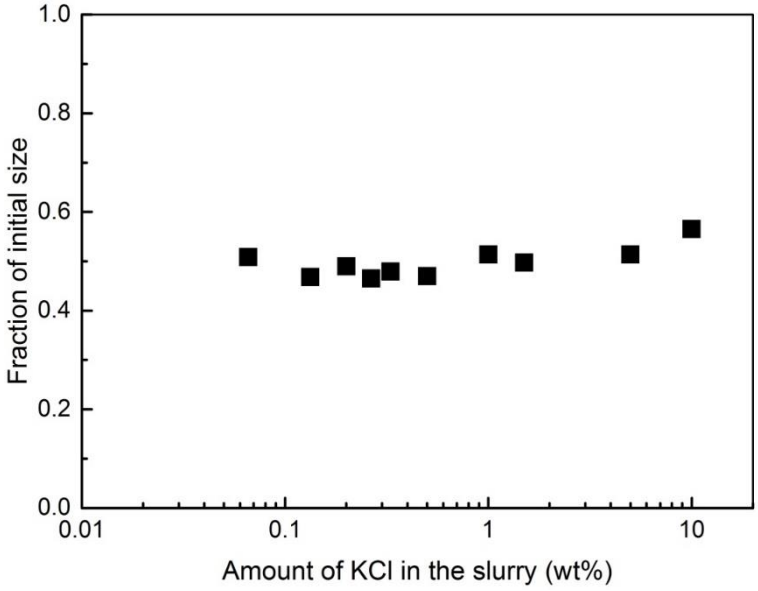

Figure 2.10 Slurry loading has no significant effect on rates of fragmentation of pota ssium chloride crystals during sonication. A potassium chloride slurry (loadings from 0.07 to 10 wt%) in 10mL dodecane was sonicated for 140 seconds using a titanium horn (10 W/cm^2 and 20 kHz).

2.3.5.2 Particle–wall collisions

Second, particle–wall decoupling experiments were performed at various ultrasonic intensities. A latex membrane was placed around the potassium chloride slurry to prevent particles from hitting the glass reactor wall (Figure 2.9b). Although particle–wall collisions did not occur for particles isolated from the wall, these particles showed slightly greater fragmentation than the particles exposed to the wall (Figure 2.11). The slight increase probably represents the effective increase in ultrasonic intensity that the confined slurry would have experienced within the membrane. These results demonstrate that particle–wall collisions were not a major mechanism of ionic crystal fragmentation.

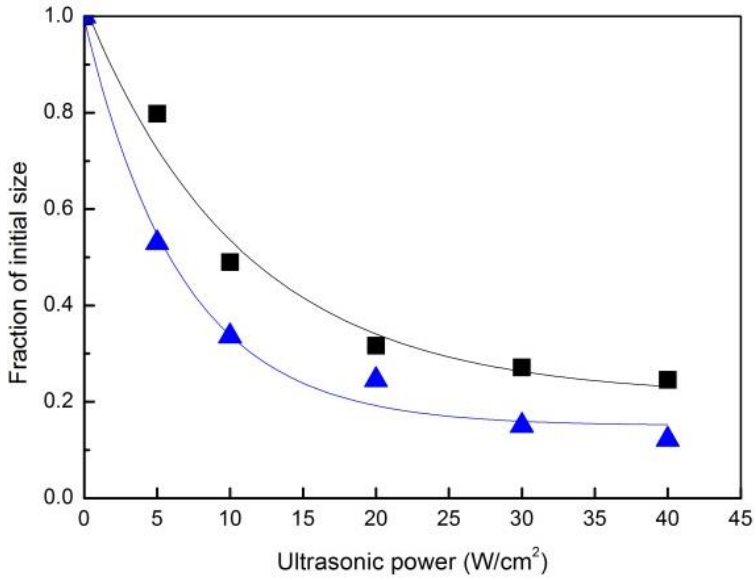

Figure 2.11 Comparison of fragmentation of potassium chloride crystals that were able to collide with the reactor wall directly (black line) versus crystals prevented from direct collisions with the reactor wall (blue line); cf. Figure 2.9a vs. 2.9b. A potassium chloride slurry (0.2 wt%) in 10 mL dodecane was sonicated for 140 seconds using a titanium horn (20 kHz). The solid line is an exponential fit.

2.3.5.3 Particle–horn collisions

Third, particle–horn decoupling experiments were carried out by isolating the potassium chloride slurry from direct contact with the horn using a latex membrane (Figure 2.9c). The solid particles were still fragmented at rapid rates (Figure 2.12), even in the absence of direct horn-particle contact. As such, these results demonstrate that particles–horn collisions were also not a major contributor to crystal fragmentation.

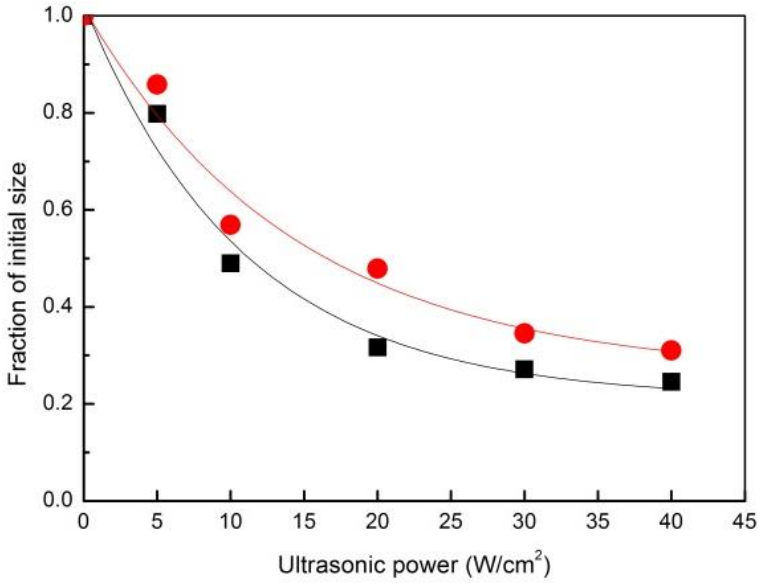

Figure 2.12 Comparison of fragmentation of potassium chloride crystals that were able to collide directly with the ultrasonic horn (black line) versus crystals prevented from direct collisions with the horn (red line); cf. Figure 2.9a vs. 2.9c. The slightly lower rates of fragmentation in the absence of direct horn contact (red line) is due to attenuation of the ultrasound by the latex membrane and the longer distances from the ultrasonic source (i.e. the horn tip). A potassium chloride slurry (loading 0.2 wt%) in 10 mL dodecane was sonicated for 140 seconds using a titanium horn (20 kHz). The solid line is an exponential fit.

Thus, as discussed elsewhere in detail for molecular crystals,[26] we must conclude that particle breakage of ionic solids irradiated with ultrasound is primarily due to interaction of

the solid particles with shockwaves and microjets formed during cavitation, *not* interparticle collisions or particle impact on hard surfaces (e.g., wall or horn).

2.3.5.4 Suggested mechanism of sonofragmentation of ionic crystals

For comparison, the mechanisms of crack formation in crystals under mechanical impact from grinding has been previously discussed.[57] When a solid particle is subjected to a strong impact, tensile stresses are formed radially outward from the initial point of contact. Cracks are generated along these radial lines, leading to eventual particle breakage. In addition, cracks can also be generated perpendicular to the radial cracking, due to the buckling of the particles.

As such, we suggest that there are two general classes of mechanisms for sonofragmentation of ionic (or molecular) crystals: shock-induced compression-expansion and shock-induced bending or torsion, as shown schematically in Figure 2.13. It is likely that the morphology of the initial crystals will determine the relative importance of these two mechanisms: high aspect ratio solids (i.e., rods, needles, or plates) are much more likely to break through bending and torsion than low aspect ratio solids (as used in these studies). Breakage of crystals ultimately is a nucleated process due to defects in solids, and *is not inherently related to the solids' hardness or bulk modulus.* One intuitively expects, however, that *the rate at which defects are generated in solid particles during strain or impact ought to correlate with the strength of materials.* This is, if one may, the mechanochemical extension of the Bell-Evans-Polanyi principle or of Hammond's Postulate: activation energies correlate with enthalpies.[58-59] Indeed, prior reports have established empirically that fracture toughness and fracture strength of glasses (both silica and metallic) are empirically proportional to Young's modulus.[60-61] There are also similar results for various minerals, and harder minerals required more energy to be broken.[62] As we have now observed for ionic

crystalline solids (Figures 2.3), the rate of breakage of ionic crystals correlates strongly with both Young's modulus and the Vickers hardness of these solids: i.e., the kinetics of crystal breakage correlates with thermodynamic properties.

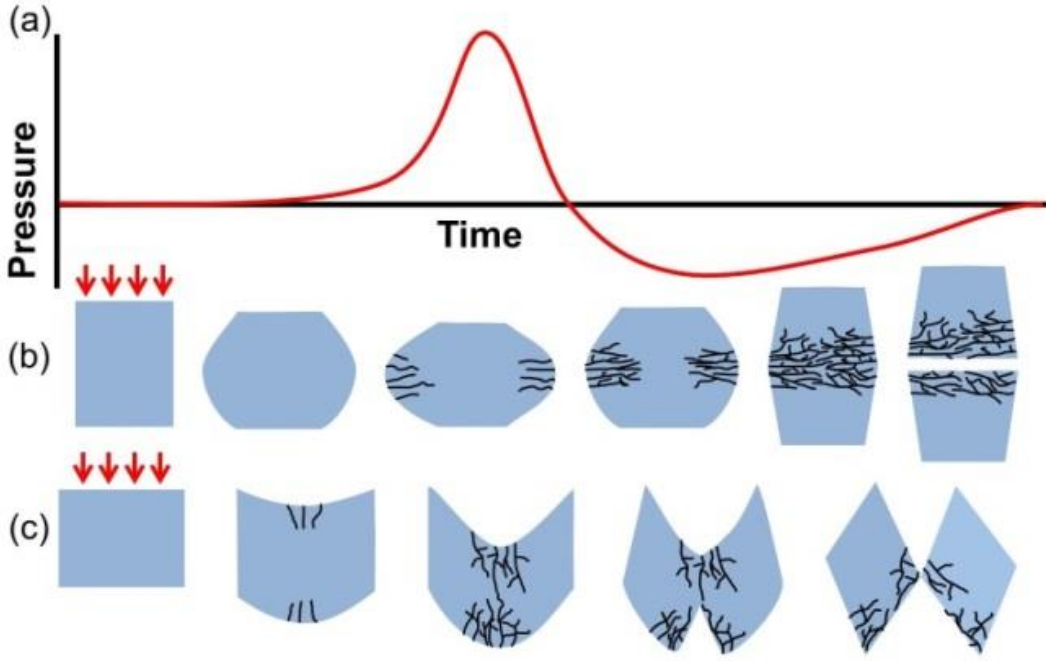

Figure 2.13 Two classes of mechanisms of shock fragmentation of crystals. (a) Pressure profile of a typical shockwave passing through a liquid; compression and expansion from shockwaves, in general, are not symmetric. (b) Particle breakage from defects formed by shock-induced compression and expansion of the initial crystal and (c) particle breakage from defects created during shock-induced bending or torsion of the initial crystal.

2.4 Conclusion

Fragmentation of various alkali halide crystals was induced by ultrasonic irradiation of slurries in organic liquids; exponential decreases in particle size were observed with length of sonication. Analysis of the fragmentation mechanism showed that direct interaction between alkali halide crystals and shockwaves or microjets, and not interparticle collisions or impaction,

were the main cause of sonofragmentation. Shockwave fragmentation of crystals may be induced by either compression-expansion or by bending-torsional effects on the solid particles. There is a strong correlation of the rate of fragmentation with materials' properties (i.e., Vickers hardness and Young's modulus).

2.5 References

1. Beyer, M. K.; Clausen-Schaumann, H., Mechanochemistry: The mechanical activation of covalent bonds. *Chem. Rev.* **2005,** *105* (8), 2921-2948.

2. Jones, W.; Eddleston, M. D., Introductory lecture: mechanochemistry, a versatile synthesis strategy for new materials. *Faraday Discuss.* **2014,** *170*, 9-34.

3. Caruso, M. M.; Davis, D. A.; Shen, Q.; Odom, S. A.; Sottos, N. R.; White, S. R.; Moore, J. S., Mechanically-induced chemical changes in polymeric materials. *Chem. Rev.* **2009,** *109* (11), 5755-5798.

4. Friscic, T.; James, S. L.; Boldyreva, E. V.; Bolm, C.; Jones, W.; Mack, J.; Steed, J. W.; Suslick, K. S., Highlights from Faraday discussion 170: Challenges and opportunities of modern mechanochemistry, Montreal, Canada, 2014. *Chem. Commun.* **2015,** *51* (29), 6248-6256.

5. James, S. L.; Adams, C. J.; Bolm, C.; Braga, D.; Collier, P.; Friscic, T.; Grepioni, F.; Harris, K. D. M.; Hyett, G.; Jones, W.; Krebs, A.; Mack, J.; Maini, L.; Orpen, A. G.; Parkin, I. P.; Shearouse, W. C.; Steed, J. W.; Waddell, D. C., Mechanochemistry: opportunities for new and cleaner synthesis. *Chem. Soc. Rev.* **2012,** *41* (1), 413-447.

6. Ralphs, K.; Hardacre, C.; James, S. L., Application of heterogeneous catalysts prepared by mechanochemical synthesis. *Chem. Soc. Rev.* **2013,** *42* (18), 7701-7718.

7. Lee, B.; Niu, Z.; Wang, J.; Slebodnick, C.; Craig, S. L., Relative mechanical strengths

of weak bonds in sonochemical polymer mechanochemistry. *J. Am. Chem. Soc.* **2015,** *137* (33), 10826-10832.

8. Cravotto, G.; Gaudino, E. C.; Cintas, P., On the mechanochemical activation by ultrasound. *Chem. Soc. Rev.* **2013,** *42* (18), 7521-7534.

9. Suslick, K. S., Mechanochemistry and sonochemistry: concluding remarks. *Faraday Discuss.* **2014,** *170*, 411-422.

10. Cintas, P.; Cravotto, G.; Barge, A.; Martina, K., Interplay between mechanochemistry and sonochemistry. In *Polymer Mechanochemistry*, Springer International Publishing: Switzerland 2015; Vol. 369.

11. Guo, Z.; Jones, A. G.; Li, N.; Germana, S., High-speed observation of the effects of ultrasound on liquid mixing and agglomerated crystal breakage processes. *Powder Technol.* **2007,** *171* (3), 146-153.

12. Wagterveld, R. M.; Boels, L.; Mayer, M. J.; Witkamp, G. J., Visualization of acoustic cavitation effects on suspended calcite crystals. *Ultrason. Sonochem.* **2011,** *18* (1), 216-225.

13. Leighton, T., *The acoustic bubble*. Academic press: Cambridge: 2012.

14. Suslick, K. S., Sonochemistry. *Science* **1990,** *247* (4949), 1439-1445.

15. Suslick, K. S.; Flannigan, D. J., Inside a collapsing bubble: sonoluminescence and the conditions during cavitation. *Annu. Rev. Phys. Chem.* **2008,** *59*, 659-683.

16. Pecha, R.; Gompf, B., Microimplosions: cavitation collapse and shock wave emission on a nanosecond time scale. *Phys. Rev. Lett.* **2000,** *84* (6), 1328-1330.

17. Blake, J. R.; Keen, G. S.; Tong, R. P.; Wilson, M., Acoustic cavitation: the fluid dynamics of non-spherical bubbles. *Philos. Trans. A Math Phys. Eng. Sci.* **1999,** *357* (1751), 251-267.

18. Lauterborn, W.; Vogel, A., Morden optical techniques in fluid mechanics. *Annu. Rev.*

Fluid Mech. **1984,** *16*, 223-244.

19. Shchukin, D. G.; Skorb, E.; Belova, V.; Mohwald, H., Ultrasonic cavitation at solid surfaces. *Adv. Mater.* **2011,** *23* (17), 1922-1934.

20. Prozorov, T.; Prozorov, R.; Suslick, K. S., High velocity interparticle collisions driven by ultrasound. *J. Am. Chem. Soc.* **2004,** *126* (43), 13890-13891.

21. Suslick, K. S.; Doktycz, S. J., The sonochemistry of zinc powder. *J. Am. Chem. Soc.* **1989,** *111* (6), 2342-2344.

22. Suslick, K. S.; Casadonte, D. J.; Doktycz, S. J., The effects of ultrasound on nickel and copper powders. *Solid State Ionics* **1989,** *32-3*, 444-452.

23. Suslick, K. S.; Casadonte, D. J.; Doktycz, S. J., Ultrasonic irradiation of copper powder. *Chem. Mater.* **1989,** *1* (1), 6-8.

24. Radziuk, D.; Grigoriev, D.; Zhang, W.; Su, D.; Moehwald, H.; Shchukin, D., Ultrasound-assisted fusion of preformed gold nanoparticles. *J. Phys. Chem. C* **2010,** *114* (4), 1835-1843.

25. Doktycz, S. J.; Suslick, K. S., Interparticle collisions driven by ultrasound. *Science* **1990,** *247* (4946), 1067-1069.

26. Zeiger, B. W.; Suslick, K. S., Sonofragmentation of molecular crystals. *J. Am. Chem. Soc.* **2011,** *133* (37), 14530-14533.

27. Deora, N. S.; Misra, N. N.; Deswal, A.; Mishra, H. N.; Cullen, P. J.; Tiwari, B. K., Ultrasound for improved crystallisation in food processing. *Food Engineering Reviews* **2013,** *5* (1), 36-44.

28. Sander, J. R. G.; Zeiger, B. W.; Suslick, K. S., Sonocrystallization and sonofragmentation. *Ultrason. Sonochem.* **2014,** *21* (6), 1908-1915.

29. Zhang, Z.; Sun, D.-W.; Zhu, Z.; Cheng, L., Enhancement of crystallization processes

by power ultrasound: current state-of-the-art and research advances. *Comprehensive Reviews in Food Science and Food Safety* **2015,** *14* (4), 303-316.

30. Gopi, K. R.; Nagarajan, R., Advances in nanoalumina ceramic particle fabrication using sonofragmentation. *IEEE Trans. Nanotechnol.* **2008,** *7* (5), 532-537.

31. Zhang, L.; Belova, V.; Wang, H.; Dong, W.; Moehwald, H., Controlled cavitation at nano/microparticle surfaces. *Chem. Mater.* **2014,** *26* (7), 2244-2248.

32. Raman, V.; Abbas, A., Experimental investigations on ultrasound mediated particle breakage. *Ultrason. Sonochem.* **2008,** *15* (1), 55-64.

33. Ambedkar, B.; Nagarajan, R.; Jayanti, S., Investigation of high-frequency, high-intensity ultrasonics for size reduction and washing of coal in aqueous medium. *Ind. Eng. Chem. Res.* **2011,** *50* (23), 13210-13219.

34. Franco, F.; Perez-Maqueda, L. A.; Perez-Rodriguez, J. L., The effect of ultrasound on the particle size and structural disorder of a well-ordered kaolinite. *J. Colloid Interface Sci.* **2004,** *274* (1), 107-117.

35. Price, G. J.; White, A. J.; Clifton, A. A., The effect of high-intensity ultrasound on solid polymers. *Polymer* **1995,** *36* (26), 4919-4925.

36. Meier, M.; John, E.; Wieckhusen, D.; Wirth, W.; Peukert, W., Influence of mechanical properties on impact fracture: Prediction of the milling behaviour of pharmaceutical powders by nanoindentation. *Powder Technol.* **2009,** *188* (3), 301-313.

37. Vogel, L.; Peukert, W., Breakage behaviour of different materials - construction of mastercurve for the breakage probability. *Powder Technol.* **2003,** *129* (1-3), 101-110.

38. Taylor, L. J.; Papadopoulos, D. G.; Dunn, P. J.; Bentham, A. C.; Dawson, N. J.; Mitchell, J. C.; Snowden, M. J., Predictive milling of pharmaceutical materials using nanoindentation of single crystals. *Organic Process Research & Development* **2004,** *8* (4),

674-679.

39. Gilman, J. J., *Chemistry and physics of mechanical hardness*. John Wiley & Sons: New York City: 2009; Vol. 5.

40. Chin, G. Y.; Van Uitert, L. G.; Green, M. L.; Zydzik, G., Hardness, yield strength and young's modulus in Halide crystals. *Scr. Mater.* **1972,** *6* (6), 475-479.

41. Rao, T. T.; Sirdeshmukh, D. B., Microhardness of rubidium halide crystals. *Cryst. Res. Technol.* **1991,** *26* (3), K53-K59.

42. Sirdeshmukh, D. B.; Subhadra, K. G.; Rag, K. K.; Rao, T. T., Hardness of crystals with NaCl structure and the significance of the Gilman-Chin parameter. *Cryst. Res. Technol.* **1995,** *30* (6), 861-866.

43. Sirdeshmukh, D. B.; Krishna, P. G.; Subhadra, K. G., Micro-macro property correlations in alkali halide crystals. *J. Mater. Sci.* **2003,** *38* (9), 2001-2006.

44. Sirdeshmukh, D. B.; Sirdeshmukh, L.; Subhadra, K. G., *Alkali halides: a handbook of physical properties*. Springer Science & Business Media: Berlin: 2013; Vol. 49.

45. Neppiras, E. A., Acoustic cavitation. *Physics Reports-Review Section of Physics Letters* **1980,** *61* (3), 159-251.

46. de Vegt, O.; Vromans, H.; Pries, W.; Maarschalk, K. V., The effect of crystal imperfections on particle fracture behaviour. *Int. J. Pharm.* **2006,** *317* (1), 47-53.

47. de Vegt, O.; Vromans, H.; den Toonder, J.; Maarschalk, K. V., Influence of flaws and crystal properties on particle fracture in a jet mill. *Powder Technol.* **2009,** *191* (1-2), 72-77.

48. Didenko, Y. T.; Suslick, K. S., The energy efficiency of formation of photons, radicals and ions during single-bubble cavitation. *Nature* **2002,** *418* (6896), 394-397.

49. Suslick, K. S.; Gawienowski, J. J.; Schubert, P. F.; Wang, H. H., Alkane sonochemistry. *J. Phys. Chem.* **1983,** *87* (13), 2299-2301.

50. Suslick, K. S.; Hammerton, D. A.; Cline, R. E., The sonochemical hot-spot. *J. Am. Chem. Soc.* **1986,** *108* (18), 5641-5642.

51. Flint, E. B.; Suslick, K. S., The temperature of cavitation. *Science* **1991,** *253* (5026), 1397-1399.

52. Suslick, K. S.; Price, G. J., Applications of ultrasound to materials chemistry. *Annu. Rev. Mater. Sci.* **1999,** *29*, 295-326.

53. Majumdar, S.; Kumar, P. S.; Pandit, A. B., Effect of liquid-phase properties on ultrasound intensity and cavitational activity. *Ultrason. Sonochem.* **1998,** *5* (3), 113-118.

54. Kass, M., Ultrasonically induced fragmentation and strain in alumina particles. *Mater. Lett.* **2000,** *42*, 246-250.

55. Chu, S.-H.; Choi, S. H.; Kim, J.-W.; King, G. C.; Elliott, J. R., Ultrasonication of bismuth telluride nanocrystals fabricated by solvothermal method - art. no. 61720A. In *Smart Structures and Materials 2006: Smart Electronics, Mems, Biomems, and Nanotechnology*, Varadan, V. K., Ed. 2006; Vol. 6172, pp A1720-A1720.

56. Price, G. J.; Mahon, M. F.; Shannon, J.; Cooper, C., Composition of calcium carbonate polymorphs precipitated using ultrasound. *Crystal Growth & Design* **2011,** *11* (1), 39-44.

57. Potapov, A. V.; Campbell, C. S., The two mechanisms of particle impact breakage and the velocity effect. *Powder Technol.* **1997,** *93* (1), 13-21.

58. Anslyn, E. V.; Dougherty, D. A., *Modern physical organic chemistry*. University Science: Sausalito, CA, 2006.

59. Dill, K. A.; Bromberg, S., *Molecular driving forces*. 2 ed.; Garland Science: New York, 2011.

60. Soga, N., Elastic moduli and fracture toughness of glass. *J. Non-Cryst. Solids* **1985,**

73 (1-3), 305-313.

61. Yuan, C. C.; Xi, X. K., On the correlation of Young's modulus and the fracture strength of metallic glasses. *J. Appl. Phys.* **2011,** *109* (3).

62. Gent, M.; Menendez, M.; Torano, J.; Torno, S., A correlation between Vickers hardness indentation values and the bond work Index for the grinding of brittle minerals. *Powder Technol.* **2012,** *224*, 217-222.

Chapter 3

Sonofragmentation of molecular crystals

3.1 Introduction

When ultrasound is applied to a slurry of molecular crystals, shockwaves generated by acoustic cavitation interact directly with the molecular crystals to cause fragmentation, *i.e.*, sonofragmentation.[1] Molecular crystals are composed of molecules held together by weak intermolecular forces consisting of dipole-dipole interactions, created by partially charged ions, and Van der Waals forces.[2] Additionally, the local length scales of these intermolecular forces are relatively short.[3-4] Thus, molecular crystals tend to be brittle and cannot usually sustain their original form and size under ultrasonic irradiation.

Sonofragmentation can occur during sonocrystallization. This can reduce crystal size in two ways: by direct fragmentation of crystals;[5-9] and by creating additional, secondary nucleation sites for new crystals.[10-14] One of the most important applications of sonocrystallization is in generating pharmaceutical drugs, many of which are molecular crystals.[15-20] Thus, it is important to understand the sonofragmentation of molecular crystals in order to predict and improve the properties of the final product of sonocrystallization with regard to factors including crystal size, size distribution, and crystal morphology.

It has been reported the effects of various control variables (e.g., acoustic power density, frequency, solvent, etc.) on sonofragmentation of molecular crystals.[1, 21-24] Also, several articles have detailed the mechanical properties of molecular crystals following milling or particle impaction.[25-28] However, no studies have revealed a direct relationship between a

material's properties and the sonofragmentation of molecular crystals.

This chapter describes the sonication of slurries of six molecular crystals and four polycyclic aromatic hydrocarbon (PAH) crystals. An ultrasonic horn (20 kHz, 10 W/cm^2) was used to examine their sonofragmentation patterns. Each of the selected crystals was distinct in its Vickers hardness (H_v) and Young's modulus (E),[29-31] two of the most critical materials' properties related to fragmentation. In addition, the relationships between Vickers hardness or Young's modulus and the sonofragmentation patterns of molecular, PAH and ionic crystals were compared. The effects of initial crystal on sonofragmentation patterns were also evaluated.

3.2 Experimental

3.2.1 Materials

Lactose, acetaminophen, hexamethylenetetramine, chrysene, 9,10-diphenylanthracene, pyrene, anthracene and dodecane were purchased from Sigma-Aldrich. Sucrose was purchase from Fisher Scientific. All chemicals were used as-received, unless otherwise indicated. Sulfadimethoxine and phenacetin (Sigma-Aldrich) were recrystallized in nanopure water (i.e., water deionized to >18 MΩ·cm resistance, scrubbed for organics, and passed through a 0.45 μm filter with a Barnstead NANOpure® ultrapure water purification system).

3.2.2 Sonofragmentation experimental setup

10 ml of dodecane was added to 15 mg of molecular crystals. The slurry was allowed to thermally equilibrate at 18 °C for 5 minutes in a temperature-controlled water bath (Isotemp 1006S). This mixture was sonicated with an exponential ultrasonic horn (Sonics and Materials

VCX-750, 20 kHz, 1 cm^2 Titanium tip, 10 W/cm^2) for different times. At 20 kHz, the maximum diameter of a cavitating bubble before collapse is ~ 150 μm.[32] All sonication experiments were performed using a duty cycle of 2 sec on and 8 sec off pulse cycle to reduce temperature variation. For all cases, steady state temperatures during sonication were 25 °C. Sonication times are reported as the total time exposed to ultrasound. For the sonofragmentation experiments of polycyclic aromatic hydrocarbon (PAH) crystals, 10 ml of DI water was added to 15 mg of PAH crystals. Other experimental conditions and processes were same as those of sonofragmentation experiments of molecular crystals.

3.2.3 Sample preparation of seven groups of sucrose having different crystal size

In order to check the effect of initial crystal size, a sonic sifter (Advantech Manufacturing, Berlin, WI) was used with various sieves (mesh opening sizes 45, 75, 106, 250, 500 and 1000 μm) to separate batches of sucrose based on their size. The sonic sifter was used for 5 minutes. Crystals that were not sieved by the sifter were removed from the sieve. The sieved crystals were collected and sieved again with same intensity and time. This process was done total 4 times for each group of sucrose. For the crystals passing the sieve with 45 μm of mesh opening size, vacuum filtration was performed with filter paper (pore size 1.2 μm) and the unfiltrated crystals were taken. For the group of the smallest size of sucrose (Group 7), sucrose was grounded by mortar and pestle and then sieved with the sieve which mesh opening size was 45 μm. Crystals smaller than 45 μm collected and dispersed into dodecane. The sucrose–dodecane slurry was sonicated with a horn (20kHz and 40 W/cm^2) for an hour. After the sonication, sucrose was collected again by centrifuge and dried in a vacuum oven at room temperature for overnight.

3.2.4 Characterization

An aliquot of sonicated slurry was removed using a disposable pipette for analysis by optical microscopy (Zeiss Axioskop optical/fluorescence microscope). The micrographs were captures using a Cannon PC1015 digital camera mounted to the microscope. Scanning electron microscopy was performed with a JEOL 7000F Analytical SEM. Crystal size analysis with optical microscopic or SEM images was performed using Image-J software (National Institutes of Health, Bethesda, MD, USA). Approximately 200 particles were measured for each experiment. Data fitting was performed using OriginPro 8.5 software (OriginLab, Northampton, MA, USA). Vickers hardness and Young's modulus of PAH crystals were measured by Leitz Wetzlar GMBH and Agilent G200 Nanoindenter, respectively.

3.3 Results and discussion

3.3.1 Sonofragmentation of molecular crystals

Molecular crystals were fragmented under ultrasonic irradiation (Figure 3.1). The rate of fragmentation for the molecular crystals is shown in Figure 3.2. The data revealed an exponential reduction in particle size as a function of sonication time. Molecular crystals with a higher Vickers hardness and Young's modulus required longer sonication times to reach half their initial crystal size (Table 3.1).

Table 3.1 Vickers hardness (H_v), Young's modulus (E), sonication time necessary to halve the initial crystal size ($\tau_{1/2}$) of molecular crystals and initial crystal size.

Molecular crystals	**H_v (GPa)**	***E* (GPa)**	**$\tau_{1/2}$ (sec)**	**Initial crystal size (μm)**
Sucrose	0.636	32.3	480	678
Lactose	0.535	24.1	440	664
Acetaminophen	0.358	18.1	380	561
Sulfadimethoxine	0.240	N/A	340	442
Phenacetin	0.172	N/A	310	1162
Hexamethylene-tetramine	0.133	9.0	260	507

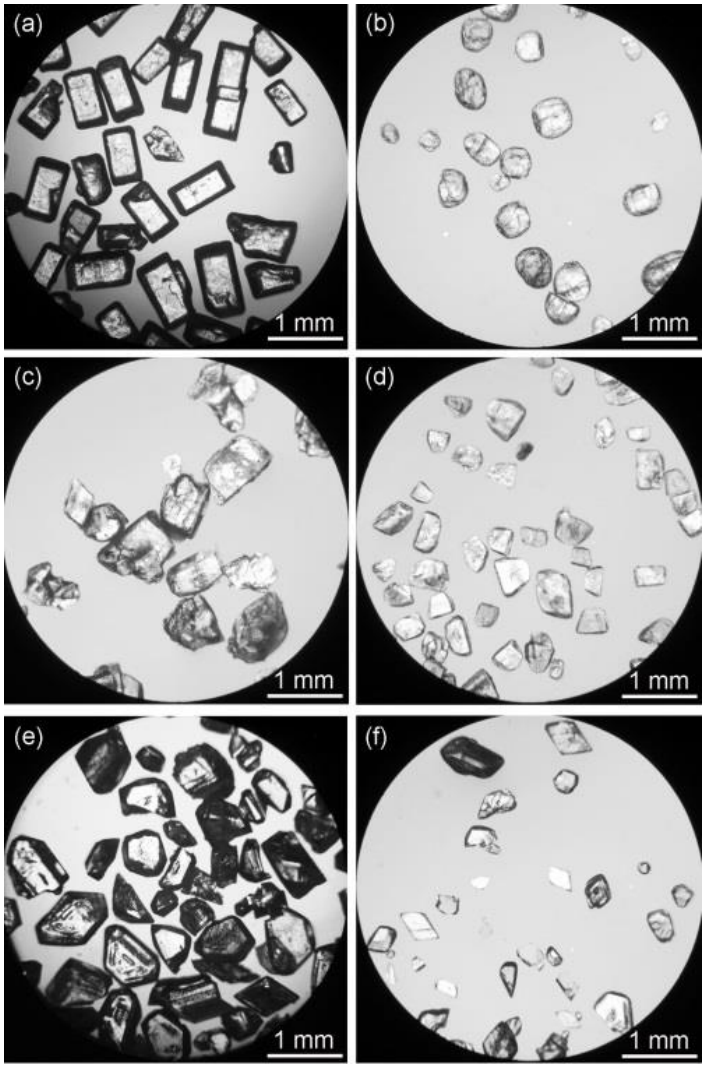

Figure 3.1 (cont.)

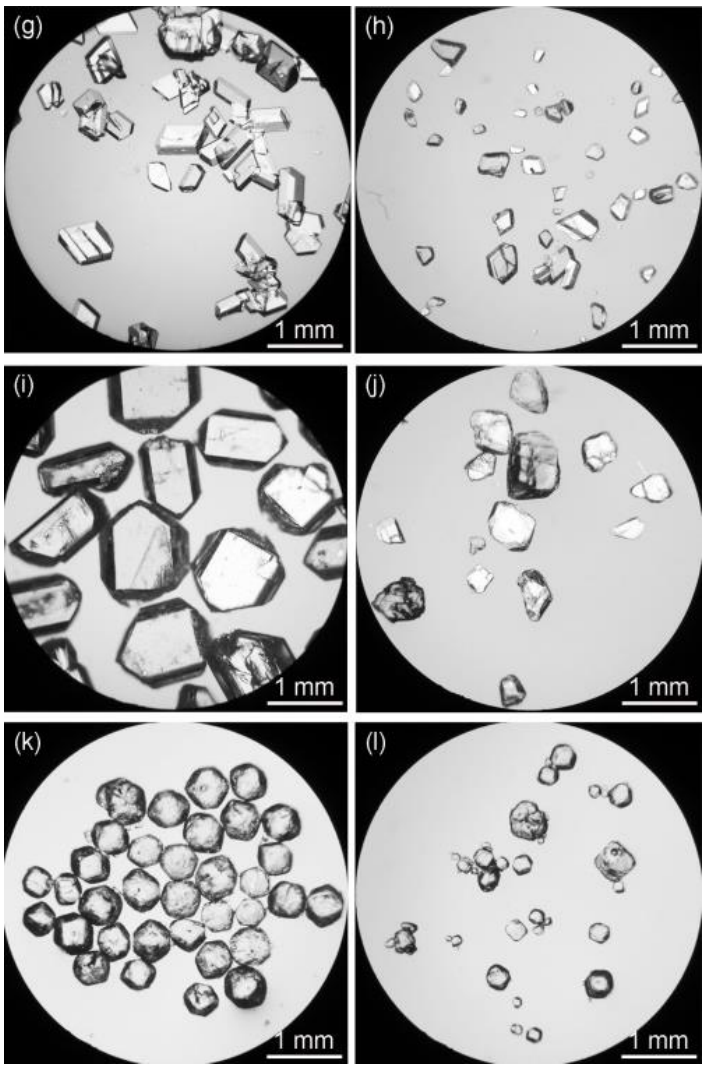

Figure 3.1 Optical micrographs of molecular crystals before and after sonication. (a) Sucrose before sonication and (b) after sonication 480 seconds, (c) lactose before sonication and (d) after sonication for 440 seconds, (e) acetaminophen before sonication and (f) after sonication 380 seconds, (g) sulfadimethoxine before sonication and (h) after sonication for 340 seconds, (i) phenacetin before sonication and (j) after sonication for 310 seconds, (k) hexamethylenetetramine before sonication and (l) after sonication for 210 seconds. Each slurry contained 0.2 wt% of molecular crystals in dodecane and was sonicated by using a titanium horn (10 W/cm^2 and 20 kHz).

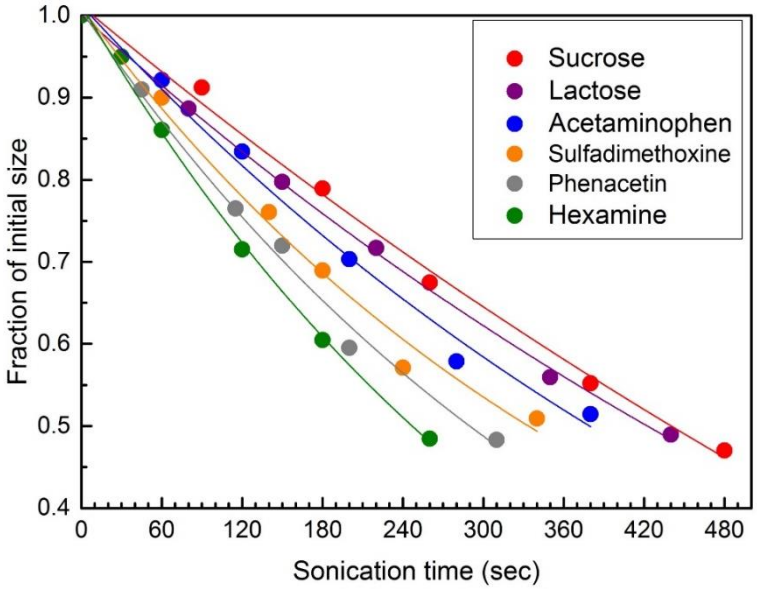

Figure 3.2 Fraction of initial crystal size versus sonication time for various molecular crystals. Slurries containing 0.2 wt% of the molecular crystals in dodecane were sonicated using a titanium horn (10 W/cm^2 and 20 kHz). Solid lines are exponential fits to the data. Standard deviation of each data point is less than 4 % of its average value.

When the sonication time was divided by the Vickers hardness$^{0.35}$ or Young's modulus$^{0.5}$, the fractions of initial crystal size were distributed near a master line (Figures 3.3b and d). Figures 3.3(a) and (c) show a quantitative relationship between hardness or elasticity and the rate of fragmentation. However, the reason for these results has not yet been determined. Other critical factors, such as the defect concentration of the starting materials, may play a role in fragmentation efficiency.

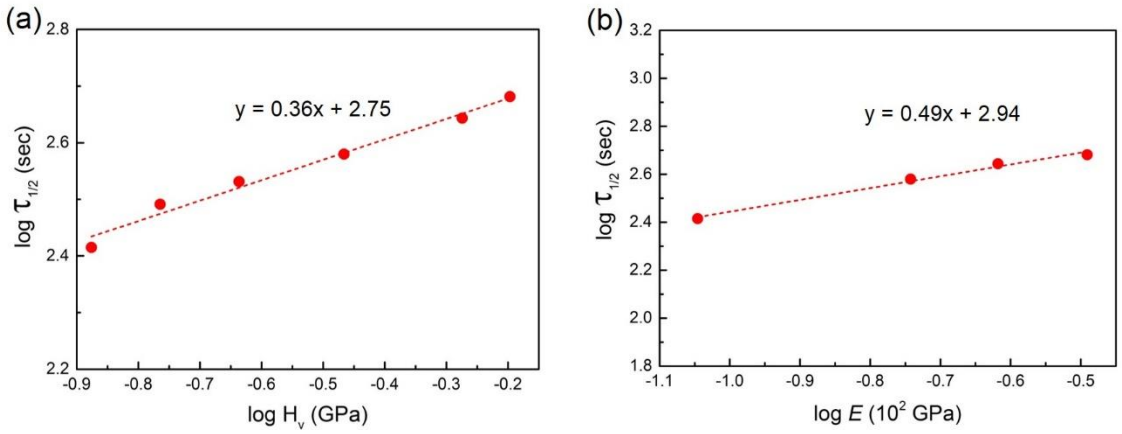

Figure 3.3 Relationship between rate of sonofragmentation and either Vickers hardness or Young's modulus. (a) log Vickers hardness (H_v) vs. log time necessary to halve the initial crystal size ($\tau_{1/2}$); and (b) log Young's modulus (E) vs. log time necessary to halve the initial crystal size ($\tau_{1/2}$). Linear fitting was applied. Standard deviation of each data point is less than 4 % of its average value.

3.3.2 Sonofragmentation of polycyclic aromatic hydrocarbon (PAH)

The relationship between the Vickers hardness or Young's modulus and sonofragmentation patterns was also examined in four polycyclic aromatic hydrocarbons (PAHs): anthracene, pyrene, chrysene, and 9,10-diphenylanthracene (Figure 3.4). PAHs are nonpolar molecular crystals that do not have hydrogen bonds. They are held together only by weak intermolecular forces such as Van der Waals forces and dipole-dipole interactions between partially charged ions.[2] These interactions are held only over very short distances.[3-4]

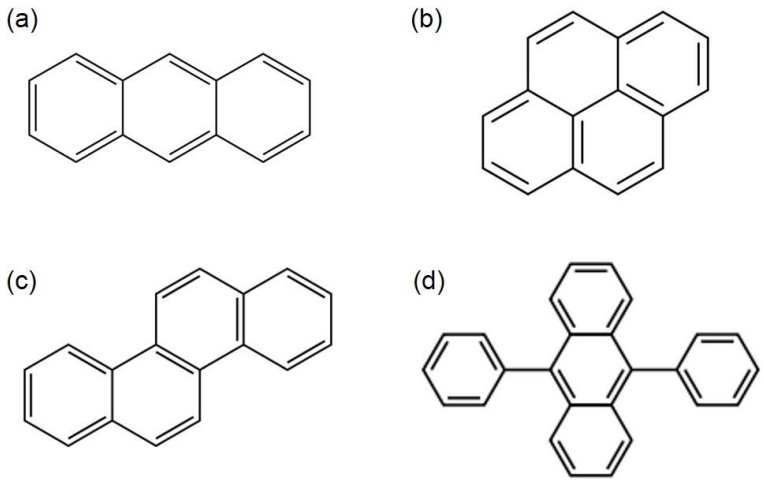

Figure 3.4 Molecular structure of four different PAH: (a) anthracene, (b) pyrene, (c) chrysene and (d) 9,10-diphenylanthracene.

The Vickers hardness and Young's modulus of PAH crystals were measured using a Vickers indenter and a nanoindenter, respectively (Table 3.2). The ranges of Vickers hardness and Young's modulus of PAH crystals partially overlapped with those of the molecular crystals described in Section 3.3.1. PAH crystals were broken during sonication of the slurries (Figure 3.5). The time required for the crystals to reach half their initial size ($\tau_{1/2}$) increased with the Vickers hardness or Young's modulus of the parent material. Figure 3.6 shows that there is a quantitative relationship between the rate of fragmentation and the hardness or elasticity of PAH crystals.

Table 3.2 Vickers hardness (H_v), Young's modulus (E), sonication time necessary to halve the initial crystal size ($\tau_{1/2}$) of PAH crystals and initial crystal size.*

PAH crystals	H_v (GPa)	E (GPa)	$\tau_{1/2}$ (sec)	Initial crystal size (μm)
9,10-diphenylanthracene	0.213 (0.025)	12.79 (2.43)	300	793
Chrysene	0.182 (0.014)	13.64 (1.73)	310	677
Pyrene	0.071 (0.012)	7.57 (0.57)	270	748
Anthracene	0.052 (0.011)	9.35 (1.6)	270	925

*H_v and E were measured three times and five times, respectively, and the values of H_v and E are average values.

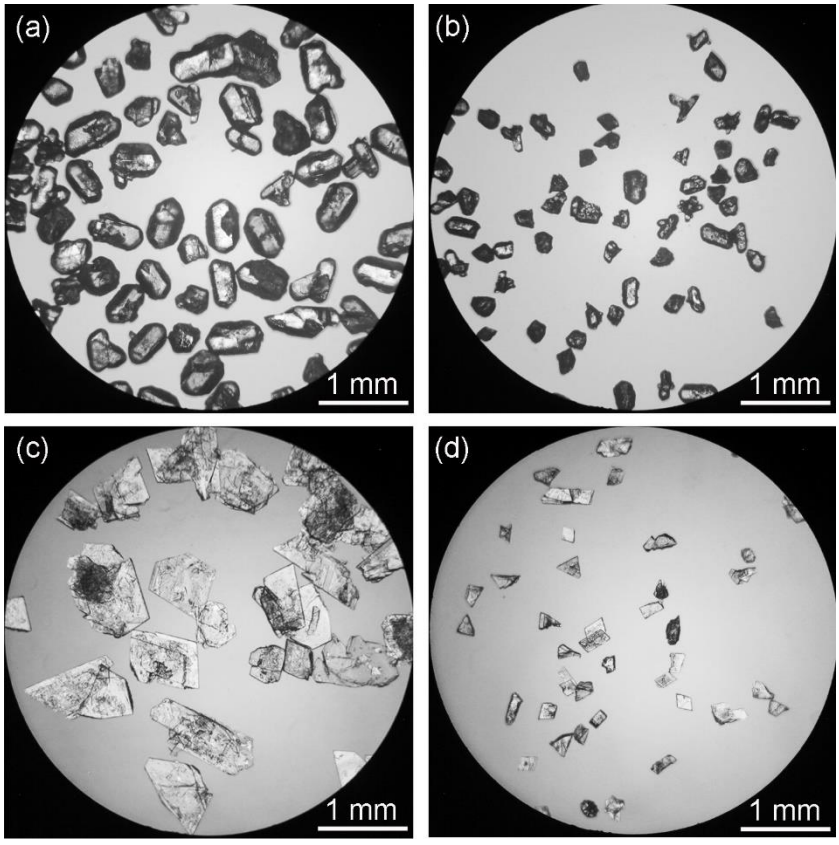

Figure 3.5 (cont.)

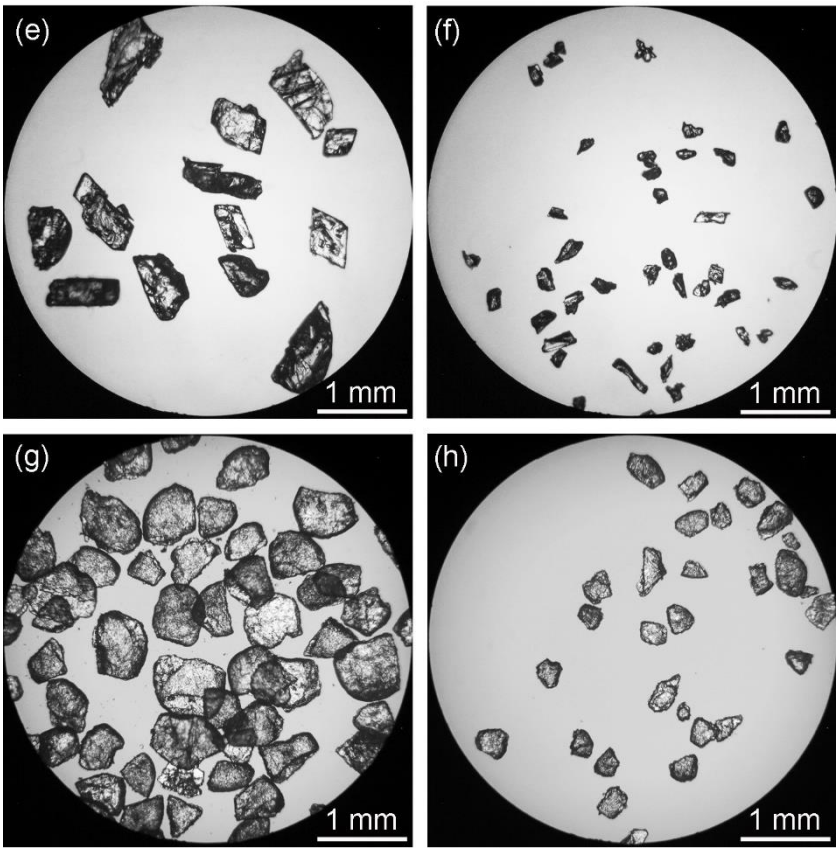

Figure 3.5 Optical micrographs of PAH crystals before and after sonication. (a) 9,10-diphenylanthracene before sonication and (b) after sonication for 300 seconds, (c) chrysene before sonication and (d) after sonication for 310 seconds, (e) pyrene before sonication and (f) after sonication 270 seconds, (g) anthracene before sonication and (h) after sonication for 270 seconds. Each slurry contained 0.2 wt% of PAH crystals in DI water and was sonicated by using a titanium horn (10 W/cm^2 and 20 kHz).

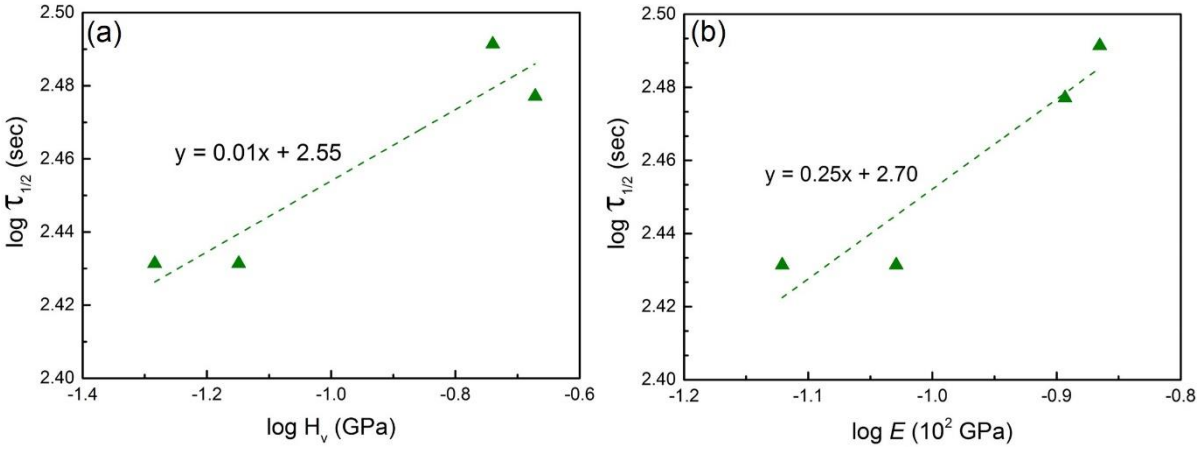

Figure 3.6 Relationship between (a) Vickers hardness (H_v) and the time necessary to halve the initial crystal size ($\tau_{1/2}$) and (b) Young's modulus (E) and the time necessary to halve the initial crystal size ($\tau_{1/2}$). The dashed lines are linear fits. Standard deviation of each data point is less than 4 % of its average value.

3.3.3 Comparison of sonofragmentation patterns between ionic, molecular and PAH crystals

Sonofragmentation occurred following sonication of slurries containing ionic, molecular, or PAH crystals. A quantitative relationship between hardness or elasticity and the rate of fragmentation was observed in each case (Section 2.3.1, 3.3.1 and 3.3.2). In Figure 3.7(a), the slope of the fitted lines of ionic crystals is the steepest among the lines representing ionic, molecular, and PAH crystals. This indicates that, among the three types of crystals, sonofragmentation of ionic crystals was the most sensitive to the change of hardness of the parent materials. However, the three types of crystals showed similar sensitivity of sonofragmentation to the change of Young's modulus (Figure 3.7b).

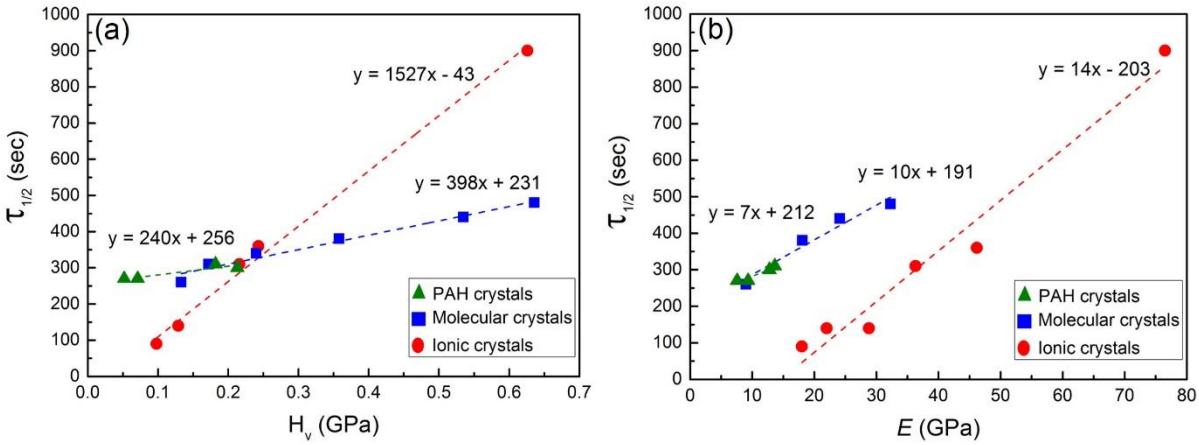

Figure 3.7 Comparison of the relationships between (a) Vickers hardness (H_v) and the time necessary to halve the initial crystal size ($\tau_{1/2}$) of ionic, molecular and PAH crystals and (b) Young's modulus (E) and the time necessary to halve the initial crystal size ($\tau_{1/2}$) of ionic, molecular and PAH crystals. The dashed lines are linear fits. Standard deviation of each data point is less than 4 % of its average value.

Ionic, molecular, and PAH crystals are held together by different types of intermolecular interactions. In ionic crystals, the major and minor intermolecular forces are ion-to-ion attraction and Van der Waals forces, respectively.[33] In contrast, molecular crystals and PAH crystals are held together by dipole-dipole interactions, created by partially charged ions, and Van der Waals forces. Additionally, the molecular crystals used herein are capable of forming intermolecular hydrogen bonds (Figure 3.8), which are not possible in PAH crystals. Ion-ion interactions are the strongest of the intermolecular forces, followed by hydrogen bonding, dipole-dipole interactions, and Van der Waals forces, respectively. Thus, the order of intermolecular bond strength with regard to the materials evaluated here is ionic crystals > molecular crystals > PAH crystals.

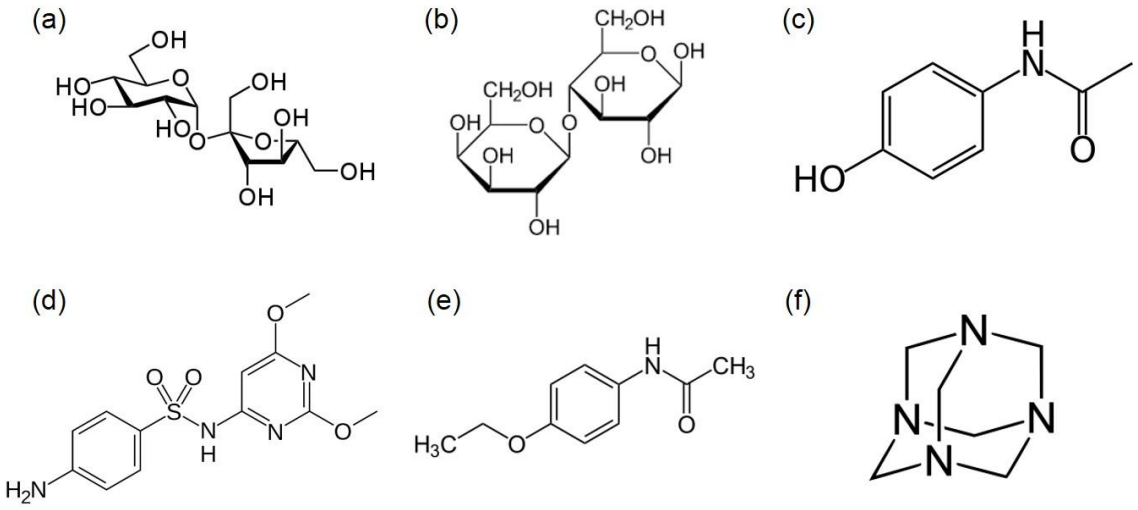

Figure 3.8 Molecular structure of six different molecular crystals: (a) sucrose, (b) lactose, (c) acetaminophen, (d) sulfadimethonxine, (e) phenacetin and (f) hexamethylenetetramine.

The length scale of order depends on the type of crystal due to the difference of the intermolecular bond strengths. Ionic crystals are held in long-range order while molecular and PAH crystals feature only short-range intermolecular interactions.[3-4] Particle breakage initiates from pre-existing defects in the particle, which propagate until cleavage is attained. The length scale of order may affect the propagation of cracks and thereby affect the sensitivity of sonofragmentation to a material's hardness. There are more parameters to affect particle breakage such as number and size of the initial defects.[34-35] Thus, the combined effect of the other parameters and the length scale of order may cause the different sensitivity of sonofragmentation to a material's hardness for ionic, molecular and PAH crystals.

3.3.4 Effect of initial crystal size

The effects of initial crystal size on sonofragmentation were also evaluated. Sucrose was prepared with seven different particle sizes by sieving in a sonic sifter (Figure 3.9). Grinding, sieving, and sonication were used to prepare the particles in Group 7. Figures 3.10 and 3.11 show the morphologies and crystal sizes of particles in each sucrose group. Initial crystal sizes ranged from 1054 μm down to 0.56 μm (Figure 3.12).

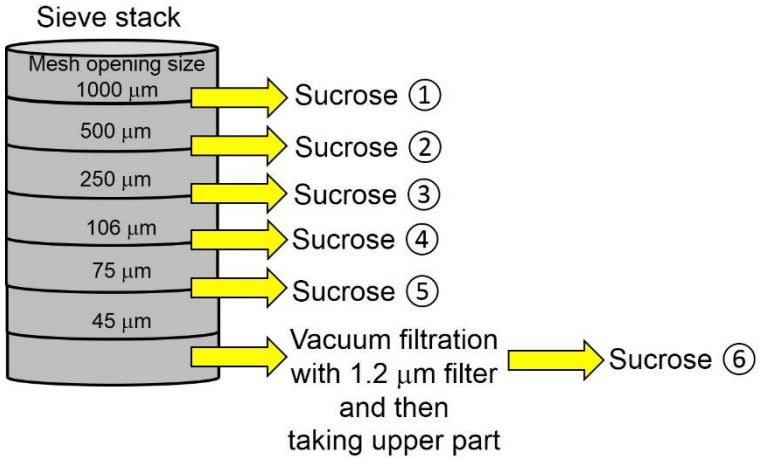

Figure 3.9 Preparation method of various sucrose groups containing different crystal size.

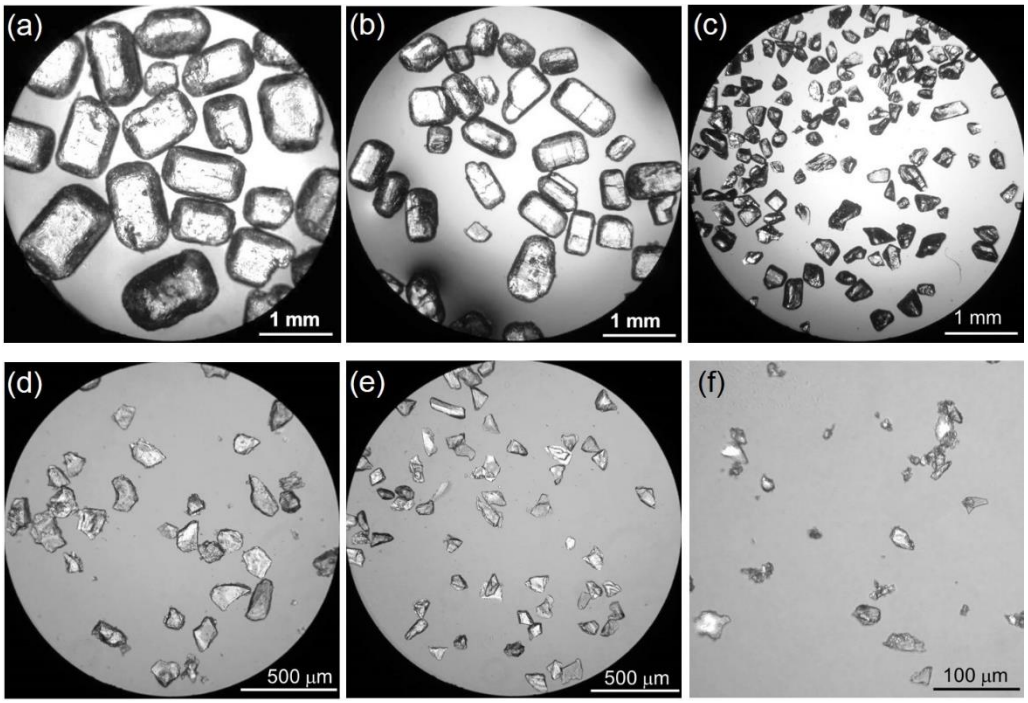

Figure 3.10 Optical microscopic images of sucrose in (a) group 1, (b) group 2, (c) group 3, (d) group 4, (e) group 5 and (f) group 6.

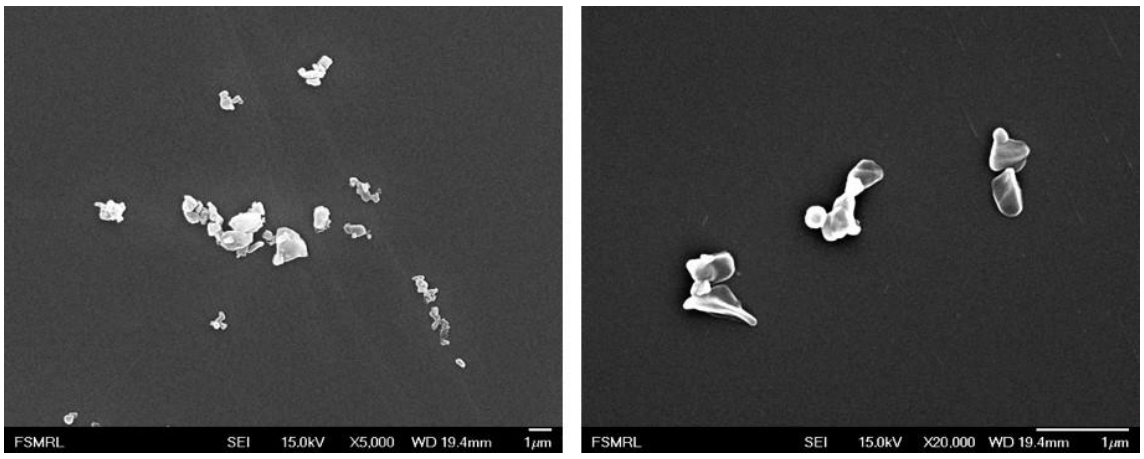

Figure 3.11 SEM images of sucrose in group 7.

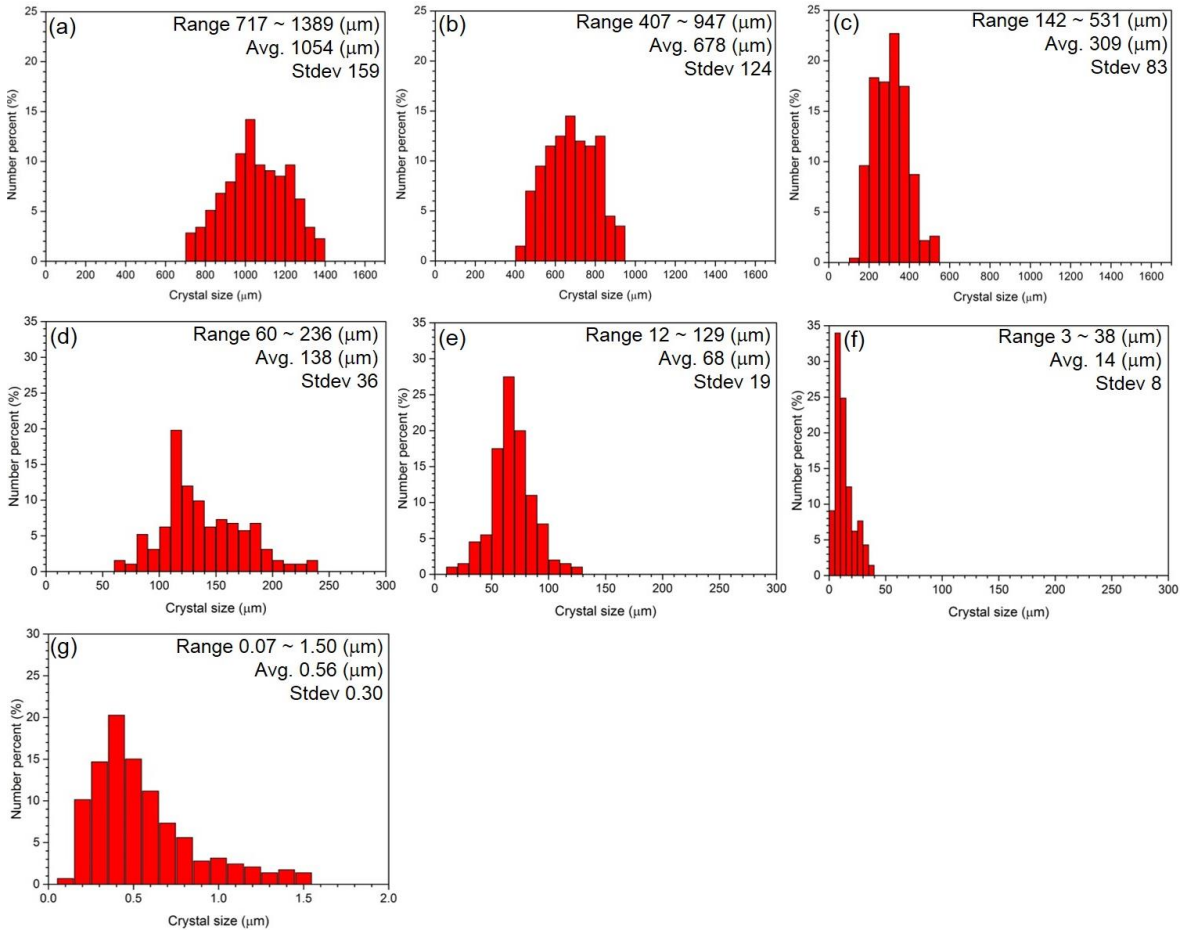

Figure 3.12 Crystal size distributions of sucrose in (a) group 1, (b) group 2, (c) group 3, (d) group 4, (e) group 5, (f) group 6 and (g) group 7.

No effects of initial crystal size were observed on the rates of fragmentation of molecular crystals when the initial crystal size was from 1054 to 68 μm (Figure 3.13). However, sonofragmentation was suppressed when the initial crystal was smaller than about 15 μm. No sonofragmentation was observed with crystals measuring about 0.56 μm. When the molecular crystal slurries were irradiated by ultrasound, the crystals were broken by direct interaction with shockwaves. Under continuous sonication, crystals kept breaking until they were too small to be fragmented by shockwaves passing through the slurry. When the crystals reach

smaller size than the minimum size for sonofragmentation, negative pressure of the irradiated ultrasound cannot exceed tensile strength over the length of the crystal. The minimum size for sonofragmentation may depend on the frequency and intensity of the irradiated ultrasound. In these experiments, performed using an ultrasound source operating at 20 kHz and 10 W/cm^2, molecular crystals smaller than about 0.56 μm did not experience any further breakdown.

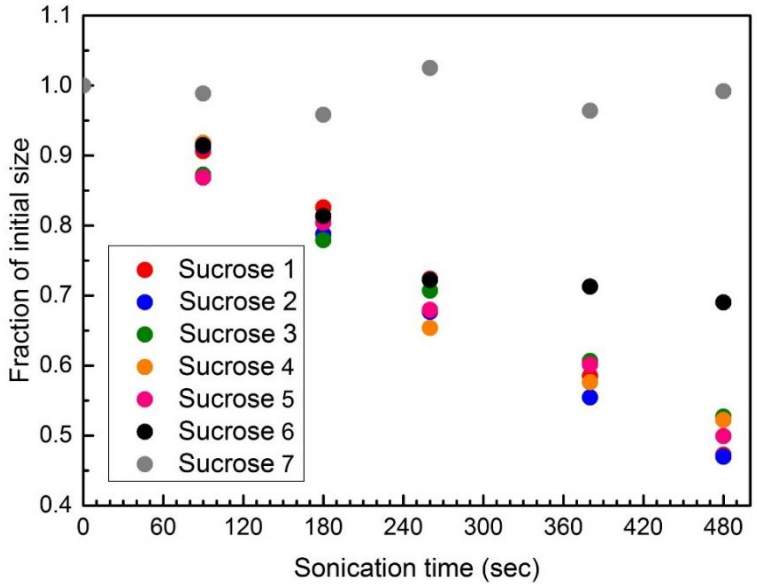

Figure 3.13 Effect of initial crystal size on fragmentation of sucrose. A slurry containing 0.2 wt% sucrose in 10 mL dodecane was sonicated using a titanium horn (10 W/cm^2 and 20 kHz). Standard deviation of each data point is less than 7 % of its average value.

3.4 Conclusion

Molecular crystals were sonofragmented by ultrasonic irradiation to the slurries of molecular crystals. The particle size of the molecular crystals decreased exponentially as the duration of sonication increased. There was a strong correlation between the rate of fragmentation and the Vickers hardness or Young's modulus of the parent material. Based on

comparisons of the sonofragmentation patterns obtained from ionic and molecular crystals, it was hypothesized that the length scale of intermolecular forces within a crystal affects sonofragmentation patterns.

3.5 References

1. Zeiger, B. W.; Suslick, K. S., Sonofragmentation of molecular crystals. *Journal of the American Chemical Society* **2011,** *133* (37), 14530-14533.

2. Atkins, P.; de Paula, J., *Physical chemistry*. 5th ed.; W. H. Freeman & Company: New York, 2009.

3. Vainshtein, B. K., *Fundamentals of crystals*. 2nd ed.; Springer-Verlag: Berlin, 1994; Vol. 1.

4. Mullin, J. W., *Crystallization*. 4th ed.; Butterworth-Heinemann: Oxford, 2001.

5. Guo, Z.; Jones, A. G.; Li, N.; Germana, S., High-speed observation of the effects of ultrasound on liquid mixing and agglomerated crystal breakage processes. *Powder Technology* **2007,** *171* (3), 146-153.

6. Gopi, K. R.; Nagarajan, R., Advances in nanoalumina ceramic particle fabrication using sonofragmentation. *Ieee Transactions on Nanotechnology* **2008,** *7* (5), 532-537.

7. Wagterveld, R. M.; Boels, L.; Mayer, M. J.; Witkamp, G. J., Visualization of acoustic cavitation effects on suspended calcite crystals. *Ultrasonics Sonochemistry* **2011,** *18* (1), 216-225.

8. Armstrong, M. R.; Senthilnathan, S.; Balzer, C. J.; Shan, B.; Chen, L.; Mu, B., Particle size studies to reveal crystallization mechanisms of the metal organic framework HKUST-1 during sonochemical synthesis. *Ultrasonics Sonochemistry* **2017,** *34*, 365-370.

9. Gao, R. X.; Gupta, I.; Boyden, E. S., Sonofragmentation of ultrathin 1D nanomaterials.

Particle & Particle Systems Characterization **2017,** *34* (1).

10. Agrawal, S. G.; Paterson, A. H. J., Secondary nucleation: mechanisms and models. *Chemical Engineering Communications* **2015,** *202* (5), 698-706.

11. Chow, R.; Blindt, R.; Chivers, R.; Povey, M., The sonocrystallisation of ice in sucrose solutions: primary and secondary nucleation. *Ultrasonics* **2003,** *41* (8), 595-604.

12. Chow, R.; Blindt, R.; Kamp, A.; Grocutt, P.; Chivers, R., The microscopic visualisation of the sonocrystallisation of ice using a novel ultrasonic cold stage. *Ultrasonics Sonochemistry* **2004,** *11* (3-4), 245-250.

13. Chow, R.; Blindt, R.; Chivers, R.; Povey, M., A study on the primary and secondary nucleation of ice by power ultrasound. *Ultrasonics* **2005,** *43* (4), 227-230.

14. Zhang, Z.; Sun, D. W.; Zhu, Z. W.; Cheng, L. N., Enhancement of crystallization processes by power ultrasound: current state-of-the-art and research advances. *Comprehensive Reviews in Food Science and Food Safety* **2015,** *14* (4), 303-316.

15. de Castro, M. D. L.; Priego-Capote, F., Ultrasound-assisted crystallization (sonocrystallization). *Ultrasonics Sonochemistry* **2007,** *14* (6), 717-724.

16. Cains, P. W.; Martin, P. D.; Price, C. J., The use of ultrasound in industrial chemical synthesis and crystallization. 1. Applications to synthetic chemistry. *Organic Process Research & Development* **1998,** *2* (1), 34-48.

17. Ruecroft, G.; Hipkiss, D.; Ly, T.; Maxted, N.; Cains, P. W., Sonocrystallization: the use of ultrasound for improved industrial crystallization. *Organic Process Research & Development* **2005,** *9* (6), 923-932.

18. Beckmann, W., *Crystallization: basic concepts and industrial applications*. John Wiley & Sons: New York, 2013.

19. Sivakumar, M.; Tang, S. Y.; Tan, K. W., Cavitation technology - a greener processing

technique for the generation of pharmaceutical nanoemulsions. *Ultrasonics Sonochemistry* **2014,** *21* (6), 2069-2083.

20. Castillo-Peinado, L. D.; de Castro, M. D. L., The role of ultrasound in pharmaceutical production: sonocrystallization. *Journal of Pharmacy and Pharmacology* **2016,** *68* (10), 1249-1267.

21. Raman, V.; Abbas, A., Experimental investigations on ultrasound mediated particle breakage. *Ultrasonics Sonochemistry* **2008,** *15* (1), 55-64.

22. Jordens, J.; Appermont, T.; Gielen, B.; Van Gerven, T.; Braeken, L., Sonofragmentation: effect of Ultrasound Frequency and Power on Particle Breakage. *Crystal Growth & Design* **2016,** *16* (11), 6167-6177.

23. Narducci, O.; Jones, A. G.; Kougoulos, E., An assessment of the use of ultrasound in the particle engineering of micrometer-scale adipic acid crystals. *Crystal Growth & Design* **2011,** *11* (5), 1742-1749.

24. Belkacem, N.; Salem, M. A. S.; AlKhatib, H. S., Effect of ultrasound on the physico-chemical properties of poorly soluble drugs: Antisolvent sonocrystallization of ketoprofen. *Powder Technology* **2015,** *285*, 16-24.

25. Meier, M.; John, E.; Wieckhusen, D.; Wirth, W.; Peukert, W., Influence of mechanical properties on impact fracture: Prediction of the milling behaviour of pharmaceutical powders by nanoindentation. *Powder Technology* **2009,** *188* (3), 301-313.

26. Taylor, L. J.; Papadopoulos, D. G.; Dunn, P. J.; Bentham, A. C.; Dawson, N. J.; Mitchell, J. C.; Snowden, M. J., Predictive milling of pharmaceutical materials using nanoindentation of single crystals. *Organic Process Research & Development* **2004,** *8* (4), 674-679.

27. Zugner, S.; Marquardt, K.; Zimmermann, I., Influence of nanomechanical crystal

properties on the comminution process of particulate solids in spiral jet mills. *European Journal of Pharmaceutics and Biopharmaceutics* **2006,** *62* (2), 194-201.

28. Mirtic, A.; Reynolds, G. K., Determination of breakage rate and breakage mode of roller compacted pharmaceutical materials. *Powder Technology* **2016,** *298*, 99-105.

29. Ichikawa, J.; Imagawa, K.; Kaneniwa, N., The effect of crystal hardness on compaction propensity. *Chemical & Pharmaceutical Bulletin* **1988,** *36* (7), 2699-2702.

30. Duncanhewitt, W. C.; Weatherly, G. C., Evaluating the hardness, Young's modulus and fracture toughness of some pharmaceutical crystals using microindentation techniques. *Journal of Materials Science Letters* **1989,** *8* (11), 1350-1352.

31. Perkins, M.; Ebbens, S. J.; Hayes, S.; Roberts, C. J.; Madden, C. E.; Luk, S. Y.; Patel, N., Elastic modulus measurements from individual lactose particles using atomic force microscopy. *International Journal of Pharmaceutics* **2007,** *332* (1-2), 168-175.

32. Neppiras, E. A., ACOUSTIC CAVITATION. *Physics Reports-Review Section of Physics Letters* **1980,** *61* (3), 159-251.

33. Atkins, P.; Overton, T.; Rourke, J.; Weller, M.; Amstrong, F., *Shriver and Atkins' inorganic chemistry*. 5th ed.; W. H. Freeman & Company: New York, 2010.

34. de Vegt, O.; Vromans, H.; Pries, W.; Maarschalk, K. V., The effect of crystal imperfections on particle fracture behaviour. *International Journal of Pharmaceutics* **2006,** *317* (1), 47-53.

35. de Vegt, O.; Vromans, H.; den Toonder, J.; Maarschalk, K. V., Influence of flaws and crystal properties on particle fracture in a jet mill. *Powder Technology* **2009,** *191* (1-2), 72-77.

Chapter 4

Spray sonocrystallization

4.1 Introduction

Controlling crystal size and size distribution are crucial in the pharmaceutical industry due to the effects of size on dissolution rates and bioavailability.[1-5] For orally-ingested drugs, pharmaceutical agents (PAs), once dissolved, must have sufficient lipophilicity to move across cell membranes but sufficient hydrophilicity to be transported within the body.[6-8] For moderately hydrophobic PAs, however, rates of dissolution after ingestion can be problematic unless the PA crystal size is sufficiently small.[9-10] Aerosol drugs also require control of the particle size and size distribution to successfully administer dosage: particles too large will not get into the deep lung, particles too small will be less easily trapped but more easily absorbed.[11] Parenteral (injected) drugs must also control particle size because potentially fatal embolisms can result with particles larger than ~5 μm.[12]

The application of ultrasound during crystallization (i.e., "sonocrystallization") has emerged as an effective means to reduce crystal size and maintain a narrow size distribution. When ultrasound is applied to a liquid, acoustic cavitation occurs: bubbles are formed in the liquid, oscillate and expand, and under certain conditions, implosively collapse.[13-15] Bubble collapse generates intense local heating (~5000 K), pressures (~10^5 kPa) and rapid heating and cooling rates (> 10^{10} K/s).[15-18] Acoustic cavitation and associated physical consequences of ultrasonic irradiation of liquids increase the number of crystals produced and decreases their size by increasing the rates of both primary and secondary nucleation of crystal growth.

The rates of primary nucleation of embryonic crystallites are increased by ultrasonic irradiation of liquids through three mechanisms: (1) Improved micro-scale mixing occurs from cavitation and associated turbulence, which accelerates diffusion rates of reactants, thus reducing induction times for crystallization.[19-22] Reduced induction time will increase the rate of nucleation by increasing the growth rates of embryonic crystallites, which prevents their redissolution.[23] (2) Through similar phenomena, ultrasound also reduces the metastable zone width (MZW, i.e., the range of metastability of a supersaturated solution in either temperature or antisolvent concentration[23]), which diminishes the rate of crystal growth and decreases crystal size.[21, 24-26] (3) The increase in gas-liquid interfaces produced by bubble formation, collapse, and fragmentation can also enhance nucleation rates.[23]

Rates of secondary nucleation are also increased by ultrasonic irradiation. Breakage of primary crystals due to interparticle collisions or more importantly shockwave fragmentation during sonication (i.e., "sonofragmentation")[27-28] increases the number of secondary nucleation sites, which results in increased numbers of smaller crystals. Turbulent flow from cavitation will also diminish crystal aggregation, which also produces smaller solid particulates with narrower size distribution.

Antisolvent crystallization (i.e., adding a miscible liquid in which the solute is poorly soluble) can generate a high level of supersaturation quickly and induce higher nucleation rates.[4, 23, 29-32] In principle, ultrasound should be beneficial for antisolvent crystallization through enhanced mixing between the antisolvent and solution; in practice, however, the ultrasound from a solid horn has been applied to the merging of fairly wide streams (25 mm) of solvent and antisolvent or to a large volume batch reactor of antisolvent into which the solute solution is pumped; this configurations lead to ineffective application of the ultrasound with relatively poor mixing, which typically generates multi-micron sized crystals.[33-38]

In this chapter, a spray sonocrystallization method is described here for the crystallization of pharmaceutical agents that provides for a tunable crystal size and narrow size distribution in the sub-micron regime. spray sonocrystallization uses a tapped, flow-through ultrasonic horn (20 kHz) to spray very fine droplets of the solute containing solution into a continuous flow of antisolvent which induces immediate crystallization with extremely effective mixing. The analgesic 2-carboxyphenyl salicylate (CPS) was explored as a test case.

4.2 Experimental

4.2.1 Materials

2-carboxyphenyl salicylate (CPS), polyvinylpyrrolidone (average mol wt 10,000) and sodium dodecyl sulfate (> 95 %) were purchased from Tokyo Chemical Industry, Sigma-Aldrich and Fisher Chemicals, respectively, and used as-received. Ethanol (100 %) was purchased from Decon Laboratory. Nanopure water (i.e., water deionized to >18 MΩ·cm resistance, scrubbed for organics, and passed through a 0.45 μm filter with a Barnstead NANOpure® ultrapure water purification system) was used as an antisolvent.

4.2.2 Spray sonocrystallization experimental setup

2-carboxyphenyl salicylate (CPS, Tokyo Chemical Industry, > 98.0 %) was dissolved in ethanol (Decon Labs, Inc., 100 %) to form a saturated CPS solution. The CPS solution was pumped with a syringe pump through a tapped ultrasonic horn (i.e., a hole drilled from top to bottom of the horn, cf. Figure 4.1; Sonics and Materials dual inlet atomizing probe VCX 130 AT, 20 kHz), exiting from the bottom (an acoustic antinode of the horn) into the mixing region of the flow cell into which the antisolvent (water) was also pumped. The CPS solution was

kept in a water bath (Fisher Scientific Isotemp 1006S) set to 18 °C prior to transferring to syringe. The solution was filtered using a syringe filter (Thermo Scientific Nalgene Syringe Filter, pore size 0.2 μm) and transferred to the syringe of a syringe pump (Harvard Apparatus Compact Infusion Pump), which was set to 0.08 mL/min. The ultrasonic horn was immersed in a flowing antisolvent of nanopure water (i.e., water deionized to >18 MΩ·cm resistance, scrubbed for organics, and passed through a 0.45 μm filter with a Barnstead NANOpure® ultrapure water purification system). The initial temperature of nanopure water was set to 18 °C using a water bath; its flow as set to 48 mL/min using a peristaltic pump (Cole-Parmer Instrument Company MasterFlex 77390-00). The CPS solution was rapidly dispersed into the antisolvent via momentum transfer from the ultrasonic horn. The ultrasonic power delivered by the tapped horn was calorimetrically determined and set to 15 W/cm^2. Aliquots of the sonicated mixture were collected every minute and diluted in 10 mL of nanopure water. For characterization, product was collected after a full steady state was reached, specifically after 6 min. The surfactants, polyvinylpyrrolidone (Sigma-Aldrich, average mol wt 10,000) and sodium dodecyl sulfate (Fisher Chemical, > 95 %) were dissolved in nanopure water, and those PVP and SDS aqueous solutions were used as the antisolvent and dilution solvent during product collection.

4.2.3 Sonocrystallization without flow experimental setup

For sonocrystallization without flow of an antisolvent, CPS solution and a round bottom flask containing 288 ml of nanopure water were kept in water bath in order to set to 18 °C. The CPS solution was filtered using a syringe filter and transferred to the syringe of a syringe pump, which was set to 0.08 mL/min. The ultrasonic horn (20 kHz, 15 W/cm^2) was immersed

in the round bottom flask and sonication was performed for 6 minutes from the time when the CPS solution and nanopure water were mixed. The equilibrium temperature, 25 °C, was reached after about 2 minutes. Aliquots of the sonicated mixture were collected and diluted in 10 mL of nanopure water. The surfactants, polyvinylpyrrolidone and sodium dodecyl sulfate were dissolved in nanopure water, and those PVP and SDS aqueous solutions were used as the antisolvent and dilution solvent during product collection.

4.2.4 Solubility test

Solutions of CPS in ethanol, 1-propanol, methanol, acetone, or a 1:600 v/v solution of ethanol in nanopure water were prepared at concentrations of 0.05, 0.10, 0.15 and 0.20 mM. UV-Vis absorption of each solution was measured by UV-Vis spectrometer (PerkinElmer Lambda 35). Molar absorptivity coefficients were calculated at the absorption peak at 308 nm. Saturated solutions in each solvent system was prepared by adding CPS in excess with stirring for 1 day at room temperature. The supernatants were filtered through a syringe filter (Thermo Scientific Nalgene Syringe Filter, pore size 0.2 μm) to remove any particulates of CPS before UV-Vis analysis. The initially saturated CPS solutions were diluted and UV-visible absorption spectra measured. In the case of pure water, the low solubility of CPS precluded measuring the molar absorptivity coefficient. For measurement of CPS solubilities in ethanol as a function of temperature, the same method was used with the ethanol solutions saturated at specific temperatures of 7, 12, 33, 46, 55. and 65 °C for 1 day.

4.2.5 Characterization

Particle size and zeta potential were measured at room temperature by Malvern Zetasizer

Nano ZS. Average values and standard deviations of results for the DLS (dynamic light scattering) measurements from eight measurements. Optical microscopy was performed with a Zeiss Axioskop optical/fluorescence microscope. The micrographs were captures using a Cannon PC1015 digital camera mounted to the microscope. Scanning electron microscopy was performed with a Hitachi S4700 High Resolution SEM and a JEOL 7000F Analytical SEM. Particle size analysis from SEM images was performed using Image-J (NIH). Powder X-ray diffraction patterns were obtained from samples mounted on a quartz sample holder using a Bruker D-5000 ($\lambda = 1.5418$ Å, 25 °C) in the 2θ range 5-50°; domain size was calculated with the Jade X-ray analysis program.

4.3 Results and discussion

4.3.1 Spray sonocrystallization system

Intense ultrasound with an antisolvent crystallization method in a continuous flow reactor equipped with a specially designed flow-through ultrasonic horn (Figure 4.1). The horn has a channel drilled down its center and the PA-solvent solution flows through that channel and is atomized upon its exit from the horn into a flowing stream of antisolvent. The momentum transfer and micromixing created by acoustic cavitation[13-15] forms a fine dispersion of the PA-solvent into the flowing antisolvent, which substantially increases the rate of solvent-antisolvent mixing and leads to rapid formation of nanocrystals at the 100 nm scale. As shown in Figure 4.2, thorough mixing of solvent and antisolvent occurs within 100 ms.

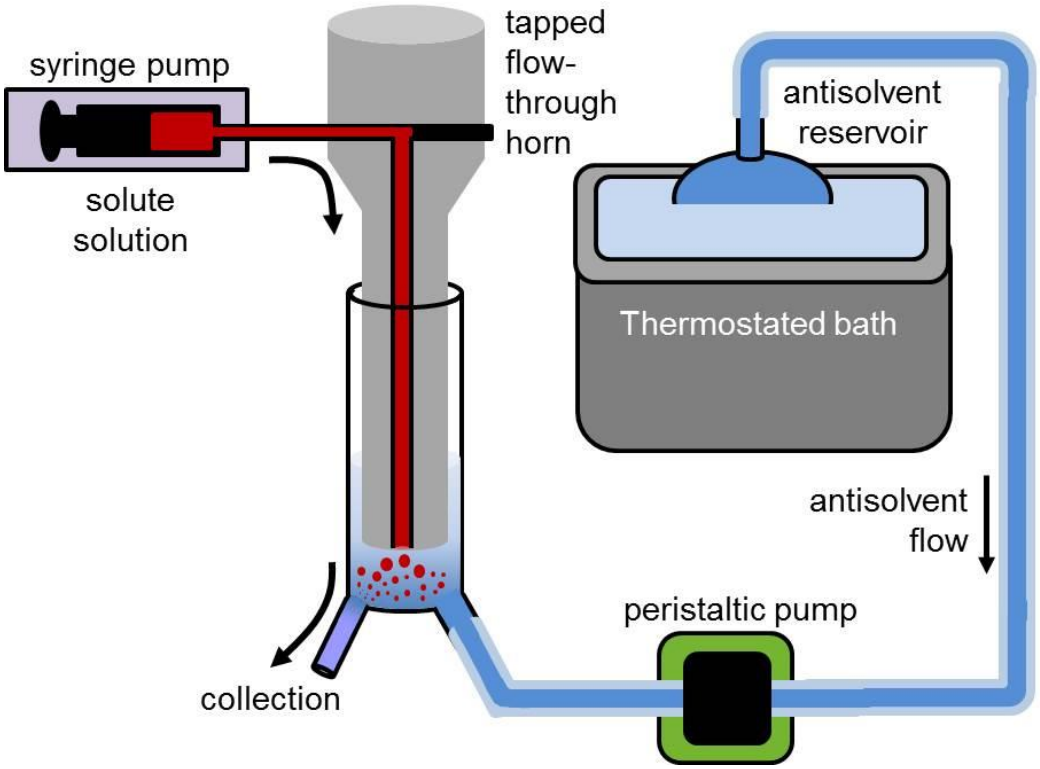

Figure 4.1 Tapped flow-through ultrasonic horn and experimental rig for spray sonocrystallization.

Figure 4.2 Mixing pattern of solution (red, flowing from the tapped ultrasonic horn) and antisolvent (white, flowing from the lower right) within the spray sonocrystallization rig. The second frame marks the start of sonication. Frames were extracted from video every 33 ms.

4.3.2 Solubility test of 2-carboxyphenyl salicylate (CPS)

The analgesic 2-carboxyphenyl salicylate (CPS) was selected as a model system. The solubility of CPS was determined at room temperature in various solvents (Table 4.1); for example, CPS has high solubility in ethanol (ca. 349 mg/ml), but is poorly soluble in water (<0.01 mg/ml). Based on solubility differences, ethanol and water were chosen as a solvent and an antisolvent, respectively. The solvent and antisolvent were mixed ultrasonically with a mixing ratio of water to CPS solution of 600:1. Thermal equilibration occurred rapidly (< 1 min) after energizing the ultrasonic horn (~7 °C rise); unless otherwise specified eaction zone temperature was 25 °C.

Table 4.1 Solubility of CPS in selected solvents.

Solvent	**Nanopure Water**	**Ethanol-Water 1:600 v/v**	**1-Propanol**	**Ethanol**	**Methanol**	**Acetone**
Solubility of CPS (mg ml^{-1})	< 0.01	0.08	257	349	494	702

4.3.3 Spray sonocrystallization of CPS

Spray sonocrystallization produced CPS nanocrystals. Particle size measurements were made by dynamic light scattering (DLS) measurements after 6 min, by which time a crystal size steady state was fully realized (Figure 4.3). The average crystal diameter is 91 ± 5 nm and 96% of crystals are in the size range between ca. 60 and 190 nm (Figure 4.4). The zeta potential of sonocrystallized CPS is -37 ± 6 mV, which is considered in the moderate stability range (± 30 ~ ± 40 mV).[39]

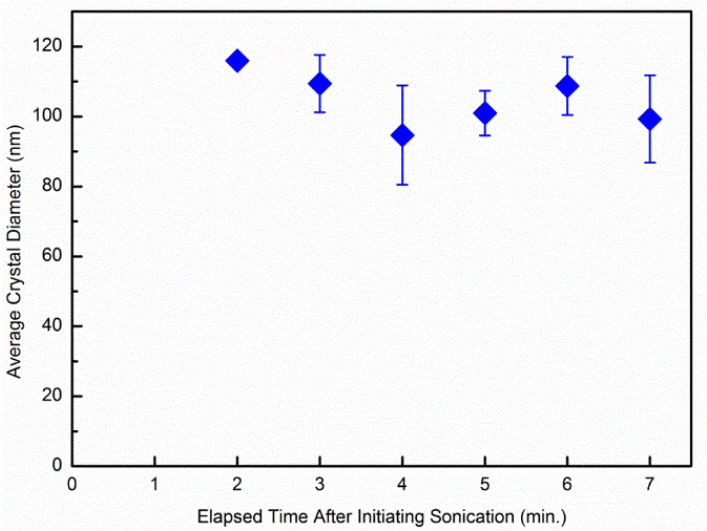

Figure 4.3 Crystal size of sonocrystallized CPS as a function of flow time. Steady state is achieved after ~3 min. Reliable DLS measurements were not available for the sample of 1 minute due to high polydispersivity. The error bar of data at 2 min. is smaller than the diamond symbol. Saturated CPS solutions in ethanol were mixed into water with a flow ratio of 1:600 at 25°C.

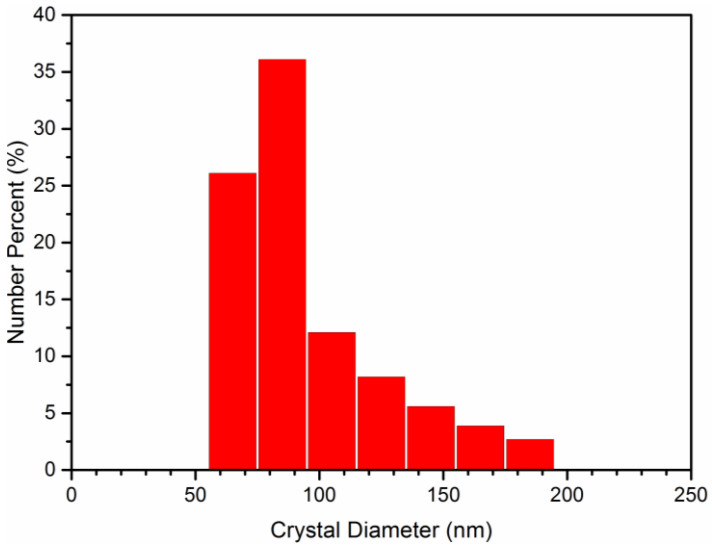

Figure 4.4 Crystal size distribution of sonocrystallized CPS from size analysis of SEM images. Sonicated CPS sample without a surfactant was collected after 6 min. after energizing the horn. Saturated CPS solutions in ethanol were mixed into water with a flow ratio of 1:600 at 25 °C.

The sonocrystallized CPS crystals in solution are well dispersed, but after centrifugation or evaporation agglomeration occurs; the agglomerates consist of ca. 100 nm crystals, which match the average crystal diameter value from solution DLS measurements (Figure 4.5).

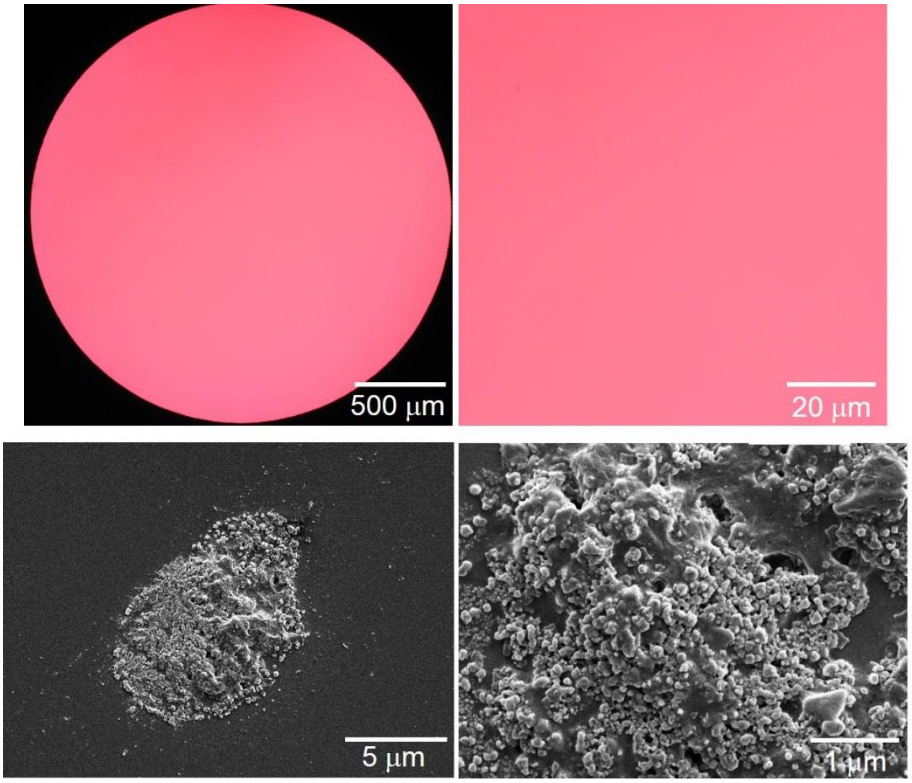

Figure 4.5 Microscopic images of sonocrystallized CPS: (Top) optical microscope images of sonocrystallized CPS in the collecting solvent (i.e. too small to see optically), (Bottom) SEM images of sonocrystallizaed CPS after evaporation.

4.3.4 Control experiments

4.3.4.1 Antisolvent crystallization of CPS with stirring

Repeating CPS crystallization in the same cell with the same flow in the absence of ultrasound, but with mechanical mixing (900 rpm, magnetic stir bar), failed to yield product measurable by DLS due to formation of large crystals and aggregation (> ~100 μm).

Mechanically stirred flow crystallization produces ~10 micron sized crystals that are heavily aggregated (Figure 4.6). Despite the agglomeration of the sonocrystallized CPS after evaporation (Figure 4.5), there is a clear size reduction of the crystals compared to crystallizations that employ the same flow but with mechanical stirring instead of ultrasound.

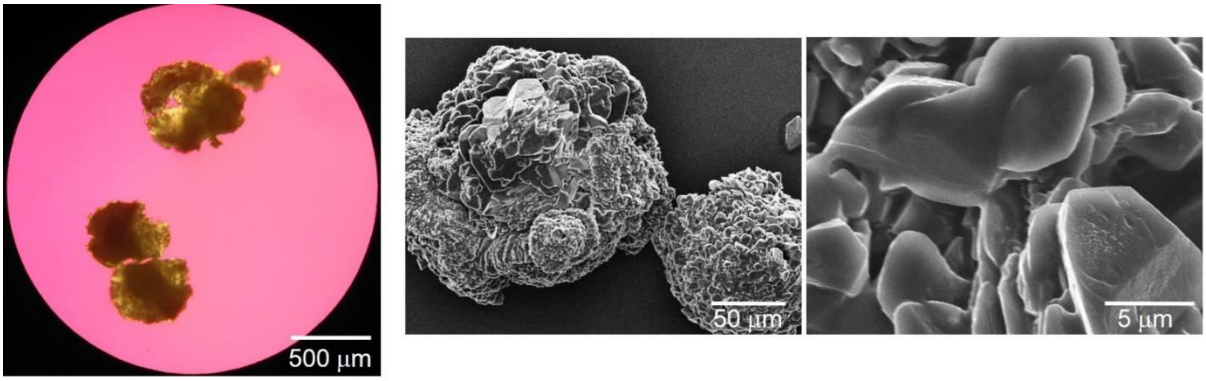

Figure 4.6 Microscopic images of CPS crystallized via 900 rpm mechanical stirring: (Left) Optical microscope images of stirred CPS in the collecting solvent, (Right) SEM images of stirred CPS after evaporation.

4.3.4.2 Spray sonocrystallization of CPS without antisolvent flow

CPS crystals were generated by sonocrystallization in the absence of antisolvent flow. The size of each crystal was ~5 micron size and crystals were heavily agglomerated. Thus, crystal size reduction was only achieved when sonocrystallization was performed in flow system (Figure 4.7).

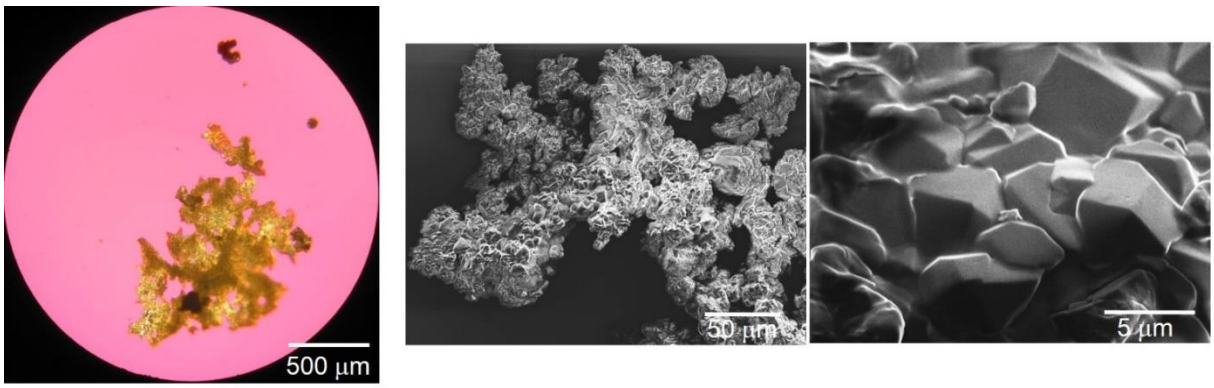

Figure 4.7 Microscopic images of sonocrystallizaed CPS without flow of the antisolvent: (Left) Optical microscope images of sonocrystallized CPS in the collecting solvent, (Right) SEM images of sonocrystallized CPS after evaporation. Saturated CPS solutions in ethanol were mixed into water with a ratio of 1:600 at 25 °C.

4.3.5 Addition of surfactant in spray sonocrystallization of CPS

Sonocrystallized CPS nanoparticels were dispersed well in the collecting solvent, but they were heavily aggregated after the evaporation of the solvent. The addition of surfactants was examined to improve the redispersion of CPS nanocrystals during their isolation (e.g., by centrifugation, or evaporation); specifically, either a nonionic (polyvinylpyrrolidone, PVP) or an anionic surfactant (sodium dodecyl sulfate, SDS) were added to the antisolvent before the spray sonocrystallization. Crystal size was only mildly affected by the surfactant addition (Table 4.2 and Figures 4.8-9).

Table 4.2 Average crystal size and zeta potential of sonocrystallized CPS from DLS Measurement.

Surfactant Concentration, wt%	No surfactant	PVP 0.001	PVP 0.01	SDS 0.001	SDS 0.01
Crystal Size, nm	91 ± 5	106 ± 4	99 ± 7	121 ± 9	127 ± 4
Zeta Potential, mV	-37 ± 6	-13 ± 2	-18 ± 2	-60 ± 4	-76 ± 9

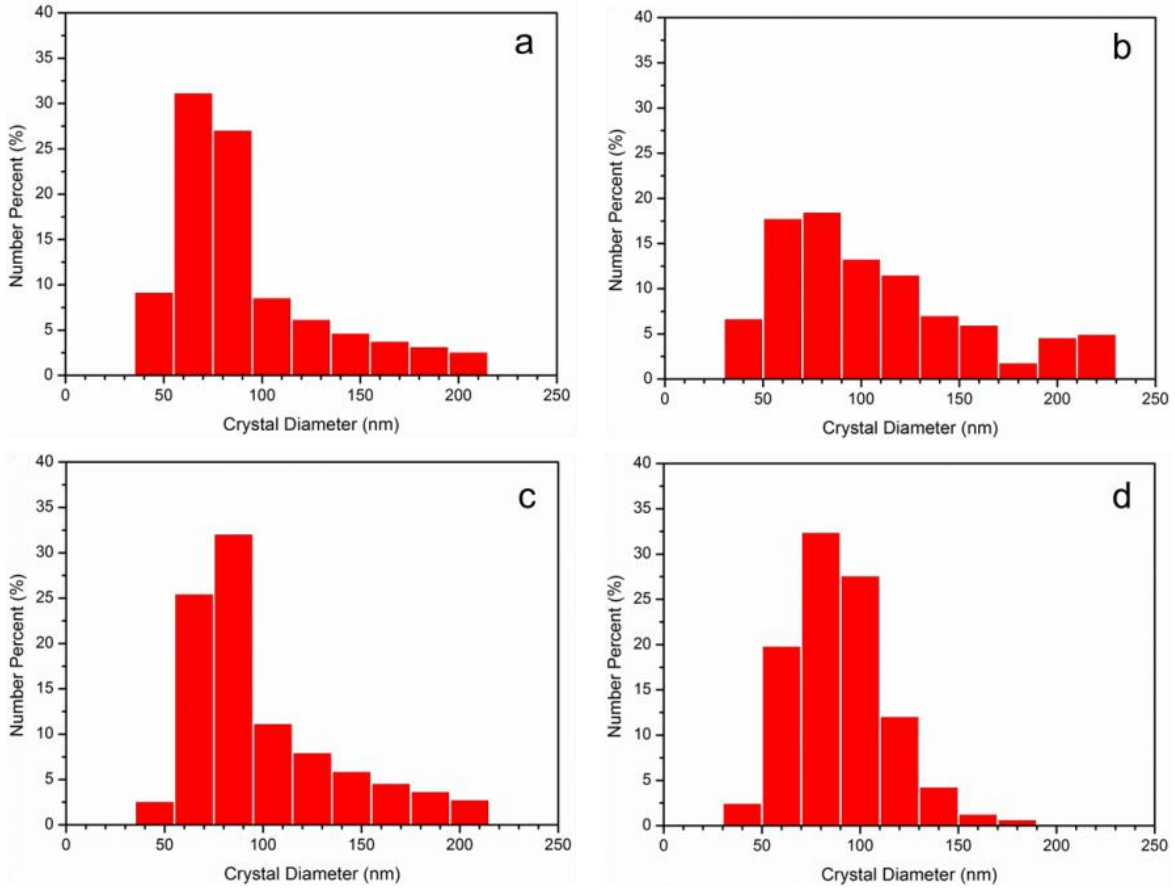

Figure 4.8 Crystal size distributions of sonocrystallized CPS-PVP 0.001 wt% from (a) DLS measurements and (b) particle size analysis of SEM images; sonocrystallized CPS-PVP 0.01 wt% from (c) DLS measurement and (d) particle size analysis of SEM images.

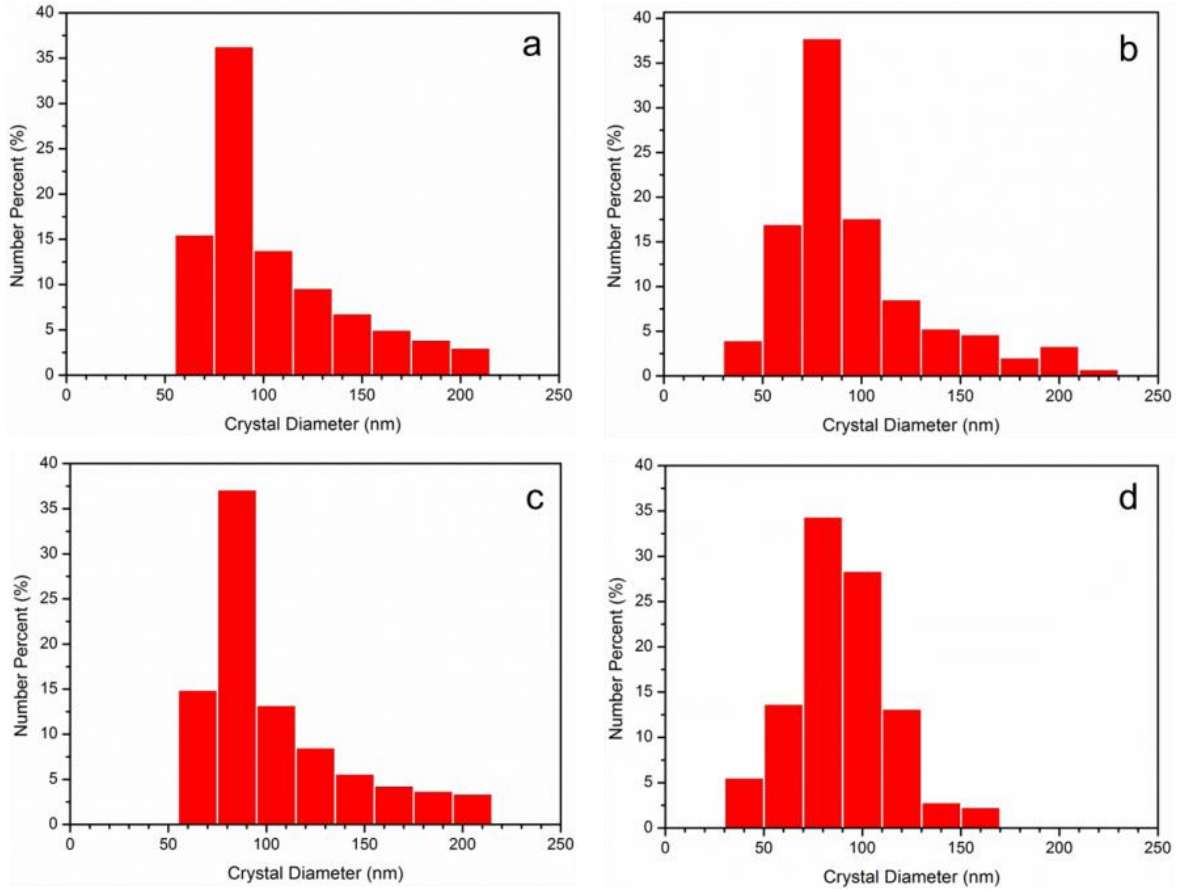

Figure 4.9 Crystal size distribution of sonocrystallized CPS-SDS 0.001 wt% from (a) DLS measurements and (b) particle size analysis of SEM images; sonocrystallized CPS-SDS 0.01 wt% from (c) DLS measurement and (d) particle size analysis of SEM images.

The surface charge (i.e., zeta potential) of sonocrystallized CPS is affected by the addition of surfactants, as expected. Addition of PVP diminishes the surface charge of the CPS-PVP nanocrystals since PVP increases the thickness of the diffuse double layer.[40] As expected, addition of SDS significantly increases the zeta potential of the CPS-SDS crystals, placing them in the excellent stability range (> ± 40),[39] and reduces the expected likelihood of aggregation.

PVP is often used as a dispersant for colloidal solutions and works as a sterically bulky coating of nanoparticles to prevent aggregation. SDS, on the other hand, has a strong negative

charge in aqueous solutions and it can prevent aggregation by providing a surface charge upon adsorption to nanoparticle surfaces. Indeed, both surfactants work well to preserve the dispersion of the sonocrystallized nanoparticles. The sonocrystallized CPS-PVP nanocrystals are well-dispersed due to the steric bulk of the PVP substituents, whereas SDS is effective at minimizing agglomeration of CPS crystals, due to the anionic nature of SDS and the resulting more negative zeta potential of CPS-SDS nanocrystals (Figure 4.10).

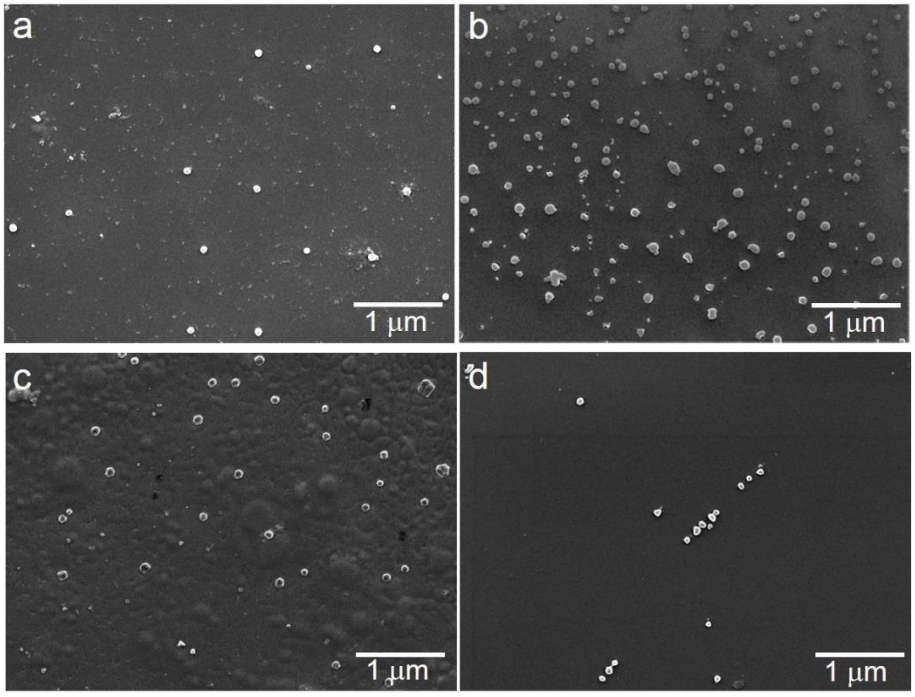

Figure 4.10 SEM images of sonocrystallized CPS with the addition of surfactants to the antisolvent (i.e., water): (a) 0.001 wt% PVP, (b) 0001 wt% PVP, (c) 0.001 wt% SDS and (d) 0.01 wt% SDS.

Addition of PVP or SDS to solutions that undergo CPS crystallization via mechanical stirring, however, still yielded massively agglomerated product (Figures 4.11-12). In the absence of antisolvent flow, sonocrystallized CPS are not dispersed and yield an agglomerated product (Figures 4.13-14) even in the presence of PVP or SDS.

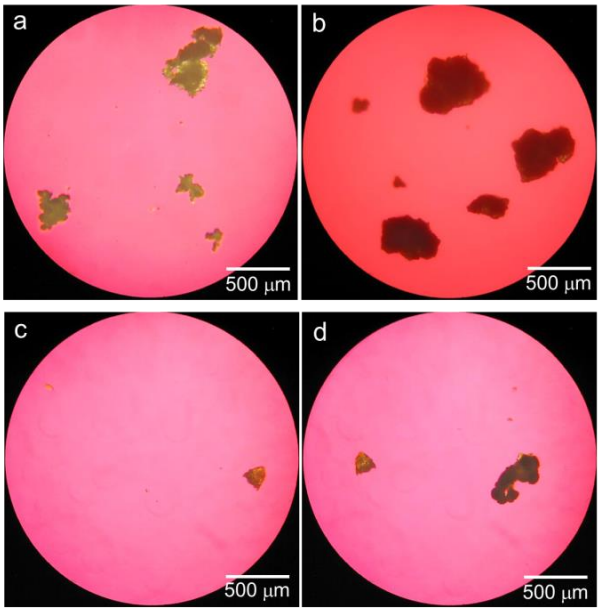

Figure 4.11 Optical microscopy micrographs of the solid obtained with rapid mechanical stirring (900 rpm) only; (a) CPS-PVP 0.001 wt%, (b) CPS-PVP 0.01 wt%, (c) CPS-SDS 0.001 wt%, (b) CPS-SDS 0.01 wt%.

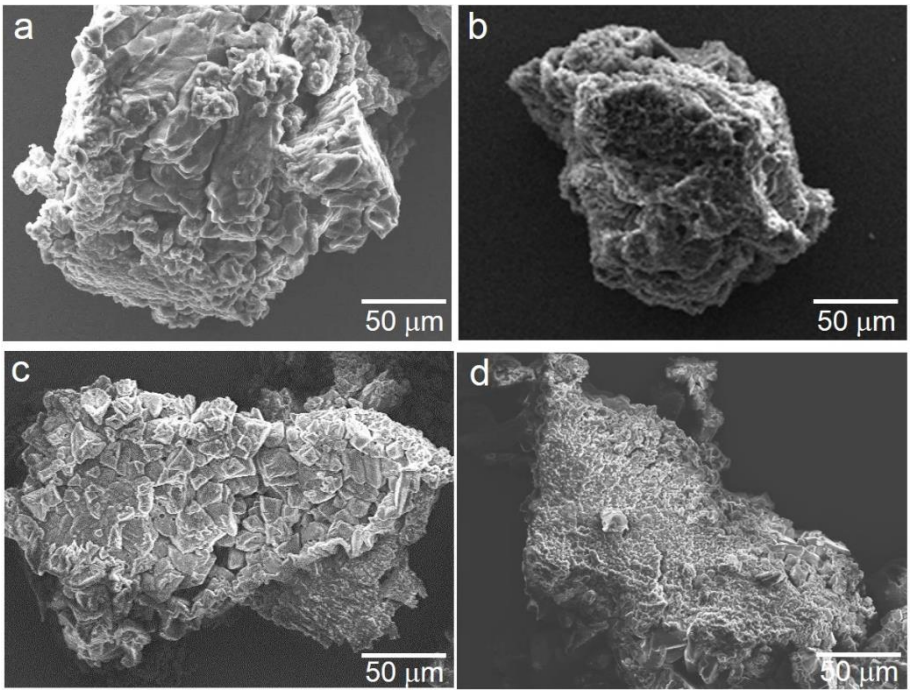

Figure 4.12 (cont.)

Figure 4.12 SEM images of mechanically stirred (900 rpm) crystallization of CPS with the addition of surfactants to the antisolvent (i.e., water): (a) 0.001 wt% PVP, (b) 0.01 wt% PVP, (c) 0.001 wt% SDS and (d) 0.01 wt% SDS.

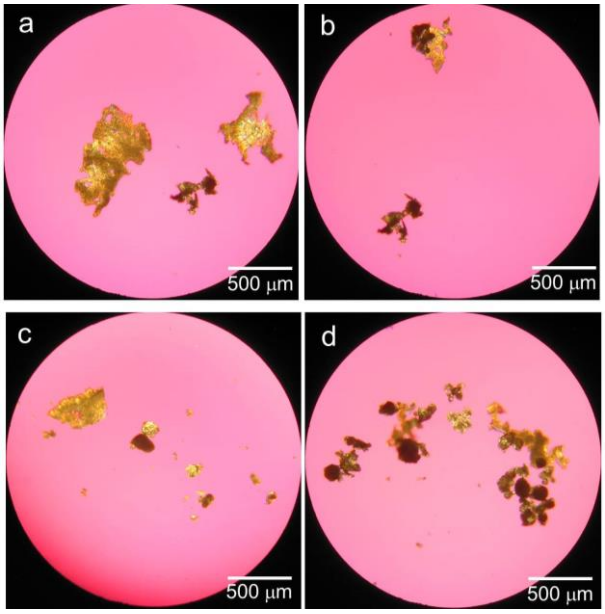

Figure 4.13 Optical microscopy micrographs of the solid obtained from sonocrystallization of CPS without flow of the antisolvent; (a) CPS-PVP 0.001 wt%, (b) CPS-PVP 0.01 wt%, (c) CPS-SDS 0.001 wt%, (b) CPS-SDS 0.01 wt%.

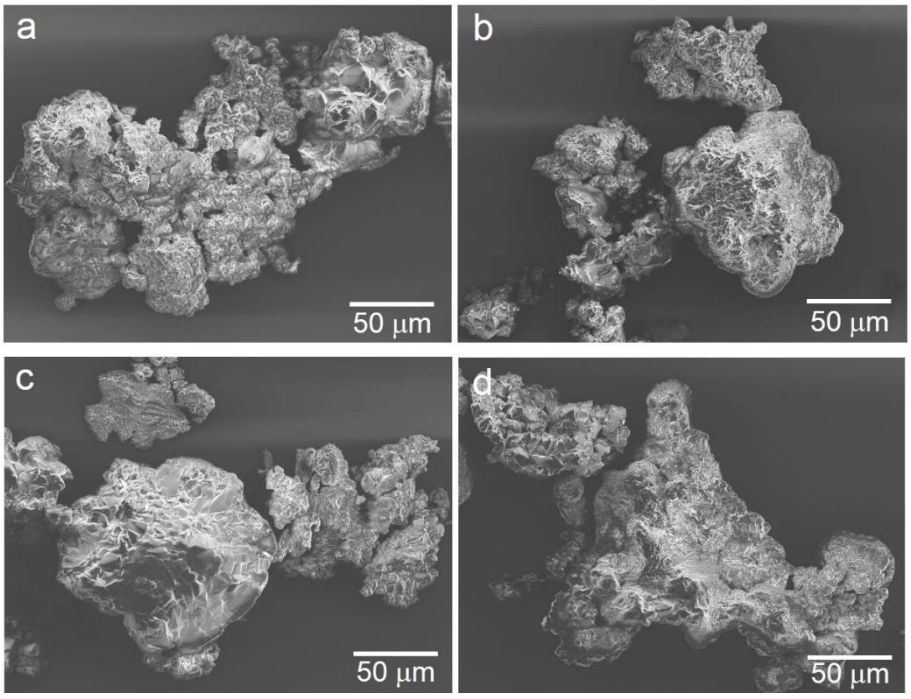

Figure 4.14 Sonocrystallized CPS with the addition of surfactants to the antisolvent (i.e., water) and the absence of the antisolvent flowing: (a) 0.001 wt% PVP, (b) 0.01 wt% PVP, (c) 0.001 wt% SDS, and (d) 0.01 wt% SDS.

4.3.6 Powder X-ray diffraction patterns

Powder x-ray diffraction established good crystallinity in sonocrystallized CPS, CPS-PVP, and CPS-SDS nanocrystals, as well as crystals from mechanical stirring (Figures 4.15-16). There was no significant change of crystal domain size for all samples (Table 4.3).

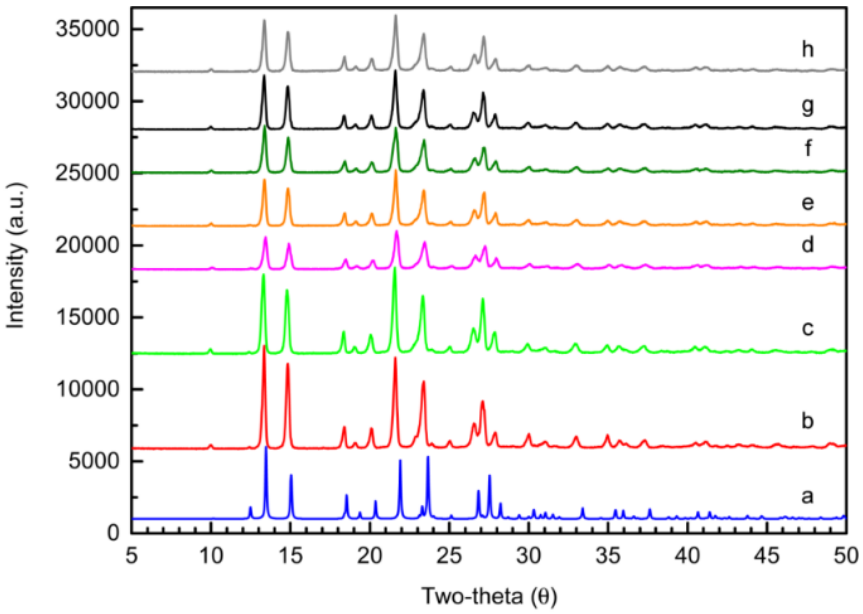

Figure 4.15 Powder X-ray diffraction patterns with and without addition of PVP. (a) CPS calculated from single crystal X-ray diffraction data, (b) as-purchased CPS, (c) sonocrystallized CPS, (d) CPS crystallized via mechanical stirring, (e) sonocrystallized CPS-PVP 0.001 wt%, (f) CPS-PVP 0.001 wt% crystallized via mechanical stirring, (g) sonocrystallized CPS-PVP 0.01 wt% and (h) CPS-PVP 0.01 wt% crystallized via mechanical stirring. Single crystal data was reported in the Cambridge Structural Database (refcode WOQDAH). Single crystal data was collected at 150 K and powder patterns were collected at room temperature.

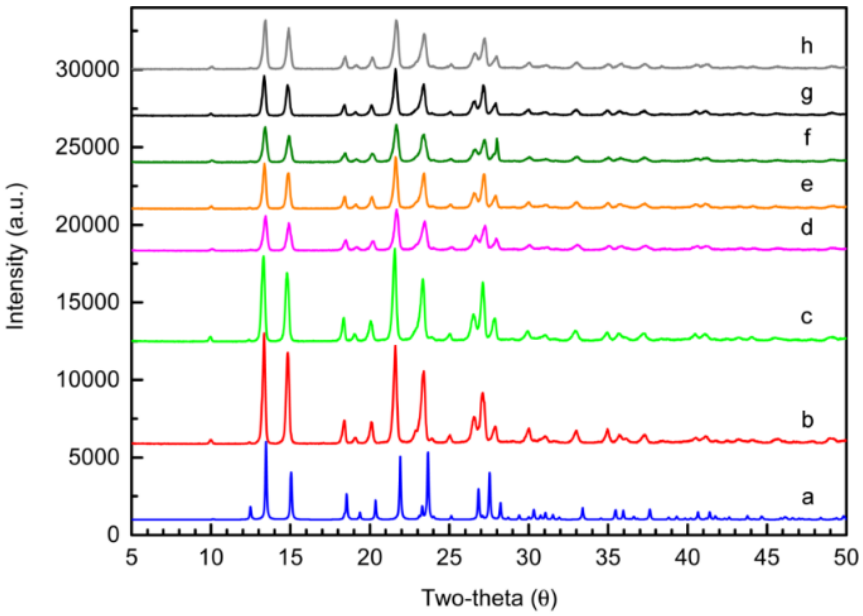

Figure 4.16 Powder X-ray diffraction patterns of (a) CPS calculated from single crystal X-ray diffraction data, (b) as-purchased CPS, (c) sonocrystallized CPS, (d) CPS crystallized via mechanical stirring, (e) sonocrystallized CPS-SDS 0.001 wt%, (f) CPS-SDS 0.001 wt% crystallized via mechanical stirring, (g) sonocrystallized CPS-SDS 0.01 wt% and (h) CPS-SDS 0.01 wt% crystallized via mechanical stirring. Single crystal data was reported in the Cambridge Structural Database (refcode WOQDAH). Single crystal data was collected at 150 K and powder patterns were collected at room temperature.

Table 4.3 Crystal domain size of CPS samples with and without addition of PVP or SDS, determined from the Debye-Scherrer equation.

Sample	Domain Size (nm)
Purchased CPS	58
Sonocrystallized CPS	51
CPS crystallized via mechanical stirring	38
Sonocrystallized CPS-PVP 0.001 wt%	51
CPS-PVP 0.001 wt% crystallized via mechanical stirring	49
Sonocrystallized CPS-PVP 0.01 wt%	47
CPS-PVP 0.01 wt% crystallized via mechanical stirring	39
Sonocrystallized CPS-SDS 0.001 wt%	49
CPS-SDS 0.001 wt% crystallized via mechanical stirring	36

Table 4.3 (cont.)

Sonocrystallized CPS-SDS 0.01 wt%	47
CPS-SDS 0.01 wt% crystallized via mechanical stirring	35

For pharmaceutical agents, a significant problem can be the conversion of metastable crystallites to other morphologies. For this reason, it was examined the powder X-ray diffraction (PXRD) of sonocrystallized CPS over a period of several months. CPS crystals, which were generated without or with a surfactant, were centrifuged and dried in a vacuum oven at room temperature immediately after sonocrystallization. They were then stored at room temperature in air as a dried powder and the powder X-ray diffraction was measured periodically: no changes in the PXRD were observed over a 10 months period (Figure 4.17).

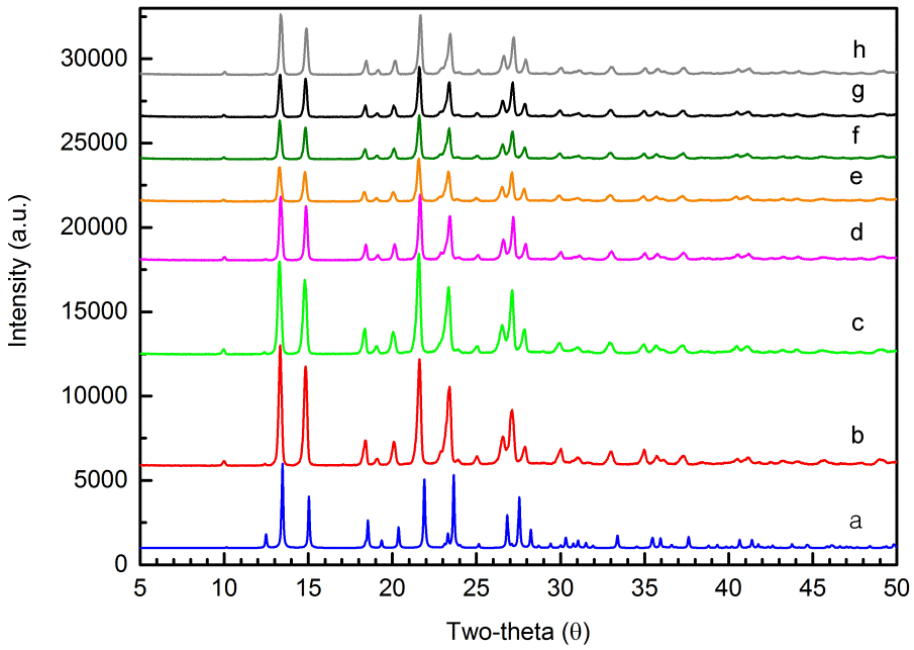

Figure 4.17 Powder X-ray diffraction patterns of (a) CPS calculated from single crystal X-ray diffraction data, (b) as-purchased CPS, (c) sonocrystallized CPS, (d) sonocrystallized CPS after 10 months, (e) sonocrystallized CPS-PVP 0.001 wt% after 10 months, (f) sonocrystallized CPS-PVP 0.01 wt% after 10 months, (g) sonocrystallized CPS-SDS 0.001 wt% after 10 months, (h) sonocrystallized CPS-SDS 0.01 wt% after 10 months Single crystal data

Figure 4.17 (cont.)

was reported in the Cambridge Structural Database (refcode WOQDAH). Single crystal data was collected at 150 K and powder patterns were collected at room temperature.

4.3.7 Modifications of control variables

In our spray sonocrystallization method, there are various parameters that might affect the sonocrystallization process, including ultrasonic power, flow rate of both antisolvent and solute solution, concentration of pharmaceutical agent, etc. We have found that the spray sonocrystallization process is robust to most of these variables: the only parameter that has a significant effect on nanocrystal size is the initial solute concentration. Based on DLS measurements, there were no significant changes to average crystal size when ultrasonic power and flow rate were systematically changed (Table 4.4-5). Similarly, the use of different solvents gave rise to only modest changes in the average crystal size.

Table 4.4 Effect of ultrasonic power. With horn turned off, CPS crystals formed micron sized aggregations, and DLS measurement was not possible.

Ultrasonic Power (W/cm^2)	**Crystal Size (± s.d.), nm**
0	N/A (large agglomerates)
5	91 (± 14)
15	91 (± 5)
25	116 (± 12)

Table 4.5 Effect of flow rate with fixed mixing ratio between antisolvent and CPS solution (600 : 1).

Flow Rate of Antisolvent (ml/min)	Flow Rate of CPS Solution (ml/min)	Crystal Size (± s.d.), nm
48	0.08	91 (± 5)

Table 4.5 (Cont.)

30	0.049	96 (± 7)
20	0.033	111 (± 11)

In contrast, however, as the concentration of CPS was increased in the acetone solute solution, the average crystal size also increased (with water as the antisolvent), as shown in Figure 4.18 and Table 4.6. The CPS concentration was also modified via temperature changes using saturated solutions initially over the range of 7 to 46 °C. As temperature increases, the solubility of CPS increases exponentially (Figure 4.19), and the average crystal size also increases (Figure 4.18, Table 4.7). Based on the results of sonocrystallized CPS in acetone and ethanol with various concentrations, it can be concluded that the higher concentration of CPS produces larger crystals (Figure 4.18), with an accessible nanocrystal size range of 80 to 180 nm, in this system.

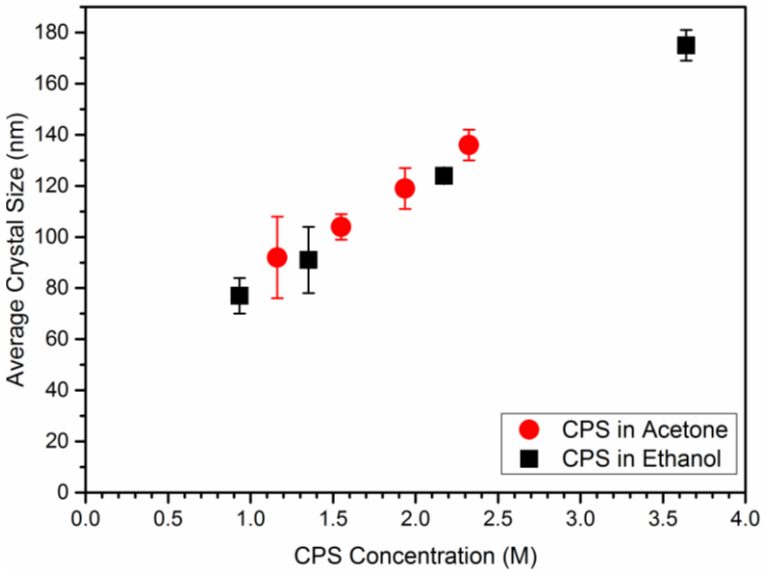

Figure 4.18 Effect of initial CPS concentration on sonocrystallized CPS size. For acetone, all experiments were at 25 °C; for ethanol, solutions were saturated and crystallizations run at different initial temperatures ranging from 7 to 46 °C.

Table 4.6 Effect of initial CPS concentration in acetone at 25 °C.

Dissolved amount of CPS, mg/ml	Initial CPS Concentration, M	Crystal Size (± s.d.), nm
100	0.39	No crystals
200	0.77	No crystals
300	1.16	91 (± 7)
400	1.55	104 (± 13)
500	1.94	119 (± 3)
600	2.32	136 (± 6)
700* (Saturated solution)	2.71	N/A (aggregation)

*For this highest concentration (a saturated solution of CPS), aggregated crystals appeared immediately upon mixing of water and CPS solution even in the presence of ultrasound, due to the large solubility difference between CPS in acetone (702 mg/ml) vs. water (< 0.01 mg/ml).

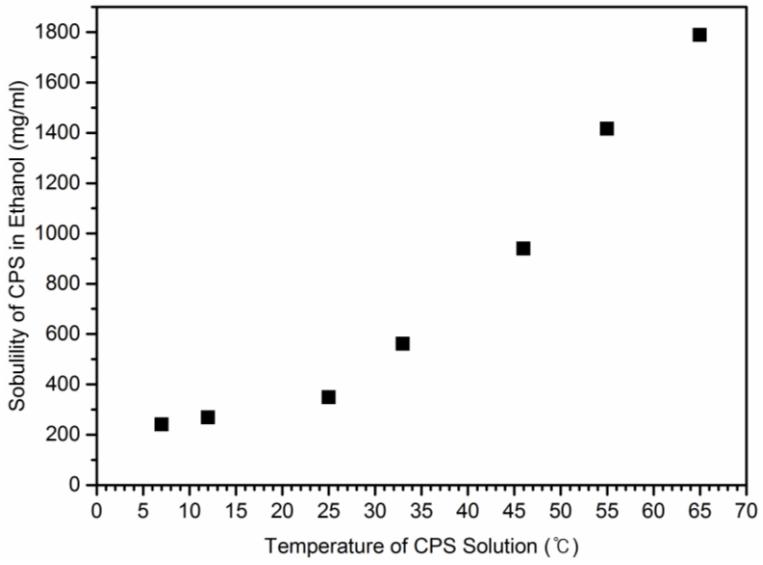

Figure 4.19 Solubility of CPS in ethanol at a function of temperature.

Table 4.7 Effect of initial CPS concentration in ethanol at different temperatures. Initial solutions of CPS were saturated at each temperature.

Temperature of Initial CPS Solution (°C)*	Dissolved amount of CPS (mg/ml)	Initial CPS Concentration (M)	Crystal Size (± s.d.), nm
7	241	0.93	77 (± 16)
25	349	1.35	91 (± 5)
33	561	2.17	124 (± 8)
46	940	3.64	175 (± 6)

* Final steady state temperatures in the mixing zone were 12, 25, 40, and 55°C, respectively.

4.4 Conclusion

The spray sonocrystallization method produces nanoscaled pharmaceutical molecular crystals with a narrow size distribution. Nanocrystal size can be easily controlled through solute concentration. Nonionic and anionic surfactants, PVP and SDS, effectively reduce aggregation of the nanocrystals. Given the lower ultrasonic power demands necessary for these laboratory scale experiments, we have some confidence that one may achieve scale-up to kg levels without great difficulty.

4.5 References

1. Erdemir, D.; Lee, A. Y.; Myerson, A. S., Nucleation of crystals from solution: classical and two-step models. *Acc. Chem. Res.* **2009,** *42* (5), 621-629.

2. Chen, J.; Sarma, B.; Evans, J. M.; Myerson, A. S., Pharmaceutical crystallization. *Cryst. Growth Des.* **2011,** *11* (4), 887-895.

3. Duncan, R.; Gaspar, R., Nanomedicine (s) under the microscope. *Mol. Pharmaceutics* **2011,** *8* (6), 2101-2141.

4. D'Addio, S. M.; Prud'homme, R. K., Controlling drug nanoparticle formation by rapid

precipitation. *Adv. Drug Deliv. Rev.* **2011,** *63* (6), 417-426.

5. Abu Bakar, M. R.; Nagy, Z. K.; Saleemi, A. N.; Rielly, C. D., The impact of direct nucleation control on crystal size distribution in pharmaceutical crystallization processes. *Cryst. Growth Des.* **2009,** *9* (3), 1378-1384.

6. Liversidge, G. G.; Cundy, K. C., Particle size reduction for improvement of oral bioavailability of hydrophobic drugs: I. Absolute oral bioavailability of nanocrystalline danazol in beagle dogs. *Int. J. Pharm.* **1995,** *125* (1), 91-97.

7. Amidon, G. L.; Lennernäs, H.; Shah, V. P.; Crison, J. R., A theoretical basis for a biopharmaceutic drug classification: the correlation of in vitro drug product dissolution and in vivo bioavailability. *Pharm. Res.* **1995,** *12* (3), 413-420.

8. Balaz, S., Modeling kinetics of subcellular disposition of chemicals. *Chem. Rev.* **2009,** *109* (5), 1793-1899.

9. Kesisoglou, F.; Panmai, S.; Wu, Y., Nanosizing—oral formulation development and biopharmaceutical evaluation. *Adv. Drug Deliv. Rev.* **2007,** *59* (7), 631-644.

10. Sun, W.; Mao, S.; Shi, Y.; Li, L. C.; Fang, L., Nanonization of itraconazole by high pressure homogenization: stabilizer optimization and effect of particle size on oral absorption. *J. Pharm. Sci.* **2011,** *100* (8), 3365-3373.

11. Kleinstreuer, C.; Zhang, Z.; Donohue, J., Targeted drug-aerosol delivery in the human respiratory system. *Annu. Rev. Biomed. Eng.* **2008,** *10*, 195-220.

12. Devadasu, V. R.; Bhardwaj, V.; Kumar, M. R., Can controversial nanotechnology promise drug delivery? *Chem. Rev.* **2012,** *113* (3), 1686-1735.

13. Leighton, T., *The Acoustic Bubble*. Academic Press: 1994.

14. Suslick, K. S., Sonochemistry. *Science* **1990,** *247* (4949), 1439-1445.

15. Suslick, K. S.; Flannigan, D. J., Inside a collapsing bubble: sonoluminescence and the

conditions during cavitation. *Annu. Rev. Phys. Chem.* **2008,** *59*, 659-683.

16. McNamara, W. B.; Didenko, Y. T.; Suslick, K. S., Sonoluminescence temperatures during multi-bubble cavitation. *Nature* **1999,** *401* (6755), 772-775.

17. Flannigan, D. J.; Suslick, K. S., Plasma formation and temperature measurement during single-bubble cavitation. *Nature* **2005,** *434* (7029), 52-55.

18. McNamara, W. B.; Didenko, Y. T.; Suslick, K. S., Pressure during sonoluminescence. *J. Phys. Chem. B* **2003,** *107* (30), 7303-7306.

19. Guo, Z.; Zhang, M.; Li, H.; Wang, J.; Kougoulos, E., Effect of ultrasound on anti-solvent crystallization process. *J. Cryst. Growth* **2005,** *273* (3), 555-563.

20. Lyczko, N.; Espitalier, F.; Louisnard, O.; Schwartzentruber, J., Effect of ultrasound on the induction time and the metastable zone widths of potassium sulphate. *Chem. Eng. J.* **2002,** *86* (3), 233-241.

21. Revalor, E.; Hammadi, Z.; Astier, J.-P.; Grossier, R.; Garcia, E.; Hoff, C.; Furuta, K.; Okustu, T.; Morin, R.; Veesler, S., Usual and unusual crystallization from solution. *J. Cryst. Growth* **2010,** *312* (7), 939-946.

22. Guo, Z.; Jones, A.; Li, N., The effect of ultrasound on the homogeneous nucleation of BaSO4 during reactive crystallization. *Chem. Eng. Sci.* **2006,** *61* (5), 1617-1626.

23. Mullin, J. W., *Crystallization*. Butterworth-Heinemann: 2001.

24. Cravotto, G.; Gaudino, E. C.; Cintas, P., On the mechanochemical activation by ultrasound. *Chem. Soc. Rev.* **2013,** *42* (18), 7521-7534.

25. Li, H.; Li, H.; Guo, Z.; Liu, Y., The application of power ultrasound to reaction crystallization. *Ultrason. Sonochem.* **2006,** *13* (4), 359-363.

26. Luque de Castro, M.; Priego-Capote, F., Ultrasound-assisted crystallization (sonocrystallization). *Ultrason. Sonochem.* **2007,** *14* (6), 717-724.

27. Zeiger, B. W.; Suslick, K. S., Sonofragmentation of molecular crystals. *J. Am. Chem. Soc.* **2011,** *133* (37), 14530-14533.

28. Sander, J. R.; Zeiger, B. W.; Suslick, K. S., Sonocrystallization and sonofragmentation. *Ultrason. Sonochem.* **2014,** *21* (6), 1908-1915.

29. Dirksen, J.; Ring, T., Fundamentals of crystallization: kinetic effects on particle size distributions and morphology. *Chem. Eng. Sci.* **1991,** *46* (10), 2389-2427.

30. Kamaraju, V. K.; Chiu, M.-S., Improved Operation of Concentration Control for Antisolvent Crystallization Processes. *Org. Proc. Res. Dev.* **2014,** *in press*.

31. Myerson, A., *Handbook of Industrial Crystallization*. Butterworth-Heinemann: 2002.

32. Thorat, A. A.; Dalvi, S. V., Liquid antisolvent precipitation and stabilization of nanoparticles of poorly water soluble drugs in aqueous suspensions: Recent developments and future perspective. *Chem. Eng. J.* **2012,** *181*, 1-34.

33. Eder, R. J.; Schrank, S.; Besenhard, M. O.; Roblegg, E.; Gruber-Woelfler, H.; Khinast, J. G., Continuous sonocrystallization of acetylsalicylic acid (ASA): control of crystal size. *Cryst. Growth Des.* **2012,** *12* (10), 4733-4738.

34. Beck, C.; Dalvi, S. V.; Dave, R. N., Controlled liquid antisolvent precipitation using a rapid mixing device. *Chem. Eng. Sci.* **2010,** *65* (21), 5669-5675.

35. Dalvi, S. V.; Dave, R. N., Controlling particle size of a poorly water-soluble drug using ultrasound and stabilizers in antisolvent precipitation. *Ind. Eng. Chem. Res.* **2009,** *48* (16), 7581-7593.

36. Narducci, O.; Jones, A.; Kougoulos, E., An assessment of the use of ultrasound in the particle engineering of micrometer-scale adipic acid crystals. *Cryst. Growth Des.* **2011,** *11* (5), 1742-1749.

37. Ramisetty, K. A.; Pandit, A. B.; Gogate, P. R., Ultrasound-Assisted Antisolvent

Crystallization of Benzoic Acid: Effect of Process Variables Supported by Theoretical Simulations. *Ind. Eng. Chem. Res.* **2013,** *52* (49), 17573-17582.

38. Sander, J. R.; Bučar, D. K.; Henry, R. F.; Zhang, G. G.; MacGillivray, L. R., Pharmaceutical Nano-Cocrystals: Sonochemical Synthesis by Solvent Selection and Use of a Surfactant. *Angew. Chem.* **2010,** *122* (40), 7442-7446.

39. Greenwood, R.; Kendall, K., Selection of suitable dispersants for aqueous suspensions of zirconia and titania powders using acoustophoresis. *J. Eur. Ceram. Soc.* **1999,** *19* (4), 479-488.

40. Verma, S.; Gokhale, R.; Burgess, D. J., A comparative study of top-down and bottom-up approaches for the preparation of micro/nanosuspensions. *Int. J. Pharm.* **2009,** *380* (1), 216-222.

Chapter 5

Sonocrystallization of carbamazepine

5.1 Introduction

It is important to control particle size of pharmaceutical agents since the particle size can affect to the solubility and dissolution rate.[1-3] Pharmaceutical agents for orally-ingested drugs should have not only sufficient lipophilicity to pass through cell membrane but also sufficient hydrophilicity to be transported within the body.[4-6] If a pharmaceutical agent has low solubility in water, transport in blood plasma is difficult and the absorption of the drug into the target organ can be problematic.[7-9] Therefore, it is crucial to improve the solubility and dissolution rate of hydrophobic pharmaceutical agents.

Reducing the size of a particle increases its solubility by increasing the surface area per unit volume.[10-17] Dissolution occurs at the interface between the particle and surrounding solvent. Therefore, an increased surface area increases the chance of molecules on the surface of a particle dissolving in the surrounding solvent. In 1900, Ostwald and Freundlich determined the following relationship between salt particle size and solubility[18]:

$$\ln\left[\frac{c(r)}{c^*}\right] = \frac{2M\gamma}{\nu RT\rho r}$$

where c(r) = solubility of particles of size r; c* = normal equilibrium solubility of the substance; M = molar mass of the substance in the solution; γ = interfacial tension of the substance in contact with the solution; ν = number of moles of ions formed from one mole of electrolyte; R = gas constant; T = absolute temperature; and ρ = density of the substance.

Decreasing particle size also increases the dissolution rate of the particles.[10, 17, 19-22] According to the Noyes–Whitney equation, the dissolution rate is affected by the surface area

and concentration of the dissolving substance, and by the thickness of the boundary layer of solvent around the dissolving substance.[23] Noyes and Whitney suggested their relationship could be written as:

$$\frac{dm}{dt} = \frac{DA(c_s - c_t)}{h_D}$$

where m = mass of the dissolving substance; t = time; D = diffusion coefficient of the dissolving substance; A = surface area of the dissolving substance; c_s = solubility of the substance; c_t = mass concentration of the substance in the bulk medium at time t; and h_D = thickness of the boundary layer of the solvent at the surface of the dissolving substance. Reducing particle size increases the surface area per unit volume dramatically. In addition, the thickness of the boundary layer decreases with reduction of particle size due to the increased relative velocity of the flowing solvent against the surface of the particle.[24] Consequently, the dissolution rate is accelerated as the particle size is reduced.

Carbamazepine is one of the most essential medications for the treatment of epilepsy, neuropathic pain and schizophrenia,[25] but it is poorly soluble in water (~125 mg/L at 25 °C).[26] Consequently, the absorption of carbamazepine in the gastrointestinal tract is delayed and irregular.[8, 27] Studies have examined ways to reduce the crystal size of carbamazepine to improve its solubility and dissolution rate. There are only a few reports, however, on carbamazepine nanoparticles generated using additives such as polymers or surfactants.[28-31] Without these additives, aggregates of carbamazepine nanoparticles are produced.[32]

In this chapter, carbamazepine micro- and nanocrystals were produced by sonocrystallization without the use of additives. Also, the carbamazepine crystals were generated using evaporation–cooling and antisolvent crystallization methods. The size,

morphology, and structure of the crystals were compared. Finally, it was investigated the effect of crystal size on the solubility and dissolution rate of carbamazepine.

5.2 Experimental

5.2.1 Materials

Carbamazepine were purchased from Sigma-Aldrich and used as-received, unless otherwise indicated. Ethanol (100%) was purchased from Decon Laboratory. For crystallization, nanopure water (i.e., water deionized to >18 MΩ·cm resistance, scrubbed for organics, and passed through a 0.45 μm filter with a Barnstead NANOpure® ultrapure water purification system) was used.

5.2.2 Crystallization of carbamazepine

5.2.2.1 Evaporation–cooling crystallization with or without seed crystals

First, 250 mg of carbamazepine was completely dissolved in 10 mL of ethanol at 60 °C and 20 mg of carbamazepine seed crystals (Sigma-Aldrich) were added to the carbamazepine solution when it reached 40 °C. The carbamazepine solution was cooled to room temperature in a vial that was covered loosely with a cap. Evaporation was completed within about 36 hours. For evaporation–cooling crystallization without seed crystals, the procedures were same, except no seed crystals were added.

5.2.2.2 Antisolvent crystallization

Excess carbamazepine was dissolved in 10 mL of ethanol at 25 °C for five hours with a magnetic stirring bar and a stirrer (900 rpm) to form a saturated carbamazepine solution. The

carbamazepine solution was added to 10 mL of nanopure water at 25 °C with a syringe pump (Harvard Apparatus Compact Infusion Pump), at a rate of 9.6 mL/min, through a syringe filter (Thermo Scientific Nalgene Syringe Filter, pore size 0.2 μM) with a syringe to prevent the injection of undissolved carbamazepine solid into the nanopure water. A magnetic stirring bar was used to mix the carbamazepine solution and nanopure water at 900 rpm. After finishing the injection, the solid was separated from the liquid by centrifugation and dried in a vacuum oven at 25 °C overnight.

5.2.2.3 Antisolvent sonocrystallization

All of the steps were the same as for antisolvent crystallization, except an exponential ultrasonic horn (VCX-750; Sonics and Materials, 20 kHz, 1 cm^2 titanium tip, 15 W/cm^2) was used to sonicate the carbamazepine solution and nanopure water instead of stirring it with a magnetic stirring bar. The sonication was done in a temperature-controlled water bath (Isotemp 1006S; Thermo Scientific) to prevent significant increase in the temperature of the mixed solution. The initial and final temperatures of the mixed solution were 18 and 25 °C, respectively. After the injection was complete, the solid was separated from the liquid by centrifugation and dried in a vacuum oven at 25 °C overnight.

5.2.2.4 Spray sonocrystallization

The experimental method for spray sonocrystallization followed our previous report.[33] Excess amount of carbamazepine was dissolved in 10 ml of ethanol at 25 °C to form saturated carbamazepine solution. The carbamazepine solution was pumped with a syringe pump through a tapped ultrasonic horn (i.e., a hole drilled from top to bottom of the horn, Sonics and Materials dual inlet atomizing probe VCX 130 AT, 20 kHz), exiting from the bottom (an

acoustic antinode of the horn) into the mixing region of the flow cell into which the antisolvent (nanopure water) was also pumped. The carbamazepine solution was pumped through the horn with a syringe pump (Harvard Apparatus Compact Infusion Pump), at a rate of 9.6 mL/min. A syringe filter (Thermo Scientific Nalgene Syringe Filter, pore size 0.2 μM) was used with the syringe to prevent the injection of undissolved carbamazepine solid into the nanopure water. The ultrasonic horn was immersed in a flowing antisolvent of nanopure water. The initial temperature of nanopure water was set to 18 °C using a water bath; its flow was set to 48 mL/min using a peristaltic pump (Cole-Parmer Instrument Company MasterFlex 77390-00). The carbamazepine solution was rapidly dispersed into the antisolvent via momentum transfer from the ultrasonic horn. The ultrasonic power delivered by the tapped horn was calorimetrically determined and set to 15 W/cm^2. Aliquots of the sonicated mixture were collected every minute and diluted in 10 mL of nanopure water. For characterization, product was collected after a full steady state was reached, specifically after 6 min.

5.2.3 Solubility tests

Solutions of carbamazepine in ethanol were prepared at concentrations of 0.05, 0.10, 0.15, and 0.20 mM. Saturated solutions in 10 mL of deionized (DI) water were prepared by adding excess carbamazepine and stirring for 2 days at 25 or 37 °C. The supernatant was filtered through a syringe filter (Thermo Scientific Nalgene Syringe Filter, pore size 0.2 μM) to remove any carbamazepine particles before UV-Vis analysis. The initially saturated carbamazepine solutions were diluted and UV-visible absorption spectra were measured. The ultraviolet-visible (UV-Vis) absorption of each solution was measured with a UV-Vis spectrometer (Lambda 35; PerkinElmer). The molar absorptivity coefficients were calculated

at an absorption peak of 285 nm. The amount of dissolved carbamazepine was calculated based on the intensity of the UV-visible absorption peak at 285 nm.

5.2.4 Dissolution tests

2.2 mg of carbamazepine was added to 10 mL of DI water and stirred with a magnetic bar (150 rpm) at 37°C in a silicon oil bath. After the stirring was stopped, the carbamazepine solution was filtered through a syringe filter (Thermo Scientific Nalgene Syringe Filter, pore size 0.2 μM) to remove any particulate carbamazepine. The filtered solution was diluted and the UV-visible absorption was measured by UV-Vis spectrometry (PerkinElmer Lambda 35). The amount of dissolved carbamazepine was calculated based on the intensity of the UV-visible absorption peak at 285 nm.

5.2.5 Characterization

Optical microscopy was performed with a Zeiss Axioskop optical/fluorescence microscope. The micrographs were captures using a Cannon PC1015 digital camera mounted to the microscope. Scanning electron microscopy was performed with a JEOL 7000F Analytical SEM. Particle size analysis from SEM images was performed using Image-J software (National Institutes of Health, Bethesda, MD, USA). Approximately 200 particles were measured for each experiment. Data fitting was performed using OriginPro 8.5 software (OriginLab, Northampton, MA, USA). Powder X-ray diffraction patterns were obtained from samples mounted on a quartz sample holder using a Bruker D-5000 (λ = 1.5418 Å, 25 °C) in the 2 theta range 10-35 theta.

5.3 Results and discussion

5.3.1 Crystallization of carbamazepine

The different crystallization methods produced carbamazepine crystals with diverse morphologies and sizes (Figure 5.1). The carbamazepine crystals from Sigma-Aldrich and carbamazepine crystals generated by evaporation–cooling crystallization with seed crystals had random rock shapes. All of the other carbamazepine crystals were needle shaped. The average crystal size ranged from 9 to 470 μM (Table 5.1). Antisolvent crystallization, antisolvent sonocrystallization, and spray sonocrystallization generated smaller crystals than evaporation–cooling crystallization, because the addition of the antisolvent reduced the metastable zone width and induction time, accelerating the rate of nucleation and producing many small crystals.[34-36] In addition to the antisolvent effect, antisolvent sonocrystallization and spray sonocrystallization showed reduction of metastable zone width and induction time, increase of nucleation sites, etc.[37-38] Consequently, the crystals produced by antisolvent sonocrystallization and spray sonocrystallization were smaller than those produced by antisolvent crystallization. For spray sonocrystallization, there was enhanced mixing of the antisolvent and saturated solution in the spray sonocrystallization system.[33] Spray sonocrystallization produced the smallest carbamazepine crystals among the five different crystallization methods.

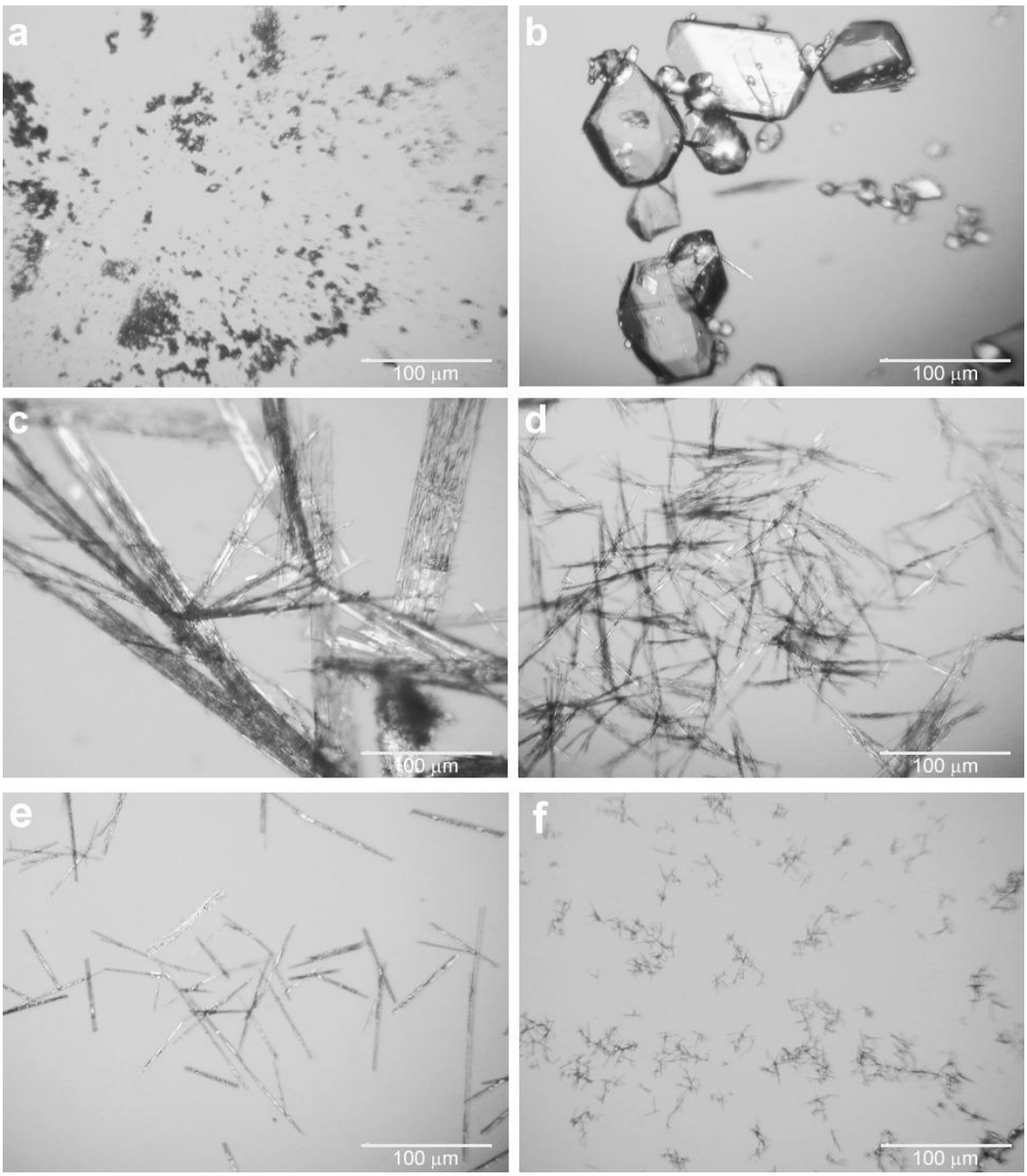

Figure 5.1 Optical microscopy images of carbamazepine crystals (a) purchased from Sigma-Aldrich Chemicals and produced by (b) evaporation–cooling crystallization without the addition of seed crystals, (c) evaporation–cooling crystallization with the addition of seed crystals, (d) antisolvent crystallization, (e) antisolvent sonocrystallization, and (f) spray sonocrystallization.

Table 5.1 Average size of carbamazepine crystals produced by various crystallization methods.

Method	Aldrich Chemical	Evaporation (without seeds)	Evaporation (with seeds)	Antisolvent	Antisolvent sono-crystallization	Spray sono-crystallization
Average crystal size (μm)	36 ± 4	473 ± 6	62 ± 4	73 ± 4	12 ± 1	9 ± 1

*Carbamazepine crystallization and crystal size analysis were performed twice for each method.

5.3.2 Spray sonocrystallization of carbamazepine with different ratios of water to carbamazepine solution

Spray sonocrystallization controlled the size of the carbamazepine crystals, and nano-scale crystals could be produced by changing the ratio of water to carbamazepine solution. When the ratio was changed from 5:1 to 240:1, the average crystal size of produced crystals was changed from about 8 μM to 140 nm (Table 5.2). Figure 5.2 shows that the average crystal size decreased exponentially as the proportion of water in the mixture of water and carbamazepine solution increased. A solution with a high mixing ratio reached a higher supersaturated level and had a more rapid nucleation rate than a solution with a low mixing ratio.[10, 39] Consequently, in the solution with a high mixing ratio, the total number of crystals produced increased and the size of each crystal decreased.

Table 5.2 Average size of carbamazepine crystals generated by spray sonocrystallization with different ratios of water to carbamazepine solution.

Mixing ratio (Water : CBZ solution)	5 : 1	10 : 1	21 : 1	37 : 1	60 : 1	120 : 1	240 : 1
Average crystal size (μm)	8.6±0.5	7.3±0.1	6.3±0.6	2.9±0.5	1.2±0.1	0.5±0.1	0.14±0.01

* Carbamazepine crystallization and crystal size analysis were performed twice for each mixing ratio.

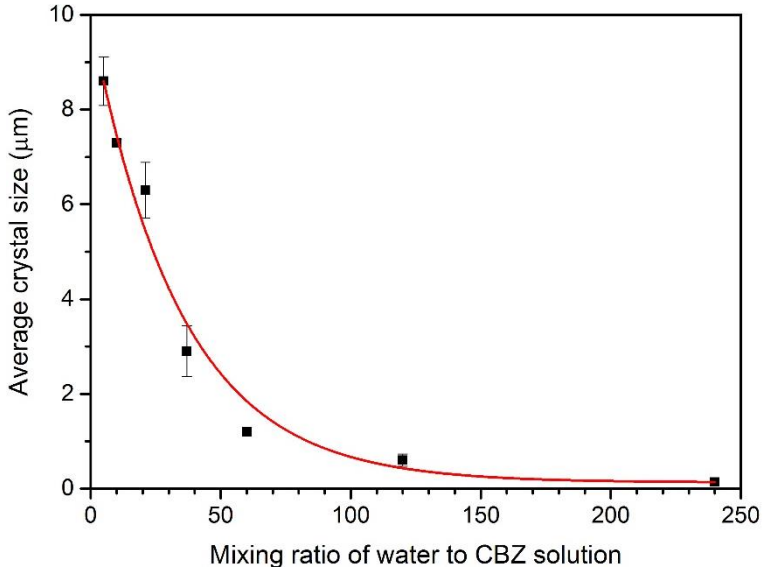

Figure 5.2 Relationship between the mixing ratio of water to carbamazepine solution and the size of carbamazepine crystals using spray sonocrystallization. For each mixing ratio, spray crystallization and crystal size analysis were performed twice. Each point is the average of two experimental results and each error bar is the standard deviation of the two results. The solid line is the exponential decay fit to the data.

The morphology of carbamazepine changed gradually with the mixing ratio (Figure 5.3). The ratio of the length to width of a crystal decreased as the mixing ratio increased: i.e. the

morphology changed from needles to rods to spheres. Figure 5.3(g) shows non-agglomerated carbamazepine nanocrystals produced by spray sonocrystallization without the use of additives.

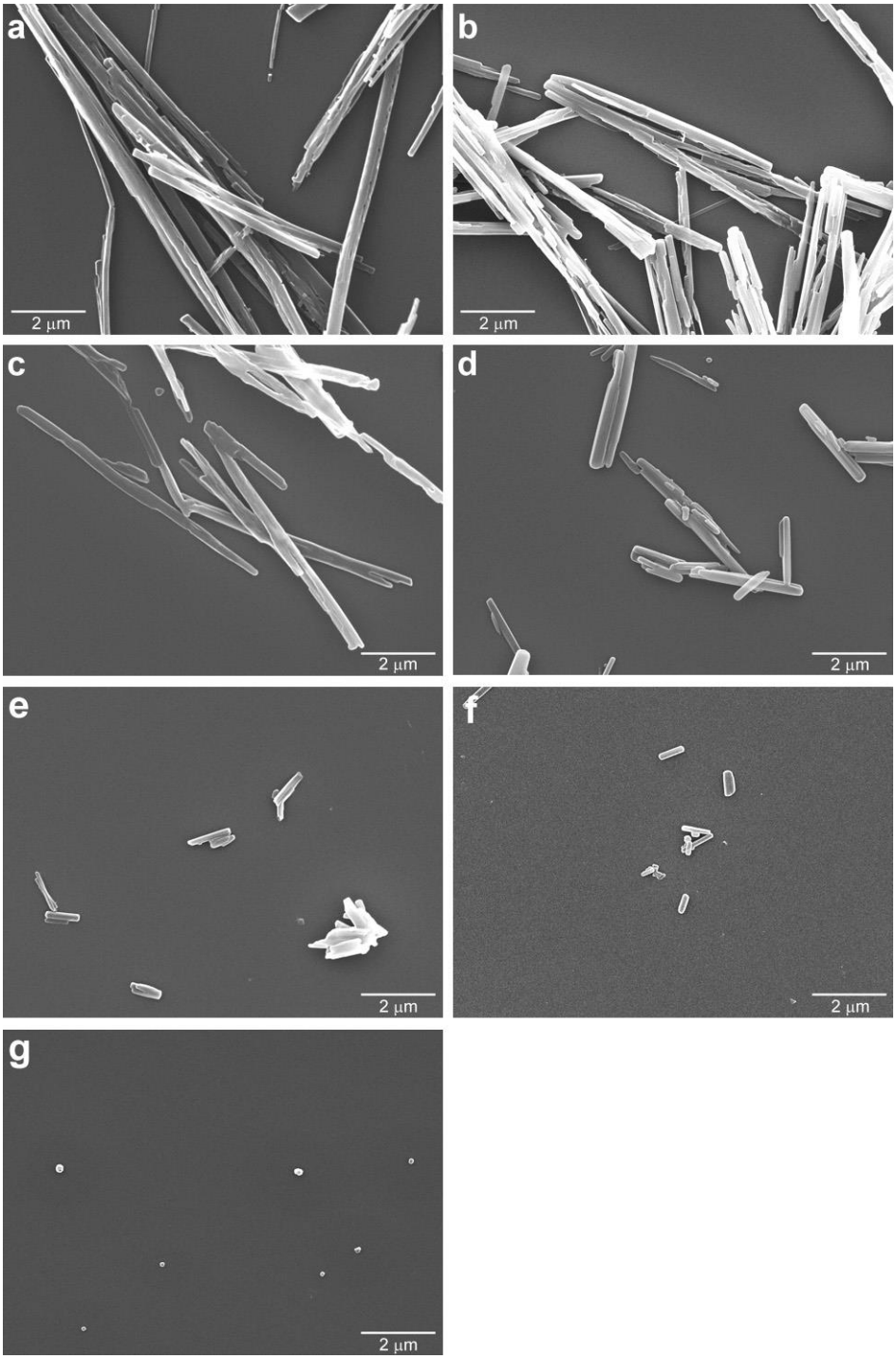

Figure 5.3 SEM images of carbamazepine crystals generated by spray sonocrystallization with

Figure 5.3 (cont.)

different mixing ratio of water to carbamazepine solution: (a) 5 : 1, (b) 10 : 1, (c) 21 : 1, (d) 37 : 1, (e) 60 : 1, (f) 120 : 1, and (g) 240 : 1.

5.3.3 Crystal structures of carbamazepine

The structures of the carbamazepine crystals were confirmed by powder X-ray diffraction. There are four different polymorphs of carbamazepine and their order of stability at ambient temperature is form III > form I > form IV > form II.[40-41] The Sigma-Aldrich carbamazepine and carbamazepine generated by evaporation–cooling crystallization with seed crystals were carbamazepine form III (Figure 5.4, left). The carbamazepine generated by evaporation–cooling crystallization without seed crystals were carbamazepine form II. Antisolvent crystallization, antisolvent sonocrystallization, and spay sonocrystallization produced carbamazepine dihydrate because of the addition of water (Figure 5.4, right).

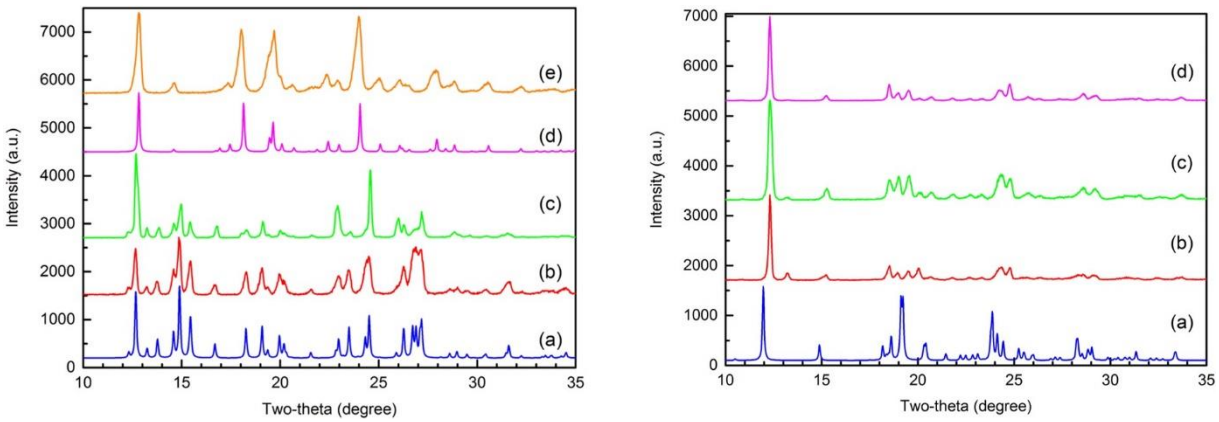

Figure 5.4 Powder X-ray diffraction patterns of carbamazepine. (Left) (a) carbamazepine form III calculated from single crystal X-ray diffraction data, (b) as-purchased carbamazepine,

Figure 5.4 (cont.)

(c) carbamazepine generated by evaporation–cooling crystallization with seed crystals, (d) carbamazepine form II calculated from single crystal X-ray diffraction data, and (e) carbamazepine generated by evaporation–cooling crystallization without seed crystals. (Right) (a) carbamazepine dihydrate calculated from single crystal X-ray diffraction data, (b) carbamazepine generated by antisolvent crystallization, (c) carbamazepine generated by antisolvent sonocrystallization, and (d) carbamazepine generated by spray sonocrystallization. Single crystal data was reported in the Cambridge Structural Database.

5.3.4 Solubility tests

Various crystallization methods generated three different carbamazepine crystals (*i.e.*, form II, form III, and dihydrate), which have different intrinsic solubilities. The intrinsic solubilities (i.e., initial solubility) of carbamazepine are in the order form III > form II > dihydrate.[42-44] The intrinsic solubility of carbamazepine differs from its equilibrium solubility (i.e., long-term solubility). Carbamazepine forms III and II are hydrated in an aqueous environment becoming carbamazepine dihydrate rapidly.[45-46] Therefore, there is no significant difference in the equilibrium solubility of form III, form II, and dihydrate.

The effect of carbamazepine crystal size on its equilibrium solubility was confirmed by solubility tests. The solubility tests were performed in water at 25 and 37°C for 2 days, respectively. It is assumed the carbamazepine crystals described in Section 5.3.1 and 5.3.2 were spheres and equivalent diameters were calculated. Although the equivalent diameter of the crystals ranged from 51 to 140 nm, their solubility did not differ significantly at 25°C (Figure 5.5). At 37°C, the solubility increased slightly as the size of the crystals decreased. Therefore, for the size range studied, crystal size had little effect on the equilibrium solubility

of carbamazepine. This is not unexpected, since size effect are most important only below about 50 nm dimensions.

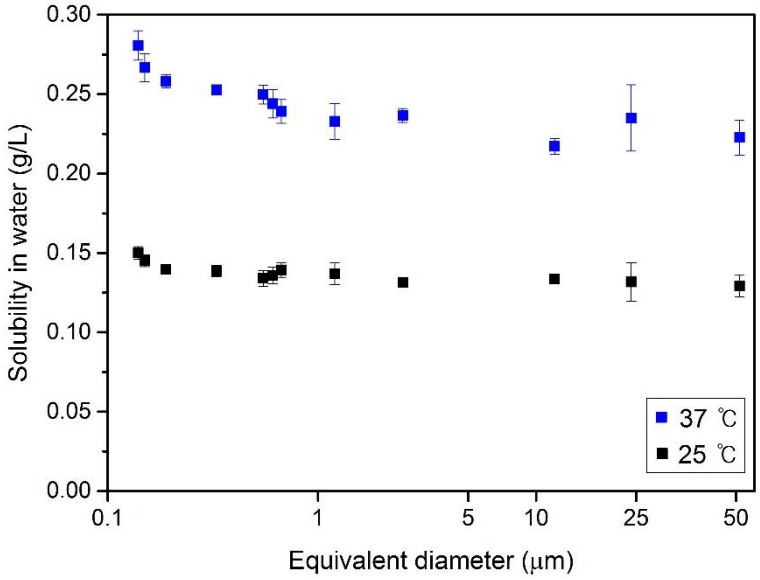

Figure 5.5 The effect of crystal size on the aqueous solubility of carbamazepine. The solubility of each sample was tested three times each at 25 and 37°C. Each point is the average value of the three trials and the error bar is the standard deviation.

5.3.5 Dissolution tests

The dissolution rate of the various sizes and forms of carbamazepine was tested in water at 37°C. The dissolution rate increased as the crystal size decreased, since smaller particles have a higher surface-area-to-volume ratio (Figure 5.6). Although carbamazepine dihydrate crystals, which have the lowest initial solubility among carbamazepine form II, form III, and dihydrate, were produced via antisolvent crystallization, antisolvent sonocrystallization, and spray sonocrystallization, their dissolution rates were more rapid than the dissolution rate of carbamazepine crystals purchased from Sigma-Aldrich or generated by evaporation–cooling crystallization with or without the addition of seed crystals. Therefore, the effect of crystal size was more important than the effect of intrinsic solubility in the dissolution tests.

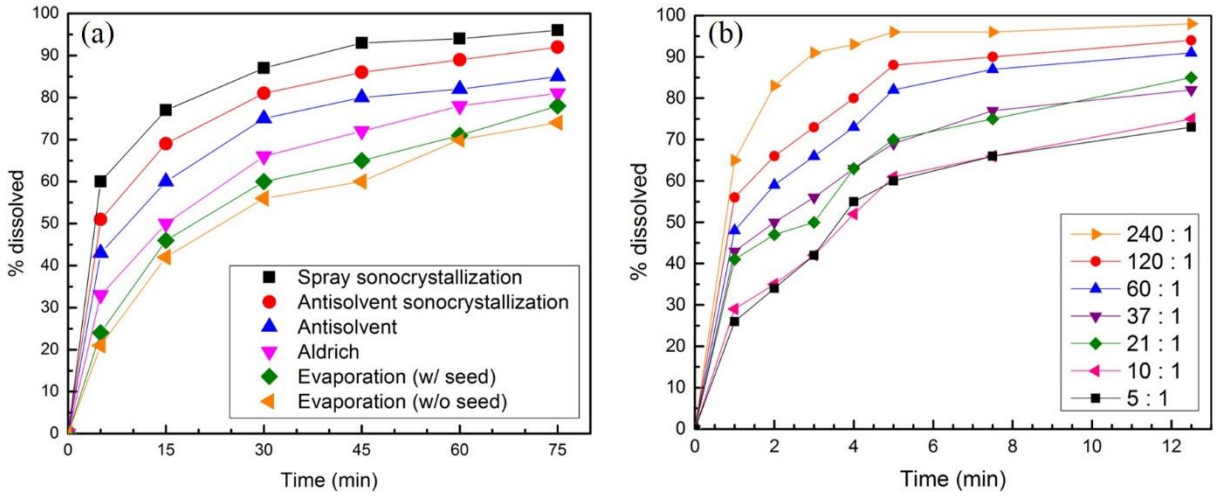

Figure 5.6 Dissolution rate of carbamazepine generated (a) by various crystallization methods and (b) by spray sonocrystallization with different ratios of water to carbamazepine solution.

The change in crystal size affected the time required to dissolve half of the initial carbamazepine (i.e., the half-time). Figure 5.7(a) shows that the half-time decreased with the equivalent diameter. According to the Noyes–Whitney equation and Prandtl's boundary layer equation,[23-24] the half-time is proportional to the (particle diameter)$^{1.5}$ when the dissolved particle is a sphere. For all samples, however, the half-time was not proportional to the (particle diameter)$^{1.5}$ (Figure 5.7a). In this experiment, the carbamazepine crystals were of three different forms (i.e., form II, form III, and dihydrate) and the initial dissolution rates were affected by the form of carbamazepine. Due to the different forms of carbamazepine, the relationship between the equivalent diameter and half-time did not follow the Noyes–Whitney equation and Prandtl's boundary layer equation. Considering only the carbamazepine dihydrate crystals, the half-time was approximately proportional to the (particle diameter)$^{1.5}$ (Figure 5.7b).

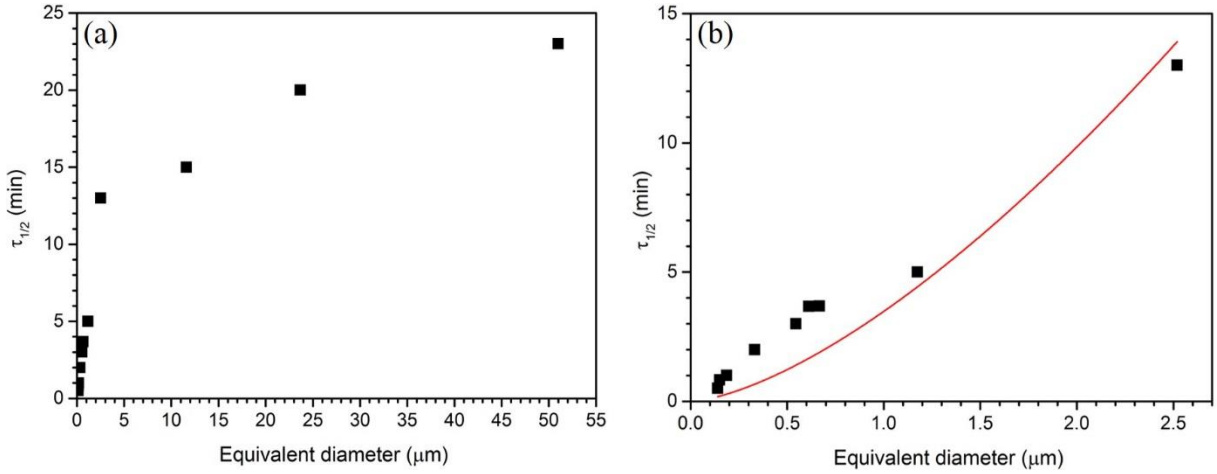

Figure 5.7 Relationship between the equivalent diameter and half-time (a) for all carbamazepine samples and (b) for carbamazepine dihydrate. In (b), the data were fitted by the exponential function $y = a \cdot x^{1.5}$ (a = constant).

5.4 Conclusion

Five different crystallization methods produced carbamazepine crystals with diverse sizes and forms. Among the methods, spray sonocrystallization controlled crystal size systematically by altering the mixing ratio between water (the antisolvent) and carbamazepine solution. Spray crystallization produced non-agglomerated carbamazepine nanocrystals without the use of additives. In the range from several hundred micrometers to one hundred nanometers, crystal size had little effect on the solubility in water. The dissolution rate in water, however, increased significantly as the crystal size decreased.

5.5 References

1. Blagden, N.; de Matas, M.; Gavan, P. T.; York, P., Crystal engineering of ac tive pharmaceutical ingredients to improve solubility and dissolution rates. *Advanced Drug Delivery Reviews* **2007,** *59* (7), 617-630.

2. Stahl, P. H.; Wermuth, C. G., *Handbook of pharmaceutical salts properties, s election, and use*. John Wiley & Sons: 2008.

3. Chen, J.; Sarma, B.; Evans, J. M. B.; Myerson, A. S., Pharmaceutical crystall ization. *Crystal Growth & Design* **2011,** *11* (4), 887-895.

4. Liversidge, G. G.; Cundy, K. C., Particle size reduction for improvement of oral bioavailability of hydrophobic drugs. *International Journal of Pharmaceutics* **199 5,** *125* (1), 91-97.

5. Amidon, G. L.; Lennernas, H.; Shah, V. P.; Crison, J. R., A theoretical basis for a biopharmaceutic drug classification - the correlation of in-vitro drug product di ssolution and in-vivo bioavailability. *Pharmaceutical Research* **1995,** *12* (3), 413-420.

6. Balaz, S., Modeling kinetics of subcellular disposition of chemicals. *Chemical Reviews* **2009,** *109* (5), 1793-1899.

7. Fincher, J. H., Particle size of drug and its relationship to absorption and acti vity. *Journal of Pharmaceutical Sciences* **1968,** *57* (11), 1825-&.

8. Dressman, J. B.; Amidon, G. L.; Reppas, C.; Shah, V. P., Dissolution testing as a prognostic tool for oral drug absorption: Immediate release dosage forms. *Pharm aceutical Research* **1998,** *15* (1), 11-22.

9. Lindenberg, M.; Kopp, S.; Dressman, J. B., Classification of orally administer ed drugs on the World Health Organization Model list of Essential Medicines accordi ng to the biopharmaceutics classification system. *European Journal of Pharmaceutics and Biopharmaceutics* **2004,** *58* (2), 265-278.

10. Mullin, J. W., *Crystallization*. Butterworth-Heinemann: 2001.

11. Buckton, G.; Beezer, A. E., The relationship between particle size and solubil ity. *International Journal of Pharmaceutics* **1992,** *82* (3), R7-R10.

12. Wu, W. J.; Nancollas, G. H., A new understanding of the relationship betwee n solubility and particle size. *Journal of Solution Chemistry* **1998,** *27* (6), 521-531.

13. Iggland, M.; Mazzotti, M., Population balance modeling with size-dependent s olubility: Ostwald ripening. *Crystal Growth & Design* **2012,** *12* (3), 1489-1500.

14. O'Mahony, M.; Leung, A. K.; Ferguson, S.; Trout, B. L.; Myerson, A. S., A process for the formation of nanocrystals of active pharmaceutical ingredients with po or aqueous solubility in a nanoporous substrate. *Organic Process Research & Develo pment* **2015,** *19* (9), 1109-1118.

15. Enustun, B. V.; Turkevich, J., Solubility of fine particles of strontium sulfate. *Journal of the American Chemical Society* **1960,** *82* (17), 4502-4509.

16. Segets, D.; Gradl, J.; Taylor, R. K.; Vassilev, V.; Peukert, W., Analysis of o ptical absorbance spectra for the determination of ZnO nanoparticle size distribution, solubility, and surface energy. *Acs Nano* **2009,** *3* (7), 1703-1710.

17. Sun, J.; Wang, F.; Sui, Y.; She, Z. N.; Zhai, W. J.; Wang, C. L.; Deng, Y. H., Effect of particle size on solubility, dissolution rate, and oral bioavailability: eval uation using coenzyme Q(10) as naked nanocrystals. *International Journal of Nanome dicine* **2012,** *7*, 5733-5744.

18. Ostwald, W., On the assumed isomerism of red and yellow mercury oxide an d the surface-tension of solid bodies. *Zeitschrift Fur Physikalische Chemie--Stochiomet rie Und Verwandtschaftslehre* **1900,** *34* (4), 495-503.

19. Kesisoglou, F.; Panmai, S.; Wu, Y. H., Nanosizing - oral formulation development and biopharmaceutical evaluation. *Advanced Drug Delivery Reviews* **2007,** *59* (7), 631-644.

20. Vogelsberger, W.; Schmidt, J., Studies of the solubility of BaSO4 nanoparticles in water: kinetic size effect, solubility product, and influence of microporosity. *Journal of Physical Chemistry C* **2011,** *115* (5), 1388-1397.

21. Radacsi, N.; Ambrus, R.; Szabo-Revesz, P.; van der Heijden, A.; ter Horst, J. H., Atmospheric pressure cold plasma synthesis of submicrometer-sized pharmaceuticals with improved physicochemical properties. *Crystal Growth & Design* **2012,** *12* (10), 5090-5095.

22. Radacsi, N.; Ambrus, R.; Szunyogh, T.; Szabo-Revesz, P.; Stankiewicz, A.; van der Heijden, A.; ter Horst, J. H., Electrospray crystallization for nanosized pharmaceuticals with improved properties. *Crystal Growth & Design* **2012,** *12* (7), 3514-3520.

23. Noyes, A. A.; Whitney, W. R., The rate of solution of solid substances in their own solutions. *Journal of the American Chemical Society* **1897,** *19* (12), 930-934.

24. Prandtl, L., Verhandlungen des dritten internationalen Mathematiker-Kongresses. *Heidelberg, Leipeizig* **1904**, 484-491.

25. WHO Model Lists of Essential Medicines. (accessed http://www.who.int/medicines/publications/essentialmedicines/en/).

26. Shayanfar, A.; Velaga, S.; Jouyban, A., Solubility of carbamazepine, nicotinamide and carbamazepine-nicotinamide cocrystal in ethanol-water mixtures. *Fluid Phase*

Equilibria **2014,** *363,* 97-105.

27. Bertilsson, L., Clinical pharmacokinetics of carbamazepine. *Clinical Pharmaco kinetics* **1978,** *3* (2), 128-143.

28. Wang, M.; Rutledge, G. C.; Myerson, A. S.; Trout, B. L., Production and ch aracterization of carbamazepine nanocrystals by electrospraying for continuous pharma ceutical manufacturing. *Journal of Pharmaceutical Sciences* **2012,** *101* (3), 1178-1188.

29. Kumar, R.; Siril, P. F., Ultrafine carbamazepine nanoparticles with enhanced water solubility and rate of dissolution. *Rsc Advances* **2014,** *4* (89), 48101-48108.

30. Tummala, S.; Satish Kumar, M.; Prakash, A., Formulation and in vitro charac terization of carbamazepine polymeric nanoparticles with enhanced solubility and susta ined release for the treatment of epilepsy. *J Chem Pharm Res* **2015,** *7,* 70-79.

31. Ueda, K.; Higashi, K.; Yamamoto, K.; Moribe, K., In situ molecular elucidati on of drug supersaturation achieved by nano-sizing and amorphization of poorly wate r-soluble drug. *European Journal of Pharmaceutical Sciences* **2015,** *77,* 79-89.

32. Duarte, I.; Corvo, M. L.; Serodio, P.; Vicente, J.; Pinto, J. F.; Temtem, M., Production of nano-solid dispersions using a novel solvent-controlled precipitation pro cess - Benchmarking their in vivo performance with an amorphous micro-sized solid dispersion produced by spray drying. *European Journal of Pharmaceutical Sciences* **2 016,** *93,* 203-214.

33. Kim, H. N.; Sander, J. R. G.; Zeiger, B. W.; Suslick, K. S., Spray sonocryst allization. *Crystal Growth & Design* **2015,** *15* (4), 1564-1567.

34. Reverchon, E., Supercritical antisolvent precipitation of micro- and nano-partic

les. *Journal of Supercritical Fluids* **1999,** *15* (1), 1-21.

35. D'Addio, S. M.; Prud'homme, R. K., Controlling drug nanoparticle formation by rapid precipitation. *Advanced Drug Delivery Reviews* **2011,** *63* (6), 417-426.

36. Chan, H. K.; Kwok, P. C. L., Production methods for nanodrug particles usin g the bottom-up approach. *Advanced Drug Delivery Reviews* **2011,** *63* (6), 406-416.

37. de Castro, M. D. L.; Priego-Capote, F., Ultrasound-assisted crystallization (son ocrystallization). *Ultrasonics Sonochemistry* **2007,** *14* (6), 717-724.

38. Sander, J. R. G.; Zeiger, B. W.; Suslick, K. S., Sonocrystallization and sonof ragmentation. *Ultrasonics Sonochemistry* **2014,** *21* (6), 1908-1915.

39. Beckmann, W., *Crystallization: basic concepts and industrial applications*. Joh n Wiley & Sons: New York, 2013.

40. Grzesiak, A. L.; Lang, M. D.; Kim, K.; Matzger, A. J., Comparison of the f our anhydrous polymorphs of carbamazepine and the crystal structure of form I. *Jour nal of Pharmaceutical Sciences* **2003,** *92* (11), 2260-2271.

41. Rustichelli, C.; Gamberini, G.; Ferioli, V.; Gamberini, M. C.; Ficarra, R.; To mmasini, S., Solid-state study of polymorphic drugs: carbamazepine. *Journal of Phar maceutical and Biomedical Analysis* **2000,** *23* (1), 41-54.

42. Lowes, M. M. J.; Caira, M. R.; Lotter, A. P.; Vanderwatt, J. G., Physicoche mical properties and x-ray structural studies of the trigonal polymorph of carbamazepi ne. *Journal of Pharmaceutical Sciences* **1987,** *76* (9), 744-752.

43. Murphy, D.; Rodriguez-Cintron, F.; Langevin, B.; Kelly, R. C.; Rodriguez-Hor nedo, N., Solution-mediated phase transformation of anhydrous to dihydrate carbamaze

pine and the effect of lattice disorder. *International Journal of Pharmaceutics* **2002,** *246* (1-2), 121-134.

44. Sehic, S.; Betz, G.; Hadzidedic, S.; El-Arini, S. K.; Leuenberger, H., Investig ation of intrinsic dissolution behavior of different carbamazepine samples. *Internationa l Journal of Pharmaceutics* **2010,** *386* (1-2), 77-90.

45. Kobayashi, Y.; Ito, S.; Itai, S.; Yamamoto, K., Physicochemical properties an d bioavailability of carbamazepine polymorphs and dihydrate. *International Journal of Pharmaceutics* **2000,** *193* (2), 137-146.

46. Tian, F.; Zeitler, J. A.; Strachan, C. J.; Saville, D. J.; Gordon, K. C.; Rades, T., Characterizing the conversion kinetics of carbamazepine polymorphs to the dihydr ate in aqueous suspension using Raman spectroscopy. *Journal of Pharmaceutical and Biomedical Analysis* **2006,** *40* (2), 271-280.